ENDOTHELIAL PROGENITOR CELL SUBPOPULATION PROFILING REVEALS A CRITICAL ROLE FOR ENDOGLIN IN RETINAL NEOVASCULARIZATION

By

Joshua McAlister Barnett

Dissertation

Submitted to the Faculty of the

Graduate School of Vanderbilt University

in partial fulfillment of the requirements

for the degree of

DOCTOR OF PHILOSOPHY

In

Pharmacology

August, 2011

Nashville, Tennessee

Approved:

Professor John S. Penn

Professor Joey V. Barnett (chair)

Professor Christopher B. Brown

Professor Frederick R. Haselton

Professor Charles C. Hong

ACKNOWLEDGEMENTS

This work would not have been possible without the financial support of the National Research Service Award (AG031036) from the NIH National Institute on Aging, a research project grant (EY07533) from the NIH National Eye Institute, a Challenge Award from Research to Prevent Blindness, and grants from the OneSight Foundation. I am especially indebted to Dr. John S. Penn, Snyder Professor in Ophthalmology and Vice Chair for Faculty Affairs, who has been incredibly supportive of my career goals and who worked actively to provide me with the time and resources to pursue these goals as well as many of my more extravagant, scientific theories. I will be forever grateful for his constant spirit of graduate student advocacy and infectious enthusiasm for scientific discovery.

I am also grateful to all of those with whom I have had the pleasure to work during this and other related projects. I would like to thank Dr. Gary McCollom, our lab's Senior Research Scientist, for his guidance and friendship. Additionally, the friendship and experimental design advice from Dr. Ashwath Jayagopal have been irreplaceable. Each of the members of my Dissertation Committee has provided me extensive scientific and professional guidance. Each of their suggestions and supportive comments throughout my time in graduate school has strengthened my dissertation work. I would especially like to thank Dr. Joey V. Barnett, the chairman of my committee. As my teacher and mentor, he has been an excellent example of a great scientist and member of the academic and local communities.

No one has been more important to me in the pursuit of this project than the members of my family. I would like to thank my parents, whose love and guidance have helped me in every endeavor that I have undertaken. Most importantly, I wish to thank my loving and supportive wife, Becca. I cannot overstate how important her patience, love, and constructive feedback have been toward helping me to finish these studies.

TABLE OF CONTENTS

Page

LIST OF FIGURES

LIST OF ABBREVIATIONS

14(0)	day of removal from oxygen treatment in the OIR model
14(3)	three days post-oxygen treatment in the OIR model
14(6)	six days post-oxygen treatment in the OIR model
°C	degrees Celsius
μl	microliter
μm	micrometer
μM	micromolar
acLDL	acetylated low density lipoprotein
ADP	adenosine diphosphate
ADPase	an enzyme that catalyses breakdown of ATP to AMP
ALK	Activin receptor-like kinase
AMD	age-related macular degeneration
ANOVA	Analysis of variance
BBS	borate buffered saline
BCA	bicinchoninic acid
BSA	bovine serum albumin
BrdU	5-bromo-2'-deoxy-uridine
CD34	cell surface glycoprotein expressed on early hematopoietic and vascular associated tissue
CD105	endoglin
CD133	(also known as Prominin-1 or AC133) an early stem and progenitor cell surface antigen

cm	centimeter
CNV	choroidal neovascularization
CO_2	carbon dioxide
CS	chondroitin sulfate
CXCR4	chemokine (C-X-C motif) receptor 4
DAPI	4’6-diamidino-2-phenylindole
DiI	1,1'-dioctadecyl-3,3,3',3'- tetramethylindocarbo-cyanine perchlorate
DNA	deoxyribonucleic acid
DR	diabetic retinopathy
EC	endothelial cell
ECL	enhanced chemiluminescence
ECM	extracellular matrix
EDTA	ethylenediaminetetraacetic acid
ELISA	enzyme-linked immunosorbent assay
EML	endothelial monolayer
EPC	endothelial progenitor cell
FACS	fluorescent activated cell sorting
FBS	fetal bovine serum
FITC	fluorescein isothiocyanate
HA	hyaluronic acid
HBSS	Hank’s buffered salt solution
hetero. EPC	heterogeneous EPC population
HHT	hereditary hemorrhagic telangiectasia

HRP	horseradish peroxidase
IB4	isolectin B4
IgG	immunoglobulin-G
LCNV	laser-induced choroidal neovascularization
LDL	low density lipoprotein
ml	milliliter
mm	millimeter
mM	millimolar
ms	millisecond
mW	milliwatt
NaCl	sodium chloride
nm	nanometer
NV	neovascularization
OIR	oxygen-induced retinopathy
PBS	phosphate buffered saline
PMSF	phenylmethylsulfonyl fluoride
PPFC	parallel plate flow chamber
QD	quantum dot nanocrystal
ROP	retinopathy of prematurity
RPE	retinal pigment epithelium
rpm	revolutions per minute
RRMEC	rat retinal microvascular endothelial cells
SD	standard deviation

SDS-PAGE	sodium dodecyl sulfate polyacrylamide gel electrophoresis
SDF-1	stromal cell-derived factor-1
SEM	standard error of the mean
SMAD	transcription factor proteins with a name that is the combination of mothers against decapentaplegic (MAD) and the *Caenorhabditis elegans* protein SMA
TBST	tris buffered saline with 0.1% tween-20
TGFβ	transforming growth factor beta
Tie2	tyrosine kinase with immunoglobulin-like and EGF-like domains 2, TEK tyrosine kinase, angiopoietin receptor
Tris	(hydroxymethyl)aminomethane
v/v	volume to volume proportions
VEGF	vascular endothelial growth factor
VEGFR2	vascular endothelial growth factor receptor 2, KDR, flk-1
VEGFR3	vascular endothelial growth factor receptor 2, flt-4

CHAPTER I

INTRODUCTION

1.1 Background and Significance

1.1.1 Endothelial Progenitor Cell Subsets in Vascular Disease

Angiogenesis characterizes of a number of blinding ocular conditions, including diabetic retinopathy, macular degeneration, retinopathy of prematurity, and vein occlusion retinopathy to name a few. In angiogenesis, new blood vessels originate from existing venules by a series of events involving extracellular matrix remodeling, endothelial cell proliferation and migration and the formation and closure of the nascent vascular tubes(1). Recent studies have found that a large portion of this may be vasculogenesis as the result of bone marrow-derived stem cells incorporating into the neovascular tissue regions from the peripheral blood circulation.

Adult bone marrow is known to contain a population of hematopoietic stem cells which are released into the blood stream where they home to sites of angiogenesis and become vascular endothelial cells. These endothelial progenitor cells (EPCs) were first isolated and characterized by Asahara et al.(2) and have been shown to be recruited to participate in a variety of vascular diseases. These cells can contribute to as much as 50% of the newly formed vessels in choroidal neovascularization (CNV)(3, 4) and have also been shown to participate in myocardial ischemia(5) and infarction(6), tumor infiltration(7), atherosclerosis(8, 9) and revascularization after a stroke(10, 11). Additionally, the impaired ability of these cells under certain diseases has been shown to

contribute to retinal degeneration(12, 13) and vascular disease in diabetes(14-17). However, a better understanding of how these cells function in vascular diseases is required in order to eventually develop a therapy that can be used to influence or control them. This understanding will most likely come in the form of studying the proteins that make up their surface.

One such protein that is common to many hematopoietic and mesenchymal progenitor cells is endoglin. Endoglin (CD105) is a potential non-VEGF pathway protein that could be targeted in the treatment of neovascularization resulting from EPC incorporation. It is a transmembrane glycoprotein that is an accessory to the transforming growth factor β (TGFβ) receptor system(18). Endoglin is also expressed on proliferating endothelial cells (ECs) and tumor types characterized by hypoxia(19-24). On endothelial and tumor cells, it is thought to be involved in differentiation, migration and proliferation(20, 25). Monoclonal antibody therapies have been shown to have some antiproliferative effects in cancer studies(26, 27). Furthermore, subsets of endothelial progenitor cells (EPCs) have been found to highly express CD105(28-30). Additionally, as marker of mesenchymal stem cells, endoglin has been shown on progenitor cells that increase vascular remodeling in models of myocardial infarction and rheumatic diseases(31, 32).Many investigators suggest that EPCs play a significant role in ocular neovascularization and that these cells could be targeted to influence that neovascularization(33, 34). Perhaps targeting EPCs through CD105 could prevent their differentiation and proliferation in the neovascular lesions seen in the angiogenic pathology of the eye. But this isn't the only potential therapeutic strategy targeting EPCs.

Several studies have demonstrated the efficacy of blocking the "homing" of EPCs in reducing vascular disease pathology. Grant et al.(4) show that by using and SDF-1 antibody to inhibit the EPCs in a choroidal neovascularization model, the mean CNV vascular lesion is decreased by approximately 60%. Other studies have shown that the inhibition of L-Selectin and β2-integrins binding have been able to decrease EPC neovascularization in models of hind limb ischemia(35, 36). There are also suggestions to use these cells as therapeutic delivery devices of drugs and proteins to specific sites and in seeding grafts(37, 38).

A common feature of most therapeutic interventions directed toward the inhibition of EPC function in disease has not differentiated among EPC subpopulations. Much work has elucidated a family of EPC subpopulations with varying cell surface expression profiles, which may have similar or distinct functions from each other in disease processes. EPCs that are CD14+ positive, a monocyte surface marker, have been shown to incorporate into developing vessels and become endothelial cells(39, 40). In a similar way, EPCs expressing lymphatic lineage markers have also been shown to target neovascular tissue and become mature endothelial cells(41). EPCs that are CD34+ /CD133+ have been found to be more prolific in cell culture and when targeted to ischemic regions in vivo(2), while CD34- /CD133+ seem to be more adherent to SDF-1 coated plastic dishes and SDF-1 expressing ischemic tissues(42). A diagram depicting several of these cell populations interacting with their respective tissue types is shown in **Figure 1.1**. VEGF is thought to be the principle mediator involved in retinal angiogenesis(43) and EPC subpopulations with VEGF receptors have been shown to have high proliferative capacities(40, 41). However, how do VEGFR expressing

subpopulations compare to others in adherence to angiogenic regions and proliferation? How do VEGFR2 expressing subpopulations differ in their effect on NV from VEGFR3 subpopulations? Are the hematopoietic lineage progenitors (CD34+)(2), which were first discovered to be involved in NV more involved in the EPC tissue targeting observed or are CD14+ cells, one of the most recent subpopulations to be shown to take part in vascular disease pathology(39, 40)? In this study, we will identify methods to elucidate the interactions of these progenitors between subtypes. We will also develop methods to distinguish the interactions between specific subtypes, preexisting mature endothelial cells, and the effect of each subtype on vascular disease in the retina.

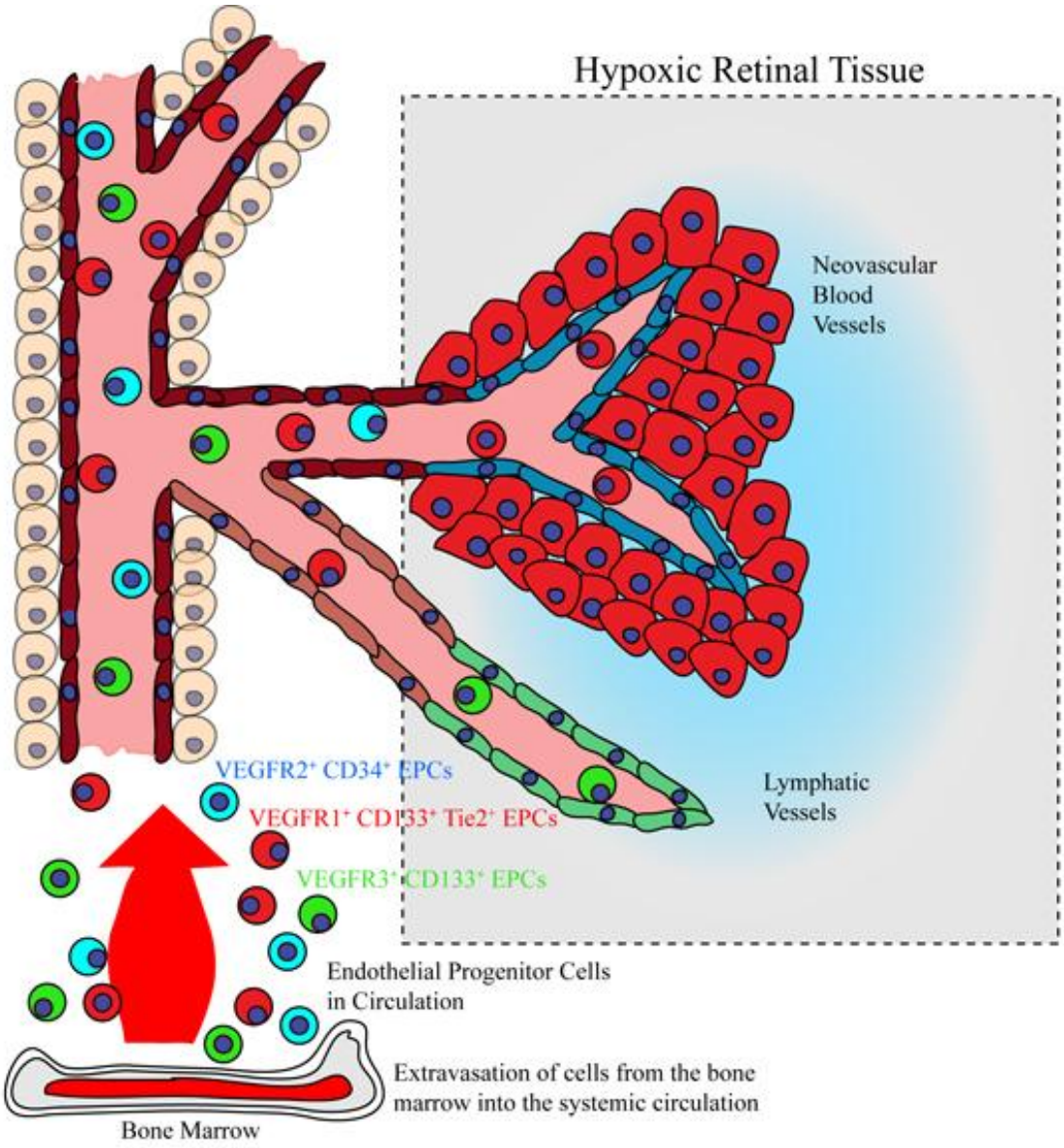

Figure 1.1. Diagram illustrating EPC subsets homing to specific vascular sites based on cell surface antigens. The EPCs originate in the bone marrow, mobilize into the systemic circulation and then extravasate into tissues determined by their individual cell surface antigens. Adapted from(44) - Nature Med. 9, 702 - 712 (2003).

1.1.2 Pre-Existing In Vitro and In Vivo Tools for the Study of Cell Trafficking

Although initial studies have demonstrated the existence of EPC subpopulations, efforts to extensively determine the significance of antigenic variation on EPC function in neovascularization are limited. Many tools are available for use exclusively within an *in vitro* environment. These include blotting techniques, which detect proteins, RNA, or DNA presence within a biological sample, and flow cytometry, a quantitative technique utilized to probe molecular expression, cell cycle phase and viability of cells. Immunohistochemistry can be utilized to visualize a protein of interest in tissue sections. For many of these observations, *in vivo* corroboration has not been obtained, primarily since the assays cannot always reflect the disease scenario in which multiple cell types and biomolecules work in concert in its progression.

No current techniques have been applied to study the complex interaction of multiple molecular and cellular participants in critical disease processes *in vivo*, such as angiogenesis, the focus of this study. Tools for such multiplexed studies have yet to be developed. Given the above limitations with *in vitro* assays, several attempts to probe in vivo activities on the single cell type or single biomolecules level have been reported(2, 36, 42), many within the disease context of inflammation. Radiolabeled monoclonal antibodies to the inflammatory cell adhesion molecules ICAM-1 and VCAM-1 were administered *in vivo*(45, 46). The method, while a useful step in the effort to develop multiplexed *in vivo* studies, was limited by low signal to noise ratios, as well as the need for multiple compensatory calculations and estimations to separate the signal of one antigen from the other. This stemmed from a lack of labeling methods that allowed for easily and accurately differentiating multiple proteins or samples of interest. Furthermore,

the method did not permit true real-time analysis. A technique with the spatial and temporal resolution to capture leukocyte motility through the circulation was established by Nishiwaki and colleagues(47) using the fluorescent DNA-intercalating dye acridine orange (AO) in conjunction with scanning laser ophthalmoscopy (SLO)(48). However, the method relies on the nonspecific staining of all nuclear material by the dye, thus making it impossible to distinguish multiple cell types. A third method has been used to characterize VCAM-1 expression *in vivo* using multimodal fluorescent Cy5.5-conjugated antibody and peptide conjugates by the Weissleder laboratory(49, 50). While this method is a significant achievement in the development of *in vivo* molecular profiling techniques, its utility in multispecies real-time imaging applications is markedly limited, since a specific laser and organic dye is required for each biomarker, raising issues of spectral overlap, photobleaching, and low signal to noise ratios. Furthermore, this application only yielded single time-point data and failed to capture real-time dynamics of molecular expression.

Efforts to image EPC trafficking *in vivo* have only recently been initiated. Jin et al.(51) used a nonspecific cell labeling dye, CMTMR, to label cells ex vivo prior to reinfusion into a tumor-bearing mouse, but no provisions for multispectral imaging in the tumor circulation. Furthermore, this study was concerned with the isolation of only CD34+ EPCs, which constitutes a very large population of EPCs and encompasses a number of cell types. However, the real-time video microscopy and spatial resolution was sufficient for capturing single cells in the circulation. Thus, if the method of Jin et al. was modified to accommodate multispecies imaging, as detailed studies of multiple cell types (e.g. genetically modified, therapeutically inhibited, etc.) would be facilitated.

1.2 Specific Aims

The field of research into endothelial progenitor cells is complex and difficult to interpret. There are a number different investigators working on their individual subpopulation that they isolated in a unique manner with a unique or semi-unique set of cell surface antigens. Each population is, additionally, assayed in a specialized way corresponding to a certain tissue or disease process. All of these variables make it difficult to determine what cell populations might be important in a particular tissue or disease state, and complicated or impossible to compare. We hypothesized that a number of separate subpopulations of endothelial progenitor cells exist, but that only a single subpopulation or small subset of these populations is significantly involved in ocular neovascularization. These studies sought to develop methods for: (1) analyzing definitive EPC populations and (2) comparing them to one another in the context of ocular neovascularization.

1.2.1 Specific Aim 1: Develop quantum dot coded EPC subpopulations and assess their recruitment to neovascular tufts

The development of quantum dot labeled EPCs is an invaluable tool used to both track EPCs in animals, but also to further develop sophisticated methods of analyzing EPCs functions *in vitro*.

1.2.2 Specific Aim 2: Develop high throughput, in vitro methods to analyze the angiogenic capacity of EPCs using quantum dot coded subpopulations

The development of *in vitro* analysis of EPC angiogenic capacity allows EPC subpopulations to be directly compared to one another, and aids in separating the individual aspects of EPC functions: homing to angiogenic sites, incorporating into and forming capillary tubes, and proliferating into neovascular lesions.

1.2.3 Specific Aim 3: Using methods to analyze the angiogenic capacity of EPCs, determine the role of endoglin in oxygen-induced retinopathy

Using the methods developed in the previous two aims to determine the biological role of an EPC associated protein demonstrates the utility of this system of analysis. With this outline as an example, multiple EPC subpopulations can be compared, and their surface antigens and angiogenic signaling can be effectively examined in the context of ocular angiogenesis.

CHAPTER II

MONITORING ENDOTHELIAL PROGENITOR CELL SUBPOPULATIONS IN ANGIOGENESIS USING QUANTUM DOT NANOCRYSTALS

2.1 Introduction

A number of blinding ocular conditions are characterized by angiogenesis, including diabetic retinopathy, macular degeneration, and retinopathy of prematurity. A number of factors including proteins, lipids and cellular interactions contribute to the pathology seen in these disorders(52, 53). In 1997, Asahara and coworkers identified and characterized a circulating population of cells originating from the bone marrow designated endothelial progenitor cells (EPCs) that have been shown to be recruited to neovascular lesions and contribute to the vascular components of a variety of diseases including diabetic retinopathy and age-related macular degeneration(2-4, 54). In these diseases, EPCs roll along and adhere to the endothelial cells of the inner vascular wall of neovascular tissue to augment pathologic angiogenesis(11, 55, 56). Several animal models, which simulate these ocular diseases have been utilized to image EPCs for elucidation of these and other functions(4, 54). However, the specific factors governing EPC homing to tissue and the spectrum of their functions remain incompletely understood. The emerging importance of EPCs in these diseases has motivated the development of methods to image EPCs in tissues with high sensitivity and specificity.

Over the last decade, research has identified a class of bone marrow-derived circulating stem cells; endothelial progenitor cells (EPCs) that are capable of homing to

vascular lesions in the eye and contributing to pathological ocular neovascularization (NV). In preclinical and biological studies, EPCs are frequently identified and tracked using a intracellularly-loaded fluorescent tracer, 1,1'-dioctadecyl-3,3,3',3'-tetramethylindocarbo-cyanine perchlorate-labeled acetylated LDL (DiI-acLDL). However, this method is limited by photobleaching and insufficient quantum efficiency for long-term imaging applications. We have developed a method for conjugation of high quantum efficiency, photostable, and multispectral quantum dot nanocrystals (QD) to acLDL for long-term tracking of EPCs with improved signal to noise ratios. Specifically, we conjugated QD to acLDL (QD-acLDL) and used this conjugated fluorophore to label a specific CD34+ subpopulation of EPCs isolated from rat bone marrow with the same specificity as DiI-acLDL. We then utilized this method to track CD34+ EPCs in a rat model of laser-induced choroidal neovascularization (L-CNV) to evaluate its potential for tracking EPCs in ocular angiogenesis, a critical pathologic feature of several blinding ocular diseases.

A majority of EPC populations cited in the literature originate from the bone marrow and are defined as being CD34 positive ($CD34^{+}$), and incorporate acetylated low-density lipoprotein (acLDL)(44, 55, 57-61). Due to the latter characteristic, dye-labeled acLDL incorporation is often used to label and track these cells using the DiI-acLDL fluorophore conjugate (DiI = 1,1'-dioctadecyl-3,3,3',3'- tetramethylindocarbo-cyanine perchlorate). However, this dye-based strategy is limited by low intensity and photostability, which complicates longitudinal studies of EPCs in disease models. In this chapter, we describe an EPC imaging strategy that incorporates quantum dot nanocrystals (QD) as the fluorophore rather than DiI. QD are superior to organic dyes in

photostability and fluorescence intensity, and thus enable more specific and prolonged visualization of EPCs in tissue. Using QD, EPCs are isolated from bone marrow and labeled *ex vivo*. The cells are then injected and imaged in a disease context using a rat model of laser-induced choroidal neovascularization (LCNV). This animal model is used to model pathologic angiogenesis in neovascular age-related macular degeneration.

2.2 Materials

1. Six, four- to six-week-old Brown Norway rats (around 100 grams each)
2. Isoflurane (Terrell)
3. Hank's Buffered Salt Solution (HBSS): (1X solution): 5 mM KCl, 0.44 mM KH_2PO_4, 137 mM NaCl, 0.34 mM Na_2HPO_4, 3.3 mM $NaHCO_3$, 5.5 mM D-Glucose, pH 7.1-7.4 [easily contaminated by bacteria if not kept in a sterile location]
4. Accutase™ (A6964, Sigma)
5. Swinging-bucket centrifuge
6. Sterile 40 nm nylon mesh (Sefar America Inc., Fisher Scientific)
7. EasySep® cell isolation system (18558, StemCell Technologies), including: EasySep® FITC Selection Cocktail (18152), magnetic nanoparticles (18150), and EasySep® magnet (18000)
8. Hemacytometer (BD Biosciences, Bedford, MA)
9. Five milliliter Falcon tube: (isolation tube): (352058, Becton Dickinson)

10. Phosphate-buffered Saline (PBS): (1X solution): 3.2 mM Na_2HPO_4, 0.5 mM KH_2PO_4, 1.3 mM KCl, 135 mM NaCl, pH 7.4
11. Isolation buffer: (1X solution): PBS, 2% fetal bovine serum (FBS), 1.0 mM EDTA [make fresh, important to keep this Ca^{++} and Mg^{++} free]
12. FcR blocking antibody (112-001-008, Jackson ImmunoResearch Laboratories Inc.)
13. Rabbit anti-CD34 FITC conjugated antibody (252268, Abbiotec)
14. EGM-2 medium (CC-3162, Clonetics): contains FBS, hydrocortisone, epidermal growth factor, and antibiotic [keeps for a few weeks at 4˚C]
15. 100X antibiotic/antimycotic solution (A5955, Sigma) [keep at -20 until needed]
16. Human Low-density lipoprotein (Biomedical Technologies Inc.)
17. Sulfo-NHS-biotin (Pierce protein research products, Thermo Fischer Scientific)
18. Borate buffered saline (BBS): (1X solution): 10 mM sodium borate, 150 mM NaCl, pH 8.2
19. G-25 Sephadex columns (GE Lifesciences)
20. Sulfo-NHS-acetate (Pierce protein research products, Thermo Fischer Scientific)
21. Sephacryl 400HR (GE Lifesciences)
22. QD655: Quantum dots emitting 655 nm light (Invitrogen)
23. DiI-acLDL (BT-902, Biomedical Technologies Inc.)
24. 4',6-diamidino-2-phenylindole (DAPI) (Sigma, D9532)
25. Chamber Slides™ (177429, Lab-Tek)
26. Light microscope similar to the AX70 (Olympus)
27. 100 Watt mercury lamp and filter cubes (Olympus)

28. Provis system digital camera DP71 (Olympus), computer (Dell) and DP controller software (Olympus)
29. Eight, 100 gram, Brown Norway rats
30. General anesthetic: 80/12 mg/kg ketamine/xylazine (K113, Sigma)
31. Local anesthetic: 0.5% proparacaine drops
32. Dilating eye drops: 2.5% phenylephrine and 1% atropine
33. 2.5% Gonak solution (Akorn) used with glass coverslips to help visualize the fundus of the retina and keep the eye moist during the procedure.
34. Slit lamp (Carl Zeiss Meditec) with a laser delivery system
35. Argon Green Laser (Coherent, Polo Alto; CA, USA)
36. 50µl Hamilton syringe (Hamilton Co.) and a 30-gauge 19˚ beveled needle (Hamilton Co.)
37. Isopropyl alcohol swabs
38. Dissection equipment: scalpel, jewelers forceps, Castroviejo scissors (Miltex, Inc., York, PA)
39. 37% formaldehyde solution (Sigma)
40. Bovine serum albumin (BSA) (Sigma)
41. FITC conjugated isolectin B_4 (L2895, Sigma)
42. Triton X-100 (Sigma)
43. Clear glass slides and Gel/Mount slide coverslipping medium with anti-fading reagents (#M01, Biomedia)

2.3 Methods

The methods below outline: (1) immunomagnetic isolation of EPCs from bone marrow, (2) intracellular loading of EPCs with QD, (3) monitoring of QD loading efficiency, and (4) imaging of QD-loaded EPCs in a rat model of LCNV. While these methods were specifically used for imaging EPCs in LCNV, the techniques herein could be applied toward the labeling and imaging of EPCs in other vascular diseases including cancer and diabetes, by selection of a relevant animal model.

2.3.1 Immunomagnetic isolation of endothelial progenitor cells from bone marrow

Cells were isolated from six, four- to six-week-old Brown Norway rats. The animals were sedated with isoflurane (Terrell) vapors, and then euthanized by decapitation. Their tibias and femurs were removed, and the bone marrow was isolated from these bones in Hank's Buffered Salt Solution (HBSS) [5 mM KCl, 0.44 mM KH_2PO_4, 137 mM NaCl, 0.34 mM Na_2HPO_4, 3.3 mM $NaHCO_3$, 5.5 mM D-Glucose, pH 7.1-7.4]. The marrow tissue was then triturated and digested in Accutase^{TM} (A6964, Sigma) for five minutes. Following the digestion, the remaining cells were washed three times in HBSS followed by centrifugation to remove extracellular matrix debris, and filtered through a double layer of sterile 40 nm nylon mesh (Sefar America Inc., Fisher Scientific, Hanover Park, IL). Following this step, the remainder of this procedure was carried out under a laminar flow hood using aseptic technique.

The cell mixture was then purified in order to enrich for $CD34^+$ cells using an immunomagnetic purification method similar to that used by Su X. et al. for the isolation of $CD31^+$ endothelial cells(62). We used the EasySep® cell isolation system (18558,

StemCell Technologies). Initially, cells were counted using a hemacytometer to ensure that no more than 2 X 10^8 cells per milliliter were in an isolation tube (352058, Becton Dickinson). These cells were then centrifuged and resuspended in 1.0 mL of an isolation buffer [3.2 mM Na_2HPO_4, 0.5 mM KH_2PO_4, 1.3 mM KCl, 135 mM NaCl, pH 7.4, 2% fetal bovine serum (FBS), 1.0 mM EDTA]. An FcR blocking antibody (112-001-008, Jackson ImmunoResearch Laboratories Inc.) was then added at 50 µl/ml. Next, 3.0µg/ml of a rabbit anti-CD34 FITC conjugated antibody (252268, Abbiotec) was added and the mixture was allowed to incubate for 15 minutes at room temperature. Following this incubation, the EasySep® FITC Selection Cocktail (18152, StemCell Technologies) was added at 100 µl/ml cells and allowed to incubate for another 15 minutes at room temperature. Finally, the magnetic nanoparticles (18150, StemCell Technologies) were mixed in at 50 µl/ml cells and allowed to incubate for 10 minutes. The cell suspension was then brought to a total volume of 2.5 mL with isolation buffer and gently mixed in the tube to ensure a homogenous suspension. The cells were then placed into the EasySep® magnet (18000, StemCell Technologies) and allowed to sit for five minutes, before the tube and magnet were carefully picked up and inverted into a waste container. This resuspension/magnetic pelleting/inversion process was repeated twice. After the third inversion, the cells were resuspended in EGM-2 media (CC-3162, Clonetics) containing 10% fetal bovine serum, 1 µg/ml hydrocortisone, 10 ng/ml epidermal growth factor and 5 ml/500 ml of 100X antibiotic/antimycotic solution (A5955, Sigma) and plated onto 60 mm plastic dishes to be expanded for one full passage before further use.

Prior to *in vitro* imaging of QD in EPCs, EPCs were seeded at 5000 cells per well on 4-well Chamber Slides™ (177429, Lab-Tek) and incubated for 2-4 days at 37°C until

60% confluence was achieved. For injection of QD-labeled EPCs in the LCNV model (3.4), EPCs were maintained in 60 mm cell culture dishes until detachment in Accutase and resuspension of EPCs to the desired density.

2.3.2 Conjugation of acLDL to QD

In order to produce fluorescently labeled acLDL, 100 µl of human low density lipoprotein (LDL) (5 mg/mL) was taken and added to 10 µl of a 20 mM solution of sulfo-NHS-biotin in borate buffered saline (pH = 8.2). The mixture was allowed to react for 30 minutes at room temperature. Following this reaction, the sample was purified for removal of excess reagent using G-25 Sephadex gravity column filtration with borate buffered saline as the elution buffer. 1.0 mg of sulfo-NHS acetate was added to the product diluted in 1.0 mL total borate buffered saline and the solution was incubated for one hour. The conjugated protein was then purified using a G-25 column with borate buffered saline, as the elution buffer, to remove excess acetylation reagent, yielding a pure solution of biotinylated acLDL. The conjugated protein was then incubated with 5.0 ul of streptavidin-functionalized QD655 (QD emitting 655 nm light) for 30 minutes at 37˚C. This solution was characterized for conjugation efficiency by size exclusion chromatography on Sephacryl HR400 resin and was found to exhibit three acLDL molecules per QD.

2.3.3 Intracellular loading of EPCs with acLDL-QD

In order to label the EPCs with QD-acLDL and DiI-acLDL (BT-902, Biomedical Technologies Inc.), the cells were incubated with 2.0 µg/ml of each acLDL in growth

media for six hours at 37˚C. Fifteen minutes prior to ending the incubation, DAPI (Sigma, D9532), a nuclear counterstain, was added to the cells in an amount to bring the final concentration to 600 nM. Following the six hour incubation, the media was removed, and the cells were washed thrice in pre-warmed (37˚C) PBS. After the wash, the cells were coverslipped to be visualized by fluorescence microscopy using Gel/Mount.

2.3.4 Monitoring of QD loading efficiency

The EPCs were imaged on Chamber Slides™ (177429, Lab-Tek) labeled directly with QD-acLDL and DiI-acLDL using fluorescence microscopy. These cells can be imaged on an upright or inverted fluorescent confocal or widefield microscope that has the appropriate filter set to distinguish the 568 nm fluorescence of the DiI, the 655 nm fluorescence of the QD, and the 454 nm fluorescence of the DAPI without significant spectral overlap. In this chapter, we used an AX70 microscope, (Olympus, Japan) containing filter cubes with 460/40 nm, 570/30 nm, and 655/20 nm emission filters. Images of the cells were captured using a digital camera attached to the Provis system (DP71, Olympus, Japan) coupled to a computer with image capture software (DP Controller, Olympus, Japan). However, this analysis can be completed with a comparable imaging system.

Imaging of the acLDL labeled EPCs

1. Position the coverglassed slides containing the labeled EPCs on the stage of the fluorescent microscope.

2. Using dim, transmitted light, bring the cells on the slide into focus.
3. Using 518 nm of incident light, excite the cells labeled by DiI-acLDL and collect an image of resulting fluorescence emission of cells with the 570/30 nm band-pass filter. Capture this image first, since DiI is the most sensitive fluorophore to photobleaching.
4. Without moving the slide, capture the next image of the DAPI-stained cell nuclei using a 360 nm incident light with the 460/40 nm band-pass filter.
5. Finally, capture the QD-acLDL labeled cells using the 360 nm incident light (or if not available, an excitation wavelength of < 480 nm) with the 655/20 nm band-pass filter. Note that the smaller wavelength incident light will produce a stronger excitation of the QDs. In addition, for optimal results, illuminate the QD-loaded cells for at least 2 minutes using these incident light settings to induce maximal QD fluorescence emission.

The images shown in **Figure 2.1** demonstrate that EPCs can be labeled with QD-acLDL with equal efficiency to DiI-acLDL labeling, however, the QD-acLDL labeling results in bright and photostable EPCs that can be tracked in culture for longer periods of time.

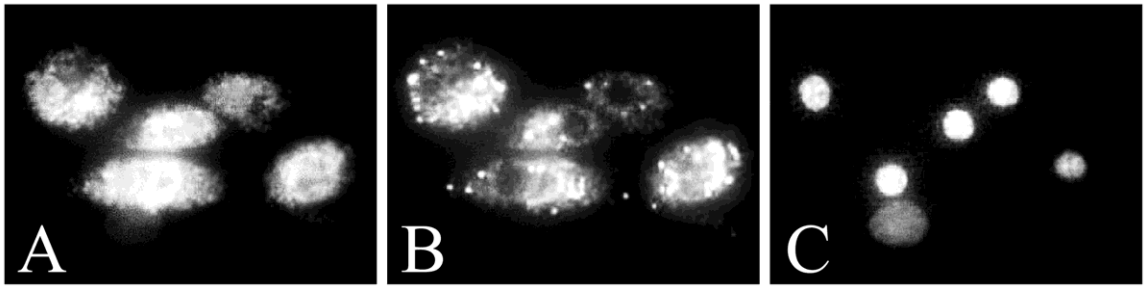

Figure 2.1. Imaging of CD34+ EPCs with fluorophore-acLDL conjugates. Panel A shows the internalized DiI-acLDL conjugate throughout the cytoplasm. Panel B shows the same field of cells as A, but with internalized, cytoplasmically-distributed QD655-acLDL. Panel C exhibits the DAPI-labeled nuclei of the cells in the same field of view. These panels demonstrate that DiI-acLDL and QD655-acLDL are targeted to and taken up by the same EPC populations. Subsequent analysis by fluorescence microscopy indicated that cells labeled with DiI became dim within 6 minutes of continuous illumination, but that QD-labeled cells lost only 3-5% of initial fluorescence for every 10 minutes of continuous illumination during a 60 minute analysis.

2.3.5 Analysis of QD-loaded EPCs in a rat model of ocular angiogenesis

Generation of LCNV model

In this study, CNV, a subretinal form of angiogenesis in which blood vessels abnormally grow beneath the retinal photoreceptors, is produced in eight, Brown Norway rats, each weighing 100 grams. This CNV was produced by administering krypton laser radiation between the major retinal vessels of the fundus as we and others have previously published(63-66). In this protocol, the animals were anesthetized with an IP injection of 80/12 mg/kg ketamine/xylazine (K113, Sigma), Proparacaine (0.5%) drops for corneal anesthesia and pupils dilated with phenylephrine (2.5%) and atropine sulfate (1%) drops. A handheld coverslip and (2.5%) Gonak solution (Akorn) was used as a contact lens for the maintenance of corneal clarity during photocoagulation. Animals were positioned before a slit lamp (Carl Zeiss Meditec, Inc; Jena, Germany) laser delivery system. An argon green laser (Coherent, Polo Alto; CA, USA) was used for photocoagulation (532 nm wavelength; 360 mW power; 0.07-s duration; and 50 μm spot size). The laser beam was focused on Bruch's membrane with the intention of rupturing it, as evidenced by subretinal bubble formation without intraretinal or choroidal hemorrhage at the lesion site. Each lesion was made between the major vessels of the retina for a total of six lesions per eye concentrically applied approximately two optic discs from the center. The choroidal capillaries proliferated through the break in Bruch's membrane into the disrupted outer layers of the retina. Laser rupture sites, which had subretinal bleeding at the time of lesion creation, were excluded from analysis and represented less than 10% of total rupture sites in each treatment group. With minor

operator training, this procedure can be completed efficiently and reliably such that up to 20 rats per day can be induced for LCNV as studies may require.

Injection of QD-acLDL labeled EPCs into LCNV model

Seven days after laser treatment, the animals received a tail vein injection of 1×10^6 EPCs labeled with QD655-acLDL in a volume of 40 µl (PBS vehicle) using a 50 µl syringe (Hamilton Co.; Reno, NV) and a 30-gauge needle with a 19˚ bevel. These cells had been labeled as previously described in subheading 'Conjugation of acLDL to QD'. For the injection, the rats were anesthetized by isoflurane (Terrell) inhalation, and the tail was wiped with an isopropyl alcohol swab. The injection was made in either of the lateral veils along the base of the animal's tail. As the needle was advanced for the injection, the plunger was pulled back slightly in order to see a flash of blood in the syringe, ensuring the needle was properly in the vein. Fourteen days following laser application, animals were sacrificed by cervical dislocation to measure the amount of CNV at the Bruch's membrane rupture sites.

Characterization of EPCs in retinal neovascular tissue

After the animals were sacrificed, eyes were immediately enucleated (removed from the orbit) and placed in fixative, and the cornea, iris, and lens were removed. The retina was peeled away from the fundus gently using a hemostat to reveal the choroid-sclera-RPE section. This section was flattened on a slide, mounted in Gel/Mount, and coverslipped. Endothelial cells and extracellular matrix components were stained to reveal the areas of neovascularization. Areas of abnormal vascular growth were

measured via computer-assisted image analysis using high-resolution digital images of the stained sclera-choroid-RPE flat-mounts. The details of this process are described below:

Dissection and analysis of neovascularization:

1. Enucleate the eyes and place them into labeled containers with 10% neutral buffered fixative solution [90% v/v PBS and 10% v/v 37% formaldehyde solution] for 2 hours at 4°C.
2. Dissect out the choroid, sclera and RPE. Make sure to remove the entire retina from the RPE surface and remove the cornea, lens and iris as well.
3. Place each dissected sample into a labeled 24-well plate well for the staining.
4. In the well, wash the samples with PBS for 5 minutes.
5. Using 5% BSA in PBS, block the samples on a shaker for 1 hour at room temperature.
6. Next wash each sample with PBS 3 times for 5 minutes each.
7. Completely cover and submerge each dissected sample with a solution of PBS with 4.0 μg/ml FITC conjugated isolectin B_4 (L2895, Sigma) and 0.1% Triton X-100, and incubate for 24 hours at 4°C on shaker.
8. Remove the staining solution and wash with PBS 3 times for 5 minutes each.
9. Mount the choroidal flat-mounts on the slides attempting to make them as flat as possible on the glass. Several cuts from the periphery of the sclera toward the optic nerve should help with this. Use Gel/Mount (#M01, Biomedia) with anti-fading reagents to prevent the FITC from bleaching.

Fluorescence imaging of LCNV lesions:

1. Position the coverglassed slides containing the choroid-sclera-RPE flat-mount on the stage of the fluorescent microscope.
2. Using dim, transmitted light, bring a one lesion of the flat-mount on the slide into focus. This is best accomplished using a 20X or 40X objective.
3. Using 488 nm of incident light, excite the cells labeled by FITC-Isolectin B_4 and obscure the fluorescence with the 525/20 nm band-pass filter. Capture this image first, since FITC is the most sensitive fluorophore to photobleaching. Isolectin B_4 labels all endothelial cells within blood vessels, *including* EPCs.
4. Without moving the slide, capture an image of the QD-acLDL labeled cells using the 360 nm or 488 nm incident light with the 655/20 nm band-pass filter. Note, again, that the smaller wavelength incident light will produce a stronger excitation of the QDs. These settings will reveal the presence of EPCs in the specimen which can be distinguished from other Isolectin B_4 positive, mature endothelial cells.

The results of our experiment shown in **Figure 2.2** demonstrate that the QD-acLDL labeled EPCs make up a large portion (62% of the total lesion size) of the lesions, and that they frequently seem to coalesce in the middle of the lesion. This would suggest that they are homing to the developing lesions through the blood stream and adding to the growth of the lesions through their own proliferation and, possibly, through the release of growth factors encouraging mature endothelial cells to proliferate. This method of cell labeling and tracking could be used to efficiently track and study the effects of these EPCs or multiple subtypes of EPCs influencing these neovascular lesions.

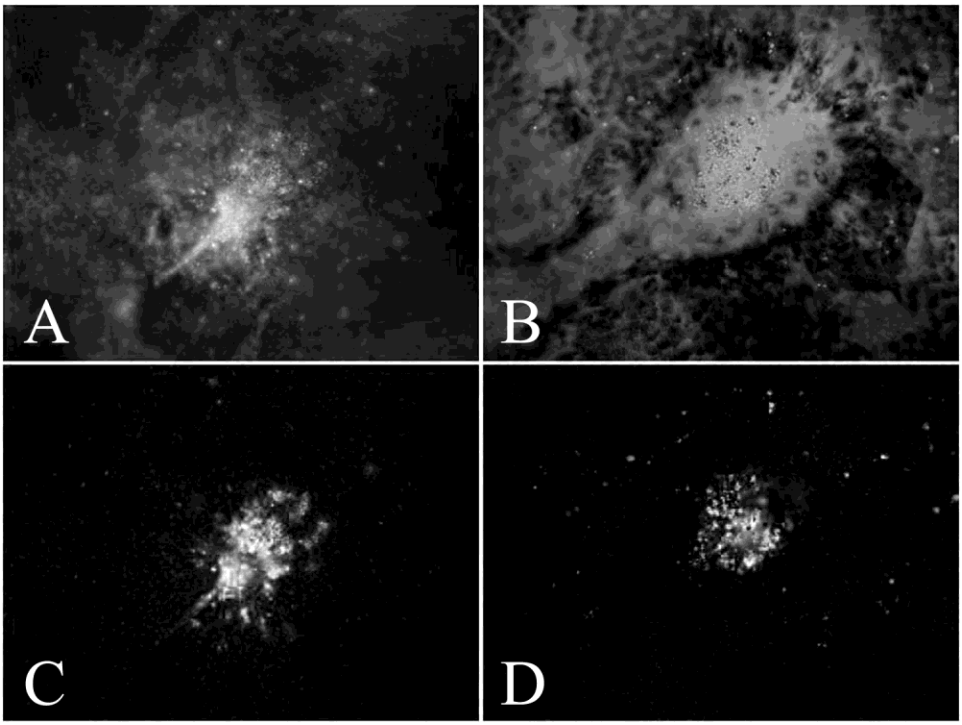

Figure 2.2. Imaging of CD34+ EPCs labeled with QD655-acLDL in the lesions of LCNV rats undergoing angiogenesis. Panels A and B show two different CNV lesions labeled with Isolectin B4-FITC conjugate (all endothelial cells). Panels C and D show the QD655-acLDL labeled CD34+ EPCs from A and B, respectively, that were injected into the tail vein of LCNV model rats seven days prior to ex vivo analysis. QD-labeled EPCs homed to the neovascular lesions in the choroid in large masses or alternatively, arrived in small numbers and proliferated to comprise up to 62% of neovascular lesion area. This is a clear demonstration that QD-acLDL labeled EPCs can be reinjected into animals, and tracked for longer periods of time relative to conventional methods, for detailed analysis of EPC function in ocular angiogenesis.

CHAPTER III

IN VITRO PARALLEL PLATE FLOW CHAMBER ASSESSMENT OF ENDOTHELIAL PROGENITOR CELL HOMING

3.1 Introduction

Bone marrow-derived endothelial progenitor cells (EPCs) have been shown to play a significant role in the neovascularization of vascular diseases. In many of these diseases, including diabetic retinopathy and age-related macular degeneration, elevated stromal derived factor-1 (SDF-1) is observed in the neovascular tissue, and this is believed to play an important role in EPC homing function. Little is known about other factors that might contribute. This study sought to develop an *in vitro* system of evaluating EPC homing capacity in conditions relevant to ocular disease states. Bone marrow was isolated from 4-6 week old Brown Norway rats and a population of EPCs was identified using the markers CD34, CD133 and CXCR4 in fluorescence-activated cell sorting experiments. EPCs were labeled with quantum dot conjugated acetylated LDL. Labeled EPCs and mature endothelial cells (ECs) were placed into a parallel plate flow chamber (PPFC) [Glycotech Corporation] in separate experiments. In the first, cells were allowed to flow at 15 dynes/cm^2 shear stress over exposed extracellular matrix (ECM) and in the second, over conditioned endothelial monolayer (EML). The ECM conditions tested were hyaluronic acid (HA) or chondroitin sulfate (CS) with and without SDF-1. EMLs were conditioned by a 24-hour pretreatment in either hypoxia (0% oxygen) or normoxia (20.9% oxygen). In the ECM studies, EPCs were found to be 3-fold

($p<0.001$) more adherent to HA than CS, and this adherence was increased 67% ($p<0.01$) with the addition of SDF-1 to HA. EPC adherence to HA + SDF-1 was reduced by 56% ($p<0.01$) by incubating the EPCs with anti-CXCR4 for 10 minutes prior to their addition to the PPFC. Compared to the ECs, EPCs were 59% ($p<0.01$) more adherent to HA alone, and 2.6-fold ($p<0.001$) more adherent to HA + SDF-1. In the EML studies, EPC adherence was increased by 33% ($p<0.05$) when EML were treated with hypoxia relative to normoxia. The *in vitro* system has demonstrated adherence of EPCs and ECs to surfaces chosen to model damaged blood vessel walls found in ocular neovascular diseases. This high throughput system can now be used to further characterize homing in more specific EPC subpopulations and to define the roles of EPCs in pathological disorders of the eye.

A number of blinding ocular conditions are characterized by angiogenesis, including diabetic retinopathy, macular degeneration, retinopathy of prematurity, and vein occlusion retinopathy to name a few. The ocular angiogenesis and neovascularization of diabetic retinopathy (DR) and age-related macular degeneration (AMD) cause the greatest blindness in working-aged Americans and individuals 65 years or older in developed countries (67, 68). A number of factors including proteins, lipids and cellular interactions contribute to the pathology seen in these disorders. In 1997, Asahara and coworkers discovered a circulating population of cells originating from the bone marrow termed endothelial progenitor cells (EPCs) that have been shown to be recruited to neovascular lesions and to contribute to the vascular components of a variety of diseases including DR and AMD (2-4, 54).

EPCs have been characterized by a number of cell surface antigens and distinguishing activities. A strong component of the "homing" ability of these cells has been linked to a chemokine receptor (CXCR4) on the surface of EPCs. The ligand for CXCR4, SDF-1 (stromal-derived factor-1), is increased in neovascular lesions and thought to attract EPCs to developing neovascular areas (57). These cells have also been isolated by the surface antigens CD133 and CD34, which are glycoproteins found specifically on stem and progenitor cells (57-59). EPCs have also been found to roll along and adhere to the endothelial cells of the inner vascular wall of neovascular tissue (55, 56). Relatively little is understood about the interactions of these characteristic surface antigens and there potential rolls in the recruitment of EPCs to specific vascular lesions and tissues. This study sought to develop an *in vitro* system of evaluating EPC homing capacity in conditions relevant to ocular disease states, but which may also have utility in modeling other tissue types and disease states.

3.2 Experimental Procedures

3.2.1 Cell Isolation and Preparation

Cells were isolated from six, four- to six-week-old Brown Norway rats. The animals were sedated with methoxyflurane vapors, and then euthanized by decapitation. Their tibias and femurs were removed, and the bone marrow was isolated from these bones. The marrow tissue was then triturated and then the remaining cells were washed once with erythrocyte-lysing solution (154mM NH_4Cl, $KHCO_3$ 10mM, EDTA 82μM) by centrifugation. The cells were then washed three times by centrifugation with phosphate

buffered saline to remove extracellular matrix debris. The cells were then further isolated according to cell surface antigens by FACS as described in section 3.2.2. This cell mixture was then plated onto plastic dishes and grown in EGM-2 media (Clonetics) containing 10% fetal bovine serum, 1ug/ml hydrocortisone, 10ng/ml epidermal growth factor and 5ml/500ml of 100X antibiotic/antimycotic solution (Sigma) for one full passage before use *in vitro* or labeled directly and used in the FACS assay to ensure the cells maintained surface expression of CD34 and CD133.

In order to label these cells with QD-acLDL or Qtracker (Invitrogen), the cells were incubated with 2ug/ml of QD-acLDL or 1ug/ml of Qtracker (as directed) for four to six hours, then removed from the dish using Accutase™ (Sigma) followed by centrifugation and resuspension to the desired concentration in PBS before use in the *in vitro* assays.

3.2.2 Fluorescence Activated Cell Sorting (FACS)

For all of the surface antigens investigated, isolated bone marrow was taken from the rats as described above and incubated in a 200 μg/ml of the appropriate blocking IgG for 10 minutes in an ice bath. A 1:500 dilution of the unconjugated primary antibody was then added to the solution. The antibodies used were anti-CXCR4 (Santa Cruz), anti-CD133 (Abcam and Santa Cruz) and anti-CD34 (Abcam). Appropriate non-labeled controls were set aside at this time as well. This suspension was incubated on ice for another 15 minutes. The cells were centrifuged at 1500×g for 3 minutes at 4°C and then resuspended in a 1:2000 dilution of the secondary antibody (Jackson Labs) conjugated to quantum dots (em. 655 and 525) using an Invitrogen antibody conjugation kit. This

solution was also incubated 15 minutes in an ice bath. The cells were then centrifuged for 3 minutes at 1500×g and 4°C. The cells were sorted on a 3-laser BD LSRII cell sorter (BD Biosciences) at the Vanderbilt Flow Cytometry Core.

3.2.3 In Vitro Parallel Plate Flow Chamber (PPFC) Assay:

PPFC and Extracellular Matrix (ECM)-Coated Adherence assay

Cells grown in culture and labeled with either QD-acLDL or Qtracker were using at 1-2 X 10^6 cells/ml. The cells were placed into a parallel plate flow chamber (PPFC) (Glycotech Corporation). The chamber used has a flow width of 1.00cm and a height of 0.010 in. Throughout these studies, a flow rate consistent with a shear stress of 15 dynes/cm^2 was used. Slides in these experiments were coated with 10μg/ml hyaluronic acid (HA) or chondroitin sulfate (CS), a similar disaccharide polymer. These were diluted in PBS (buffered with 20mM bicarbonate at pH 8.5) in the presence of 2μg/ml bovine serum albumin (BSA) carrier. Coated slides were allowed to sit at 37°C for two hours and then washed three times with PBS and blocked with (20μg/ml) BSA for 2 hours at room temperature. For the slides also coated with SDF-1, 10μg/ml SDF-1 diluted in PBS with 2μg/ml bovine serum albumin (BSA) carrier was allowed to sit for 30 minutes at room temperature before being blocked. The slides were assembled as the lower wall of the PPFC and mounted on the stage of an inverted microscope. Cells that were pre-treated to block the CXCR4 receptor were treated for 30 minutes with a 1:500 dilution of the antibody before being used in the assay. Images were captured of the flowing cells every 300ms for 5 to 15 minutes and cell counts and rolling velocities were determined at

frequent time points using Image Pro-Plus tracking software. A diagram of this PPFC is shown in **Figure 3.1**.

Hypoxia and Scratch Endothelial Monolayer Injury Assays

These studies functioned similarly to those in the adherence assay, with the substitution of the ECM-coated slides with slides having a confluent monolayer of endothelial cells cultured on their surface. These cells were either mature endothelial cells, cultured under normoxic conditions, or hypoxic conditions for 24 hours prior to their use in the PPFC. Monolayers of EPCs were also used. Additionally, monolayers of endothelial cells were cultured to confluence and then scraped down the middle of the culture removing a small line of ECs approximately 15 minutes before being used in the assay. This models a mechanical injury to the cells and exposes the ECM on which the cells were growing. Again, images were captured of the flowing cells every 300ms for 5 to 15 minutes and cell counts and rolling velocities were determined at frequent time points using Image Pro-Plus tracking software.

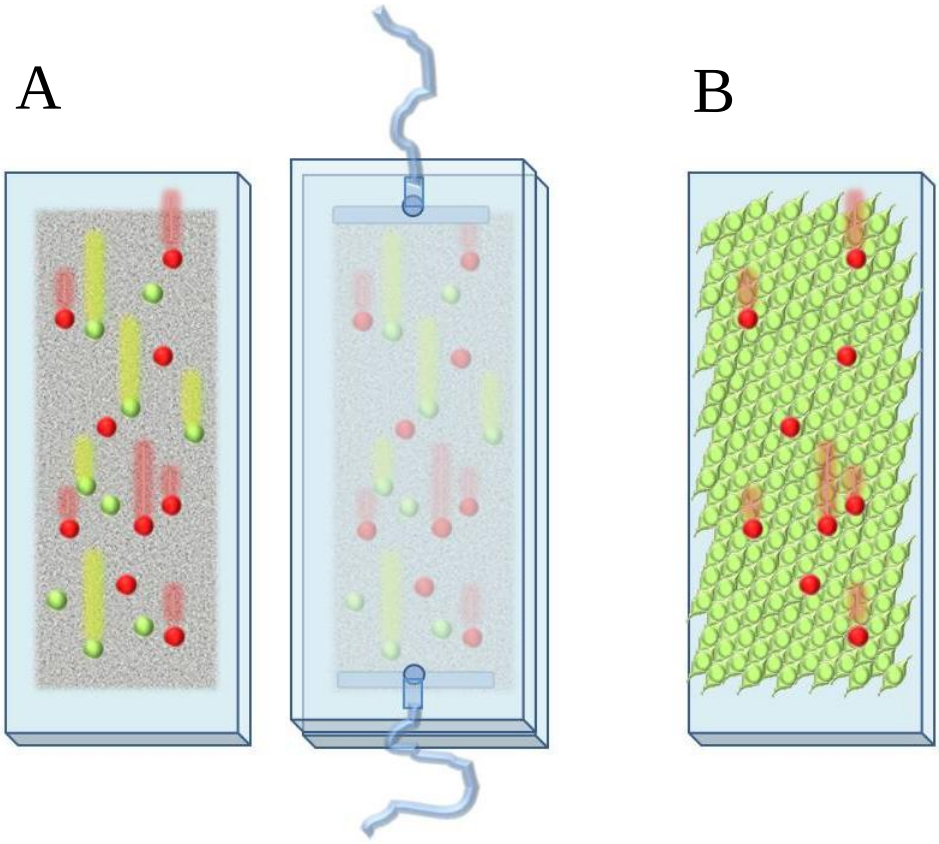

Figure 3.1. Parallel plate flow chamber diagram. (A) This diagram depicts the bottom slide of the PPFC with two separate populations of cells [in red and green] flowing at varied speeds. To the right, this same slide is shown with its top cover slide and attached tubing. (B) This diagram depicts the bottom slide with a cell monolayer in green and a separate cell population in red flowing over the monolayer.

3.3 Results

3.3.1 In Vitro Homing of EPCs to Specific Surfaces in a Parallel Plate Flow Chamber

In these experiments, EPCs were used in a parallel plate flow chamber to determine the homing and adherent ability of the EPCs *in vitro*. The EPCs were propelled in a media solution at 37°C at a speed to ensure a shear stress on the observed plate surface of 15 dynes/cm^2. In **Figure 3.2**, panels A and B show surface plots made from images like those in panels C-F. These surface plots aid in determining the number of cells adhering to a surface at any particular point in time. Here it can be observed that the surface CS (A) has much less adherence than SDF-1 (B). Panels C-F represent still images of the chamber's plate surface after 5 minutes of flow. It can be seen from the panels that SDF-1 (E) has the greatest cell adherence, which was reduced by anti-CXCR4 treatment of the EPCs. Hyaluronic acid alone had a moderate amount of attachment of the EPCs and a similar disaccharide polymer, chondroitin sulfate, had very little adherence by the EPCs.

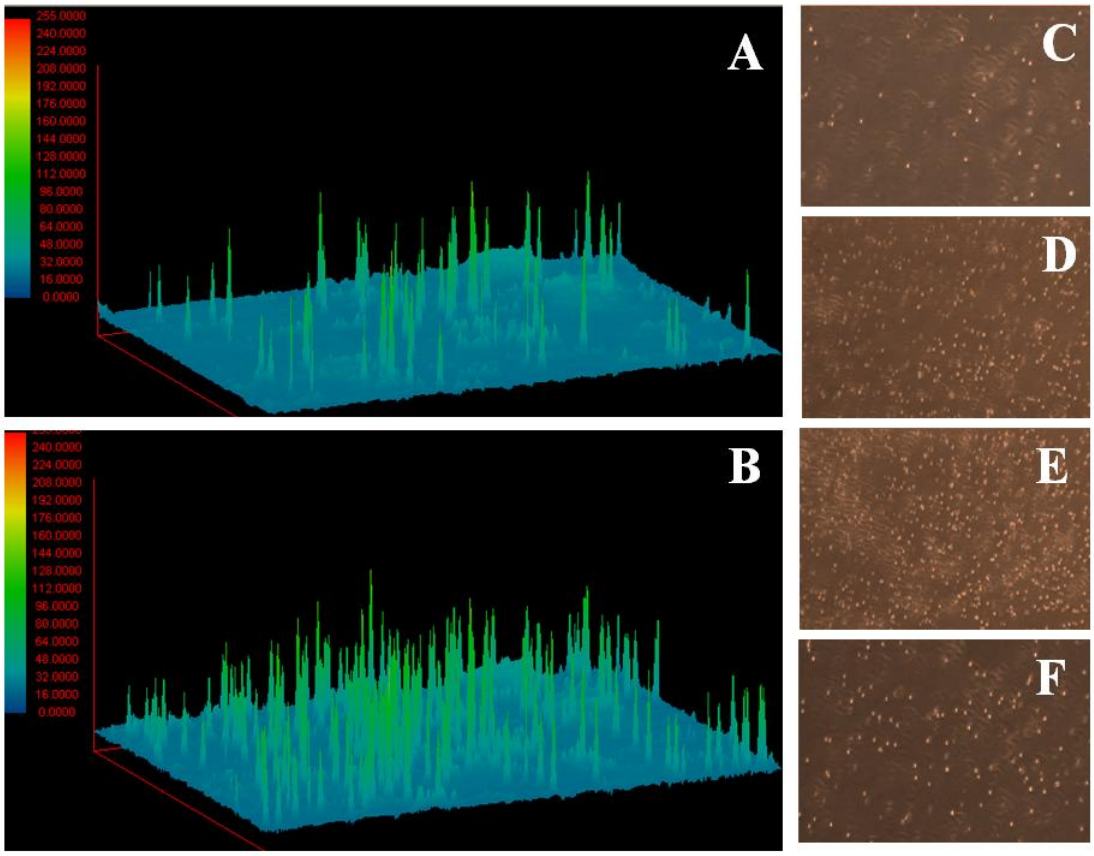

Figure 3.2. Analysis of EPCs adhesion to specifically coated surfaces. (A, B) Surface plots of cell adhesion to chondroitin sulfate and SDF-1, respectively. Photographs of cellular adhesion on (C) chondroitin sulfate (CS), (D) hyaluronic acid (HA), (E) HA+ SDF-1, (E) SDF-1 + anti-CXCR4 pre-treatment of EPCs.

Figures 3.3 and **3.4** go into more depth in this experiment showing twelve second time intervals of the attachment of the cells to each of the coated surfaces with SDF-1 and a control SDF-1 + anti-rat antibody pre-treatment demonstrating the greatest cell adherence followed by HA and a commercially available extracellular matrix, attachment factor (Invitrogen). Finally, SDF-1 + anti-CXCR4 pretreatment and CS demonstrated the least amount of adherence of EPCs under these conditions for the entire time course. **Figure 3.4** specifically shows the relative accumulation of adherent cells over the course of the five minutes observed.

Figures 3.5 and 3.6 depict a set of experiments where the adherence of EPCs is directly compared to that of mature vascular endothelial cells on HA, CS and SDF-1. Under these circumstances, mature ECs did increase their adherence to HA in comparison to CS, but were unaffected by the addition of SDF-1. On the contrary, EPCs attached much more readily to HA in comparison to their own CS adherence in addition to that of ECs to HA at all time points observed. **Figure 3.6** specifically shows the relative accumulation of adherent cells over the course of the five minutes observed. Over the observed flow period, EPC adherence to SDF-1 was the greatest by nearly 2-fold above that to HA and nearly 3-fold better than the adherence of ECs to SDF-1.

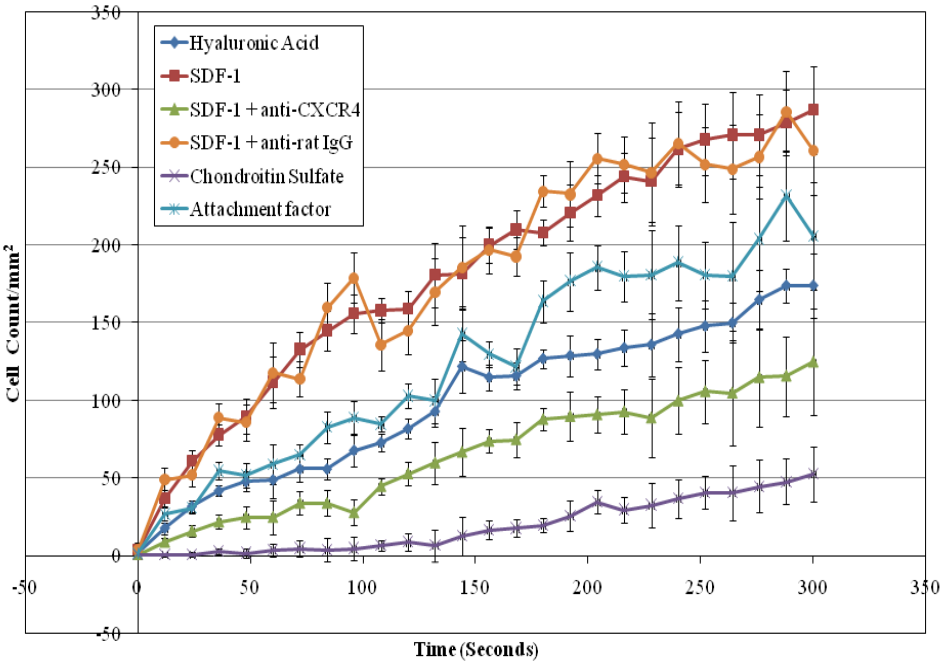

Figure 3.3. The adherence of EPCs over a period of 5 minutes to a variety of proteins coated onto a glass surface. Cell count per mm^2 at 12 second intervals for each coated surface.

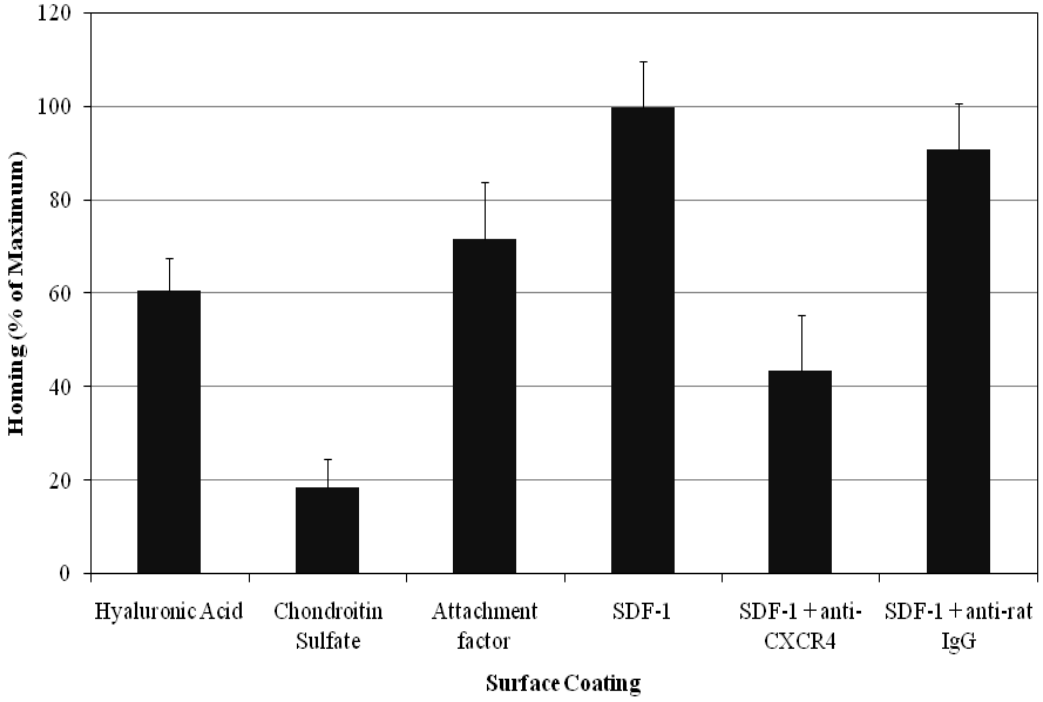

Figure 3.4. Relative adherence of EPCs to varied surface coatings and treatment after five minutes of continuous flow at 15 dynes/cm^2.

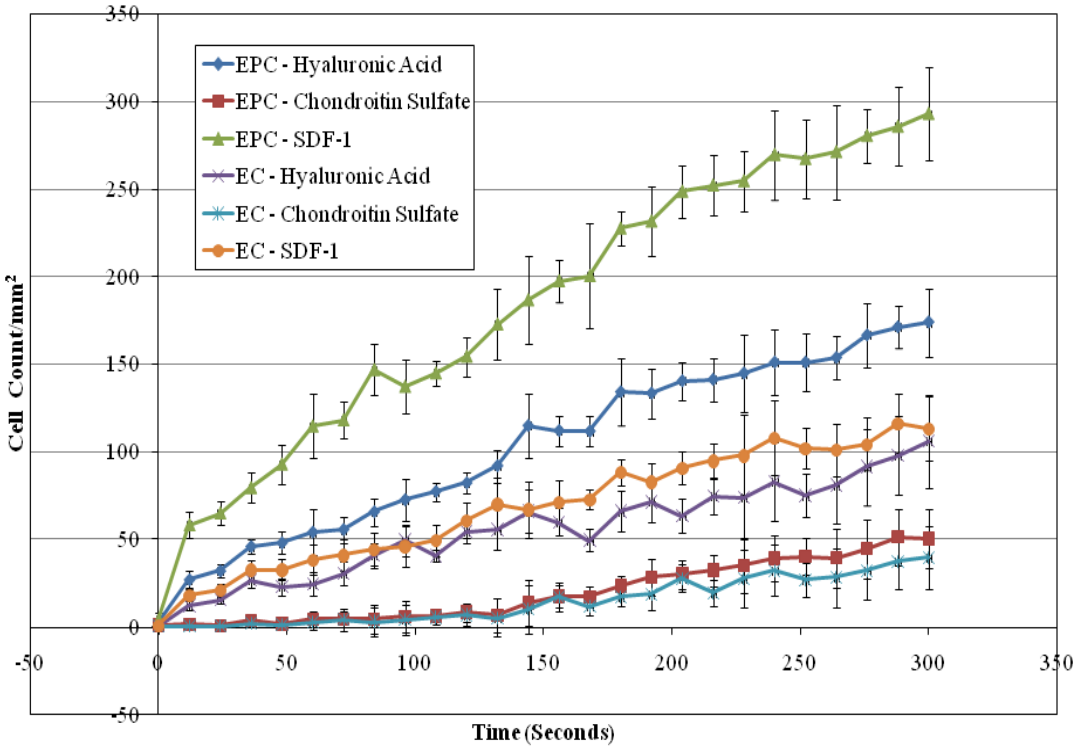

Figure 3.5. The adherence of EPCs to a variety of proteins coated onto a glass surface compared to the adherence of vascular endothelial cells (ECs) over a period of 5 minutes. The graph shows cell counts per mm^2 at 12 second intervals for each coated surface.

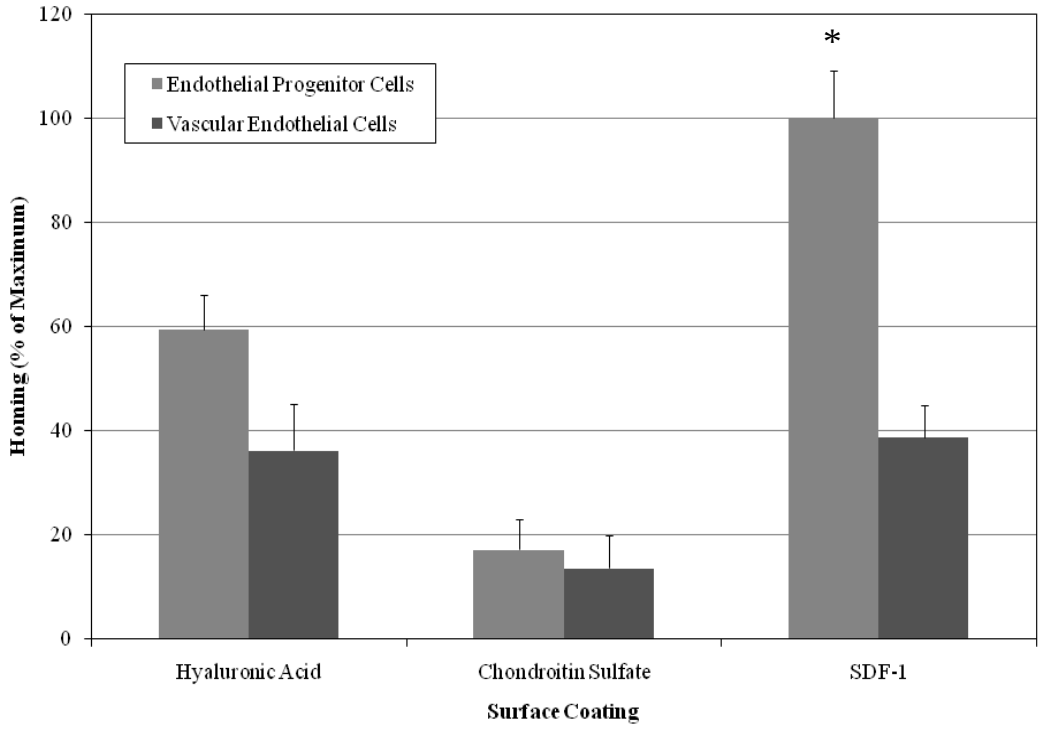

Figure 3.6. The Relative adherence of EPCs and ECs to a variety of proteins coated onto a glass surface over a period of 5 minutes at a continuous flow of 15 dynes/cm^2. * $p<0.02$ using a Student's T-test relative to hyaluronic acid control.

3.3.2 Assessment of EPC Homing and Recruitment on Endothelial Monolayers

In this set of experiments, EPCs are either propelled over a surface of endothelial cells in a monolayer culture or over an extracellular matrix (ECM)-coated surface. As the cells are flowing over the monolayer culture, they are assessed for recruitment to this monolayer by reduced rolling velocities. **Figure 3.7** illustrates the staining of EPCs labeled with Qtracker (Invitrogen, 655nm emission Q-dots) adhering and rolling on an endothelial monolayer also labeled with a different wavelength quantum dot (525nm em. Q-dots). The monolayers tested were either cultured in normoxic conditions, in hypoxia (<1% oxygen for 24 hrs), a monolayer of EPCs or, as a control, a monolayer of mature EC cultured in normoxic conditions with mature endothelial cells flowing over them rather than EPCs. The experiments with ECM-coated surfaces were similar to those done in section 3.3.1 above with the rolling velocities measured rather than the cell adherence.

Figure 3.8 depicts the slightly decreased velocities of endothelial cells on HA in comparison to CS. Just as in section 3.3.1, SDF-1 had no effect on the recruitment of mature ECs. However, EPCs showed a significant decrease in rolling velocity on a HA relative to EPCs on CS and ECs on HA, and a further decrease in velocity with the addition of SDF-1.

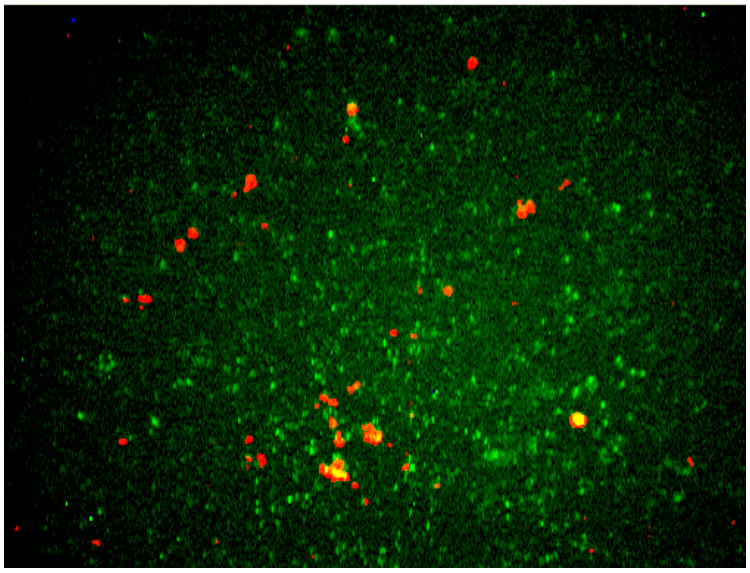

Figure 3.7. EPCs labeled in red (655nm em. Q-dots) adhering and rolling on an endothelial monolayer labeled in green (525nm em. Q-dots). This Q-dot system was used in conjunction with Image Pro-Plus software to more easily track the movement of the EPCs in a single plane of focus.

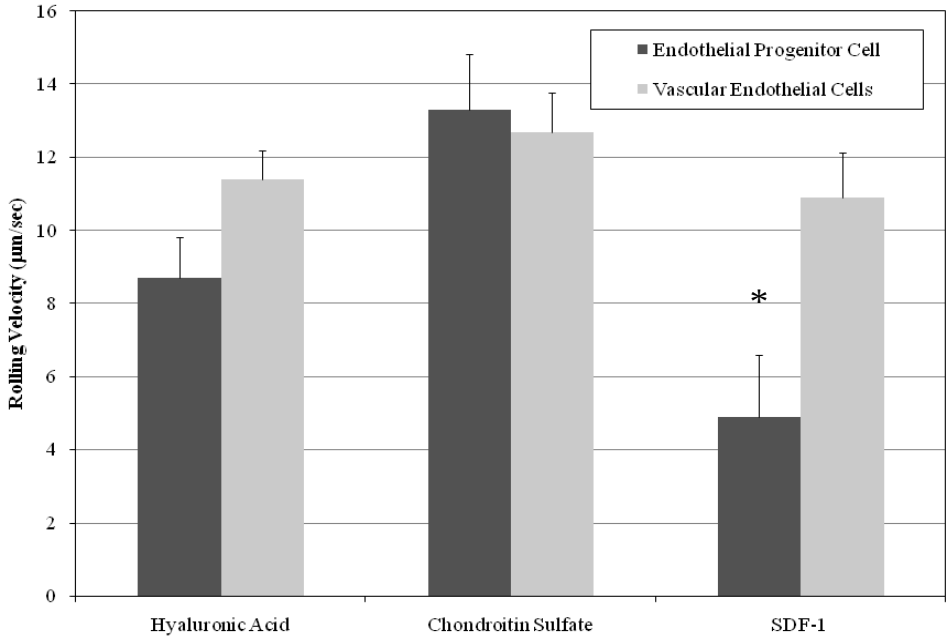

Figure 3.8. Analysis of adherence of EPCs and ECs to endothelial monolayers and specific adherence surfaces. Measurements of the rolling velocities of EPCs and ECs on HA, CS and SDF-1 for comparison to the homing adherence studies in section 3.3.1. * $p<0.05$ using a Student's T-test relative to hyaluronic acid control.

Figure 3.9 demonstrates the increased recruitment (decreased rolling velocity) of EPCs on hypoxia treated endothelial monolayers. This decrease is more than that of EPCs on normoxic EC monolayers, which show slower rolling velocities than either EPCs rolling over EPC monolayers or ECs rolling over EC monolayers.

3.3.3 Assessment of EPC Homing and Recruitment in an Endothelial Injury Model

In an attempt to further study the recruitment of EPCs to injured endothelium, EPCs were propelled over an endothelial monolayer scratch injury model. **Figure 3.10** illustrates the edge of the scratch where unaltered endothelial cells and injured cells can be seen in the same frame. The monolayer is shown in green (Qtracker; Invitrogen, 525nm em. Q-dots) while the EPCs are stained red (Qtracker; Invitrogen, 655nm em. Q-dots). Here it can be seen from panel A to panel B that cells adhere over the course of the 10 minutes that the tissue is observed.

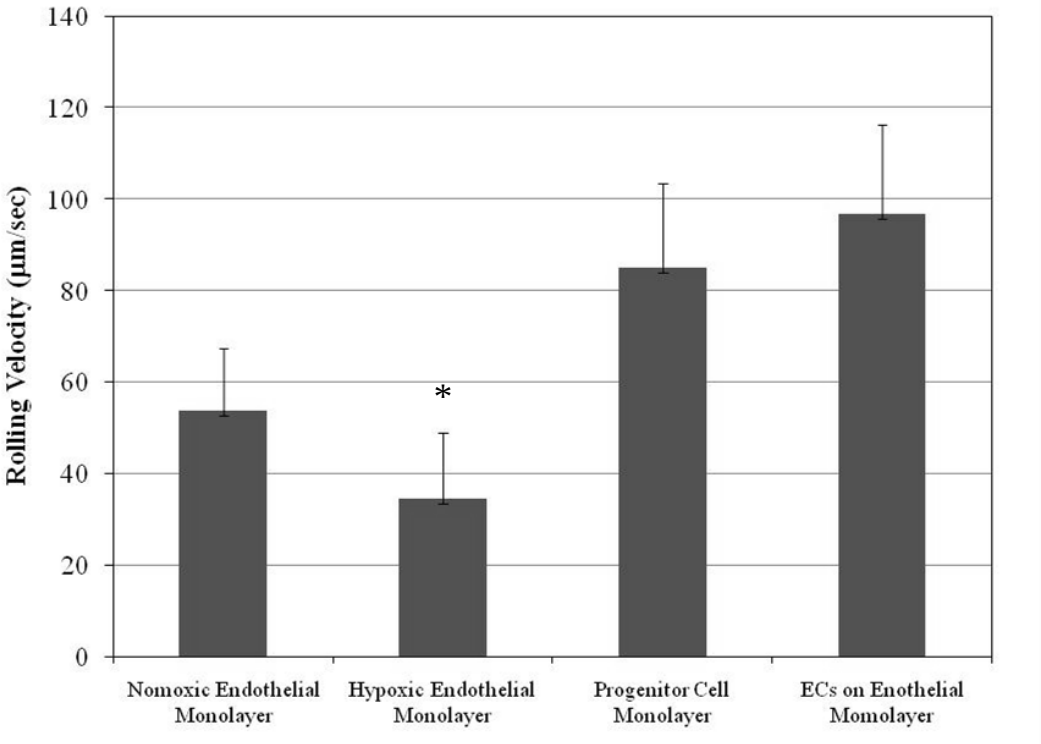

Figure 3.9. Rolling Velocities of EPCs on the following endothelial monolayer types [from left to right]: normoxic ECs, hypoxic ECs, EPC monolayer, and EC rolling velocities on an EC monolayer [control]. * $p<0.05$ using a Student's T-test relative to normoxic endothelial monolayer control.

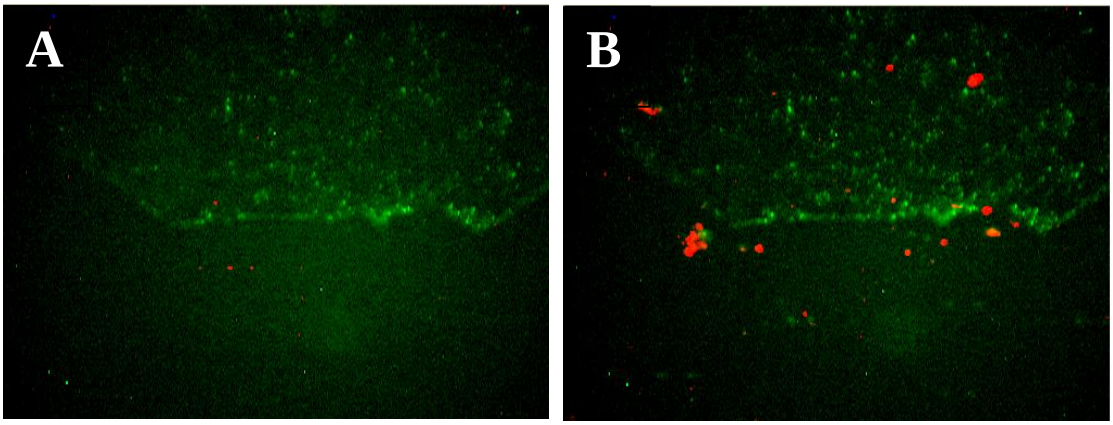

Figure 3.10. Images of an endothelial monolayer injury model with the endothelial cells labeled in green (525nm em. Q-dots) and recruited and adhering EPCs labeled in red

Figure 3.11 is more specific in describing the rolling velocities of EPCs and mature ECs over both the injured and noninjured tissue. There was no significant decrease in the rolling velocities of the ECs. However, EPCs showed decreased velocities in comparison to ECs on both types of tissue, and a significantly slowed velocity on the injured endothelium with a rolling velocity nearly half that on the noninjured tissue.

3.4 Discussion

Ultimately these studies demonstrate the utility of a parallel plate flow chamber method for analyzing the homing capabilities of EPCs. As an *in vitro* model system for the luminal surface of blood vessels, it can be used to study EPC homing and recruitment in a number of organ systems and disease processes including, atherosclerosis, vascular complications of diabetes and retinopathy. Several of the experiments also show the importance of the CXCR4 receptor in the recruitment of EPCs to injured tissues as has been reported by several studies in the literature. Furthermore, when this receptor was blocked, there was decreased binding of the EPCs to the HA + SDF-1 coated surface. Further studies are needed to block this receptor in the hypoxia and scratch endothelial injury models to further test this receptor's contribution to EPC homing.

The assays of cellular adherence to ECM-coated surfaces proved EPCs to be superior to mature ECs at adherence to the ECM as well as to the specific antigen SDF-1. This is crucial since this antigen has been shown to be upregulated in hypoxia-injured tissues such as those in ocular disorders like DR and AMD. Testing further subpopulations against this antigen as well as through blockade of their defining surface

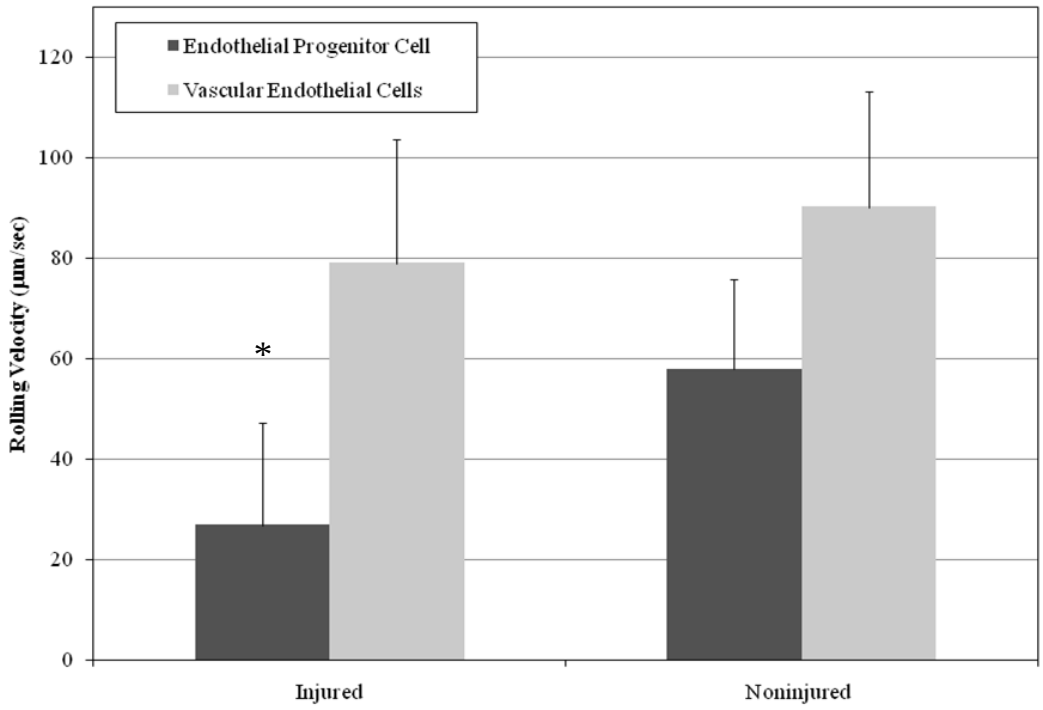

Figure 3.11. Analysis of adherence of EPCs and ECs to an endothelial monolayer injury model divided by either injured or noninjured portions of the tissue. * $p<0.05$ using a Student's T-test relative to noninjured endothelial progenitor cell control.

antigens should help determine the full extent of the homing mechanism of EPCs and how the various subpopulations interact with one another.

It is also very crucial that there was increased recruitment and slowed rolling velocity of EPCs to the hypoxic endothelial monolayers and scratch injured endothelial tissue. The slowed velocity suggests that there would be increased adherence of these cells over time. Quantum dots were an invaluable help in these injury models because the bright fluorescence allowed the cells to be captured in motion and the color allowed the different types to be distinguished. This will be of further help in future experiments, where multiple subpopulations will be added to the parallel plate flow chamber at once. There was a slowed adherence of EPCs on the EC monolayer in comparison to the ECM-coated surfaces most likely due to decreased access to "recruiting antigens" like SDF-1 and ECM components on the EC monolayer. This is expected since these cells would not adhere to a healthy vessel lumen.

Further studies using these models will help to expand the understanding of the specific role of individual EPC subpopulations within CNV. Pharmacological manipulation as well as the incorporation of isolated EPC subpopulations into the models will also facilitate further understanding of EPC involvement in ocular diseases as well as how these cells can be used to deliver preventative therapeutics to specific neovascular regions. The method outlined here for the flow chamber injury models will be invaluable in these studies, allowing for the simultaneous observation of several subpopulations and their interactions in an environment that is relevant to the disease state being studied, easy to manipulate, and relatively easy to replicate quickly.

CHAPTER IV

IN VITRO SYSTEMIC ANALYSIS OF ENDOTHELIAL PROGENITOR CELL SUBPOPULATION NEOVASCULAR CAPACITIES

4.1 Introduction

A number of blinding ocular conditions are characterized by angiogenesis, including diabetic retinopathy, macular degeneration, retinopathy of prematurity, and vein occlusion retinopathy to name a few. The ocular angiogenesis and neovascularization of diabetic retinopathy (DR) and age-related macular degeneration (AMD) cause the greatest blindness in working-aged Americans and individuals 65 years or older in developed countries(67, 68). A number of factors including proteins, lipids and cellular interactions contribute to the pathology seen in these disorders. In 1997, Asahara and coworkers discovered a circulating population of cells originating from the bone marrow termed endothelial progenitor cells (EPCs) that have been shown to be recruited to neovascular lesions and to contribute to the vascular components of a variety of diseases including DR and AMD(2-4, 54).

EPCs have been characterized by a number of cell surface antigens and distinguishing activities. A strong component of the "homing" ability of these cells has been linked to a chemokine receptor (CXCR4) on the surface of EPCs. The ligand for CXCR4, SDF-1 (stromal-derived factor-1), is increased in neovascular lesions and thought to attract EPCs to developing neovascular areas.7 These cells have also been isolated by the surface antigens CD133 and CD34, which are glycoproteins found

specifically on stem and progenitor cells(57-59). Takayuki Asahara, who is cited for first isolating and describing a population of EPCs, describes CD34 and Tie2 as important antigenic determinants of EPCs involved in postnatal vasculogenesis and neovascularization(69). EPCs have also been found to roll along and adhere to the endothelial cells of the inner vascular wall of neovascular tissue(55, 56). Relatively little is understood about the interactions of these characteristic surface antigens and there potential roles in the recruitment of EPCs to specific vascular lesions and tissues. The studies in this report have sought to better define the EPC cell populations that are involved in the angiogenesis and neovascularization that is seen in retinopathies. In further efforts to define and compare EPC subpopulations, novel in vitro methods were also used to model EPC homing capacities and the ability to influence endothelial cell capillary formation.

Bone marrow-derived endothelial progenitor cells (EPCs) play a significant role in the neovascular component of retinal diseases such as diabetic retinopathy and age-related macular degeneration. A variety of cell surface antigens have been shown to modulate this neovascular capacity, but little is known about the potential synergistic or competitive roles of these subpopulations in ocular pathology. This study sought to evaluate and compare different EPC subpopulations in tube formation and proliferation assays, under conditions relevant to ocular disease. Bone marrow was isolated from 4-6 week-old Brown Norway rats. EPC subpopulations were identified by fluorescence-activated cell sorting, using antibodies directed against CD34, CD133, Tie2 and CXCR4. Distinct EPC subpopulations were labeled with quantum dot-conjugated acetylated LDL, and mature endothelial cells (ECs) were labeled with Qtracker®. Tube formation and

proliferation assays were used to compare ECs and EPC subpopulations under conditions of VEGF or serum induction. CD34+/CD133+ cells demonstrated increased tube formation relative to ECs in serum-free, VEGF and 10% serum-stimulated conditions; tube formation was increased 612% ($p<0.001$), 78% ($p<0.01$) and 67% ($p<0.01$), respectively. Tie2+/CD133+ cells also demonstrated increased tube formation in VEGF and serum-stimulated conditions relative to ECs; tube formation increased 43% ($p<0.05$) and 22% ($p<0.05$), respectively. The proliferative capacity of CD34+/CD133+ cells was greatest, with a 70% ($p<0.01$) increase in VEGF-induced proliferation and a 44% increase in serum-induced proliferation, relative to ECs. Compared to EC controls, Tie2+/CD133+ cells demonstrated a 38% reduction ($p<0.05$) in VEGF-induced proliferation, while the Tie2-/CD133+ population demonstrated a 17% reduction in serum-induced proliferation. We have shown various EPC populations to exhibit different neovascular responses using two in vitro models of retinal angiogenic cell behavior. In both assays, the CD34+/CD133+ cells demonstrated the greatest neovascular capacity, suggesting that this EPC population may provide the greatest contribution to retinal disease. These results emphasize the importance of characterizing the angiogenic capacity of diverse EPC subpopulations in retinal vascular disease, as the knowledge may lead to better-targeted therapies for ocular diseases.

4.2 Experimental Procedures

4.2.1 Western Blot Analysis

All animal procedures used in this study were approved by the Vanderbilt University Institutional Animal Care and Use Committee and were performed in

accordance with the ARVO Statement for the Use of Animals in Ophthalmic and Vision Research. Litters of Sprague-Dawley rat pups and their mothers (Charles River Laboratories, Wilmington, MA) were transferred within 4 hours of birth to oxygen exposure chambers, where they received alternating 24-hour periods of 50% oxygen and 10% oxygen for 14 days(70, 71). On postnatal day (P) 14, the oxygen-exposed rats were returned to room air. From P14 until six days after removal to room air, on P20, rats were sacrificed, and their retinas were removed and collected for protein analysis.

For Western blot analysis, the retinas of three eyes were pooled in 300 μL cold lysis buffer (150 mM NaCl, 1.0% TritonX-100, 0.1% SDS, 50 mM Tris-HCl, 100 μg/mL PMSF, 1 mM orthovanadate, 0.3 μg/mL EDTA, 0.5% deoxycholate acid, 50 μM NaF, 0.5 μg/mL leupeptin, 0.7 μg/mL pepstatin A, and 1.0 mg/mL aprotinin) and homogenized by sonication at 4°C. The samples were incubated at 4°C for 30 minutes and then centrifuged at 5000 rpm for 15 minutes at 4°C. Protein concentrations of the supernatants were determined with the BCA kit (Pierce). The volume of each sample was adjusted to a protein concentration of 2.5 μg/μL with cold lysis buffer containing protease inhibitors. Twenty microliters (50 μg) was mixed with 20 μL of 2× Laemmli buffer (Sigma, St Louis, MO) and heated at 95°C for 10 minutes. The samples were resolved by SDS-PAGE and were transferred to 0.2 μm nitrocellulose membranes (Bio-Rad). Nitrocellulose membranes were blocked with TBST-1% bovine serum albumin (Sigma) and were probed with primary antibodies. Either goat anti-mouse IgG HRP (Chemicon, Temecula, Ca), goat anti-rabbit IgG-HRP (Chemicon), or donkey anti-goat IgG-HRP (Santa Cruz Biotechnology, Santa Cruz, CA) secondary antibodies were applied to the membranes and were developed with enhanced chemiluminescence (ECL; Amersham,

Piscataway, NJ). The following primary antibodies were used in this study: anti-CXCR4 (Neuromics), anti-SDF-1 (Santa Cruz Biotechnology) and anti–CD34 (Santa Cruz Biotechnology); anti–CD105 (NeoMarkers) and anti-CD133 (Santa Cruz Biotechnology); anti-Tie2 (BD Pharmagen Biosciences). Each Western blot was repeated at least three times.

4.2.2 Cell Isolation and Preparation

Cells were isolated from six, four- to six-week-old Brown Norway rats. The animals were sedated with methoxyflurane vapors, and then euthanized by decapitation. Their tibias and femurs were removed, and the bone marrow was isolated from these bones. The marrow tissue was then triturated and then the remaining cells were washed once with erythrocyte-lysing solution (154mM NH_4Cl, $KHCO_3$ 10mM, EDTA 82μM) by centrifugation. The cells were then washed three times by centrifugation with phosphate buffered saline to remove extracellular matrix debris. At this point, the cells were further isolated and characterized into subpopulations by FACS as described in section 4.2.3. These individual cell mixtures were then plated onto plastic dishes and grown in EGM-2 media (Clonetics) containing 10% fetal bovine serum, 1ug/ml hydrocortisone, 10ng/ml epidermal growth factor and 5ml/500ml of 100X antibiotic/antimycotic solution (Sigma) for one full passage before use *in vitro* or labeled directly and used in the FACS assay to confirm the lack of significant surface antigen drift.

In order to label these cells with QD-acLDL or Qtracker (Invitrogen), the cells were incubated with 2ug/ml of QD-acLDL or 1ug/ml of Qtracker (as directed) for four to six hours, then removed from the dish using Accutase™ (Sigma) followed by

centrifugation and resuspension to the desired concentration in PBS before use in the *in vitro* assays.

4.2.3 Fluorescence Activated Cell Sorting (FACS)

For all of the surface antigens investigated, isolated bone marrow was taken from the rats as described above and incubated in a 200 μg/ml of the appropriate blocking IgG for 10 minutes in an ice bath. A 1:500 dilution of the unconjugated primary antibody was then added to the solution. The antibodies used were anti-CXCR4 (Santa Cruz), anti-CD133 (Abcam and Santa Cruz) and anti-CD34 (Abcam). Appropriate non-labeled controls were set aside at this time as well. This suspension was incubated on ice for another 15 minutes. The cells were centrifuged at 1500×g for 3 minutes at 4°C and then resuspended in a 1:2000 dilution of the secondary antibody (Jackson Labs) conjugated to quantum dots (em. 655 and 525) using an the Invitrogen antibody conjugation kit. This solution was also incubated 15 minutes in an ice bath. The cells were then centrifuged for 3 minutes at 1500×g and 4°C. The cells were sorted on a 3-laser BD LSRII cell sorter (BD Biosciences) at the Vanderbilt Flow Cytometry Core.

4.2.4 In Vitro Parallel Plate Flow Chamber (PPFC) Assay

PPFC and Hypoxic Endothelial Monolayer Adherence assay

Cells grown in culture and labeled with either QD-acLDL or Qtracker were using at 1-2 X 10^6 cells/ml. The cells were placed into a parallel plate flow chamber (PPFC) (Glycotech Corporation). The chamber used has a flow width of 1.00cm and a height of 0.010 in. Throughout these studies, a flow rate consistent with a shear stress of 15

dynes/cm^2 was used. Slides in these experiments had a confluent monolayer of endothelial cells on their surface. These cells were either mature endothelial cells cultured under normoxic conditions or hypoxic conditions for 24 hours prior to their use in the PPFC. Monolayers of EPCs were also used. The slides were assembled as the lower wall of the PPFC and mounted on the stage of an inverted microscope. Images were captured of the flowing cells every 300ms for 5 to 15 minutes and cell counts and rolling velocities were determined at frequent time points using Image Pro-Plus tracking software.

4.2.5 Proliferation and Tube Formation Assays

Rat endothelial progenitor cells as well as rat retinal microvascular endothelial cells (RRMECs) were seeded in 10% serum EBM at 3000 cells/well in a 96-well plate and were allowed to attach and settle. The cells were serum-starved for 12 hours and then treated with 1% serum medium in the absence or presence of 50 ng/mL VEGF. Cells were then labeled with BrdU for 12 hours, and BrdU incorporation was quantified with a colorimetric ELISA (Roche, Indianapolis, IN) according to the manufacturer's instructions. The experiment was independently repeated three times.

Twelve-well tissue culture plates were coated with 200 μL growth factor-reduced basement membrane matrix (Matrigel; Becton Dickinson, Franklin Lakes, NJ). RRMECs labeled with 525nm Qtracker (Invitrogen) were seeded at 20,000 cells/well and treated with serum-free EBM alone, EBM containing 50ng/ml VEGF, or 10% serum. The cells were cultured for 4 hours at 37°C in a 5% CO_2 atmosphere to allow tubes to begin to form. Then mature endothelial cells or specific subpopulations of EPCs were added at

20,000 cells/well and kept in culture for 12 hours more. Tubes were observed with an IMT-2 inverted microscope (Olympus, Melville, NY), and images were captured with a DMC digitizing camera (Polaroid Corporation, Waltham, MA). Six fields per well were captured for quantitative analysis. The digitized images were imported into ImageJ software (developed by Wayne Rasband, National Institutes of Health, Bethesda, MD; available at http://rsb.info.nih.gov/ij/index.html). Capillary-like structures of more than two cell lengths were assessed, and the mean tube length per field of each well was calculated. The average tube length of each treatment group was reported. The experiment was independently repeated three times.

4.3 Results

4.3.1 Assessment of Rat Oxygen-Induced Retinopathy (OIR) Tissue for EPC-Associated Antigens

CXCR4 is the chemokine receptor for SDF-1 and was highly expressed on the surface of bone marrow-derived cells relative to cells resident to the retina. This receptor has also been implicated in the majority of the homing ability of EPCs. In the retinal tissue of OIR model rats, CXCR4 levels were elevated 1.8-fold when the animals were initially removed from treatment (having most recently came from an environment of 10% oxygen) and 2.5- and 2.1-fold, respectively, at three and six days following removal of the animals from oxygen treatment. These times are associated with the initial onset and peak neovascular growth in these animals (**Figures 4.1 and 4.2**). CD133 is a cell surface marker expressed by undifferentiated stem/progenitor cells and is quickly lost after cell differentiation. Similarly to CXCR4, at post-treatment days three and six,

CD133 levels were elevated 4.5-fold relative to earlier time points in the oxygen-treated samples and every time point in comparison to the room air-raised control animals (**Figures 4.1 and 4.2**).

SDF-1 is a chemokine that binds exclusively to CXCR4, attracting cells that express this receptor. In the retinal tissue of oxygen treated animals, there were elevated levels of SDF-1 that closely corresponded to those of CXCR4 appearing to precede that of the receptor by about a day, however, the SDF-1 levels were much more strongly elevated to 5-fold levels relative to earlier time points in the OIR tissue and all room air-raised samples (**Figures 4.1 and 4.2**).

CD34 is a glycoprotein cell surface receptor that has been shown to be expressed on the surface of many progenitor and stem cells, and was the original antigen used to identify EPCs by Asahara et al.(2) Tie2 was also suggested in this initial manuscript describing EPCs as well as later manuscripts(69) by this group as being an important determinant of EPCs involved in vasculogenesis. This analysis, however, found no significant differences in the levels of either of these proteins when comparing any of the time points or either of the treatments (**Figure 4.2**).

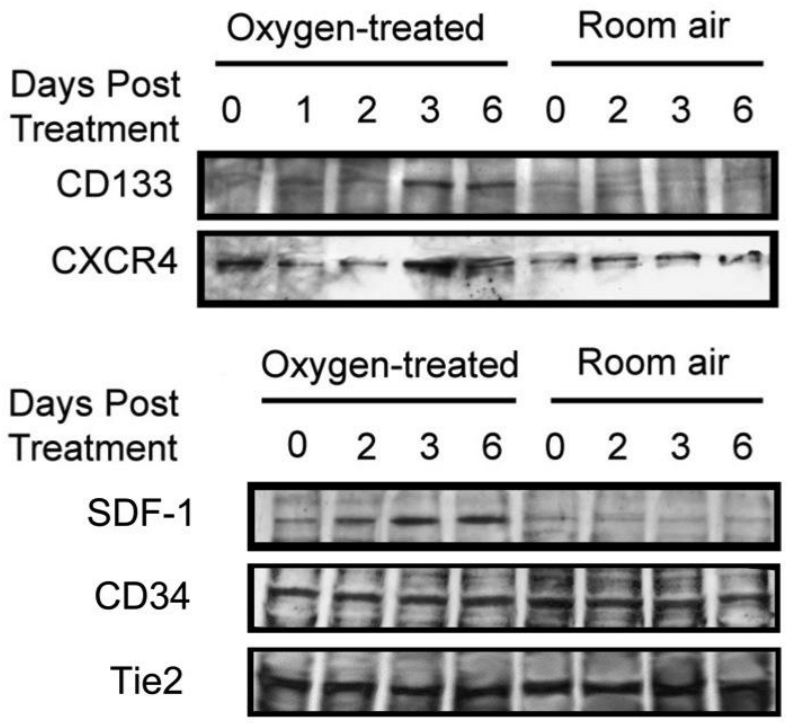

Figure 4.1. Western blots showing EPC-associated antigens at several time points in post-oxygen treated retinal tissue from OIR and room air-raised control animals. Samples in every lane were matched for protein concentration and ultimately compared to one another after being normalized to relative beta-actin levels.

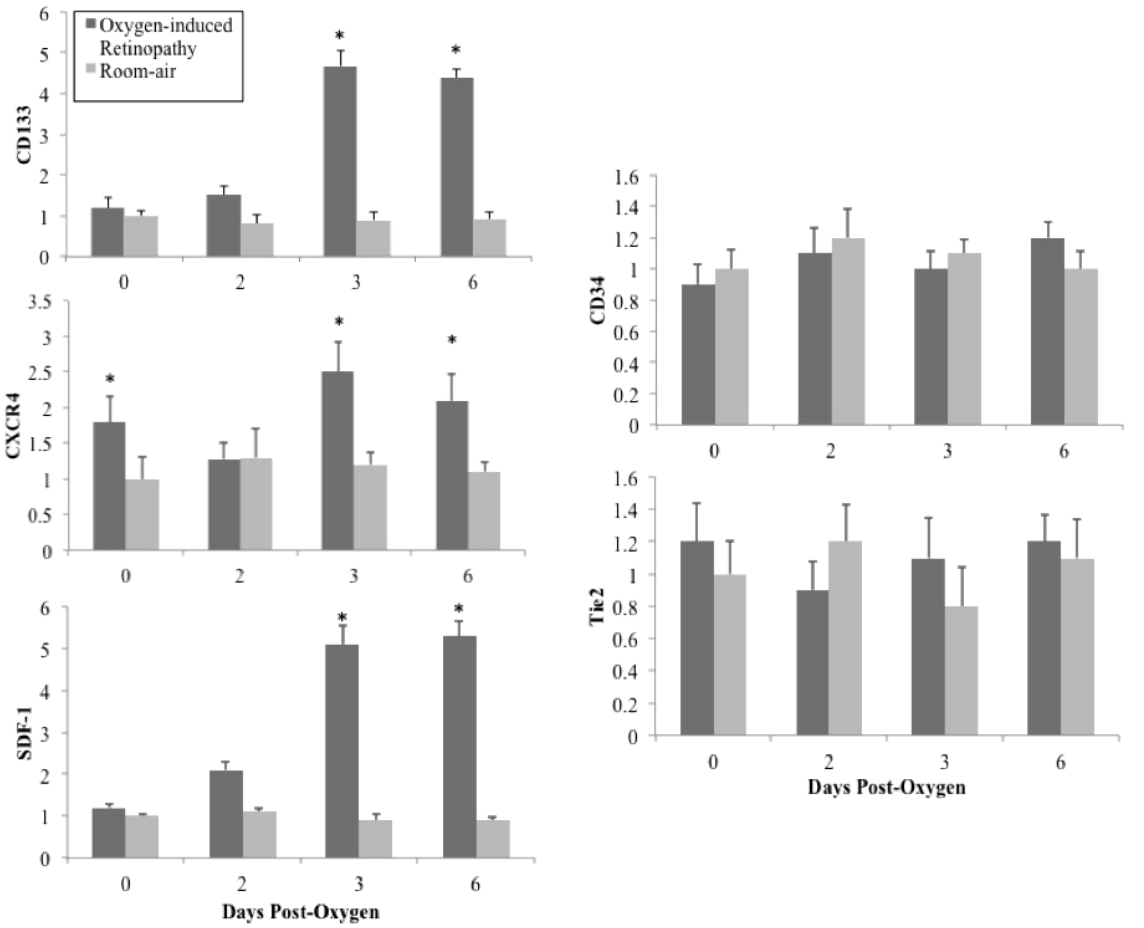

Figure 4.2. This shows the normalized and averaged results of the Western blot protein quantities for the EPC-associated antigens shown in **Figure 4.1**. Each protein was normalized to beta-actin and every Western blot was independently repeated at least three times. An "*" indicates a significance level of $p<0.05$, and a "†" indicates a significance level of $p<0.02$.

4.3.2 Assessment of EPC Homing and Recruitment in a Hypoxic Endothelial Monolayer Adherence Model

This assay is meant to model the adherence of circulating EPCs in the vascular system to the luminal wall of blood vessels in healthy and in hypoxic tissue. In this set of experiments, EPCs are propelled over a surface of endothelial cells in a monolayer culture and assessed for recruitment to this monolayer by reduced rolling velocities. **Figure 4.3** illustrates the assessment of EPCs labeled with Qtracker (Invitrogen, 655nm emission Q-dots) adhering and rolling on an endothelial monolayer also labeled with a different wavelength quantum dot (525nm em. Q-dots). The monolayers tested were either cultured in normoxic conditions or in hypoxia (<1% oxygen for 24 hrs). The cells that were flowing in suspension in the parallel plate flow chamber (PPFC) were mature endothelial cells, a heterogeneous EPC population and the CD133+/CD34+ subpopulation of EPCs.

The findings in **Figure 4.3** demonstrate the lack of adherence or very slight adherence of mature endothelial cells to themselves. This adherence was unaffected by the treatment of the endothelial monolayer in hypoxia. The heterogeneous EPC population (Hetero. EPC), shows greater adherence to the endothelial monolayer under normoxic conditions relative to the mature endothelial cells, and the hetero. EPCs demonstrated significantly decreased rolling velocities (16%, $p<0.05$) relative to the velocity of these cells on normoxic-treated (20.9% oxygen) monolayers. The CD133+/CD34+ subpopulation of EPCs, however, showed an even greater decrease in rolling velocity (40%, $p<0.02$) relative to the velocity of these cells on normoxic treated monolayers. There was no significant difference between the rolling velocities of the EPC populations on normoxic treated endothelial monolayers.

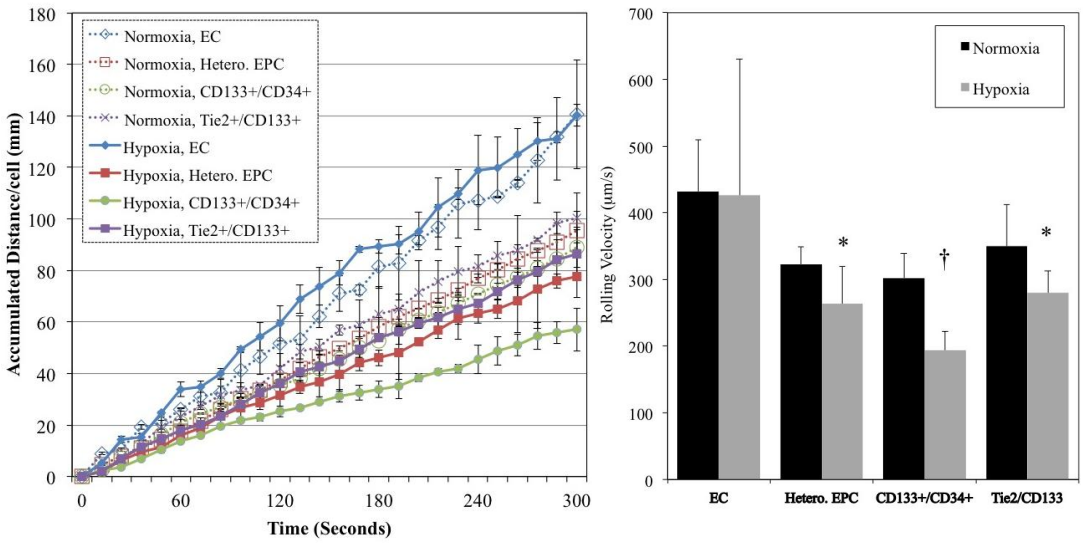

Figure 4.3. The homing ability of EPCs is tested in a parallel plate flow chamber using endothelial monolayers that have been exposed to 24 hours of hypoxia or normoxia immediately before the assay begins. Rolling velocities of the cells are measured and a slower rolling velocity is indicative of increased adherence to the endothelial monolayer. The graph to the left is the average accumulated distance of the cells at each time point during the assay and the graph to the right shows the average rolling velocity of each cell type for the entire assay. An "*" is indicative of a significance level of $p<0.05$, and a "†" indicates a significance level of $p<0.02$.

4.3.3 VEGF- and Serum-Mediated Endothelial Cell Capillary Tube Formation Influence by EPC Subpopulations

This assay should model the effect that homing EPCs would have on endogenous endothelial cells that are proliferating and forming new capillary networks in angiogenic or neovascular tissue. The first column of **Figure 4.4** shows that endothelial cells alone do not respond by forming tubes in an environment that is free of serum, but have progressively increased responses with VEGF and serum treatment. The second column depicting the addition of a hetero. EPC population to the endothelial cells shows a slight increase in tubes being formed in the serum free panel. There is also a similar capacity for tube formation in the VEGF-stimulated row of this column, however, an apparent increase in tube formation in the serum stimulated panel relative to the mature endothelial cells alone. This heterogeneous population of cells seems to cause more clumping of the endothelial cells as they are forming tubes, however, a majority of the tubes seem to be formed by the green-labeled endothelial cells and not the red-labeled EPCs. The right column of the panel shows the addition of CD133+/ C34+ EPCs to the endothelial cells forming tubes. This EPC subpopulation demonstrates a strong clumping effect on the endothelial cells in the serum free panel incorporating themselves into these clumps. The EPCs in this column also demonstrate an increased tube formation influence on the endothelial cells in both the VEGF- and serum-stimulated panels. With both stimuli, the red-labeled EPCs are shown forming tubes as frequently as the green-labeled EPCs.

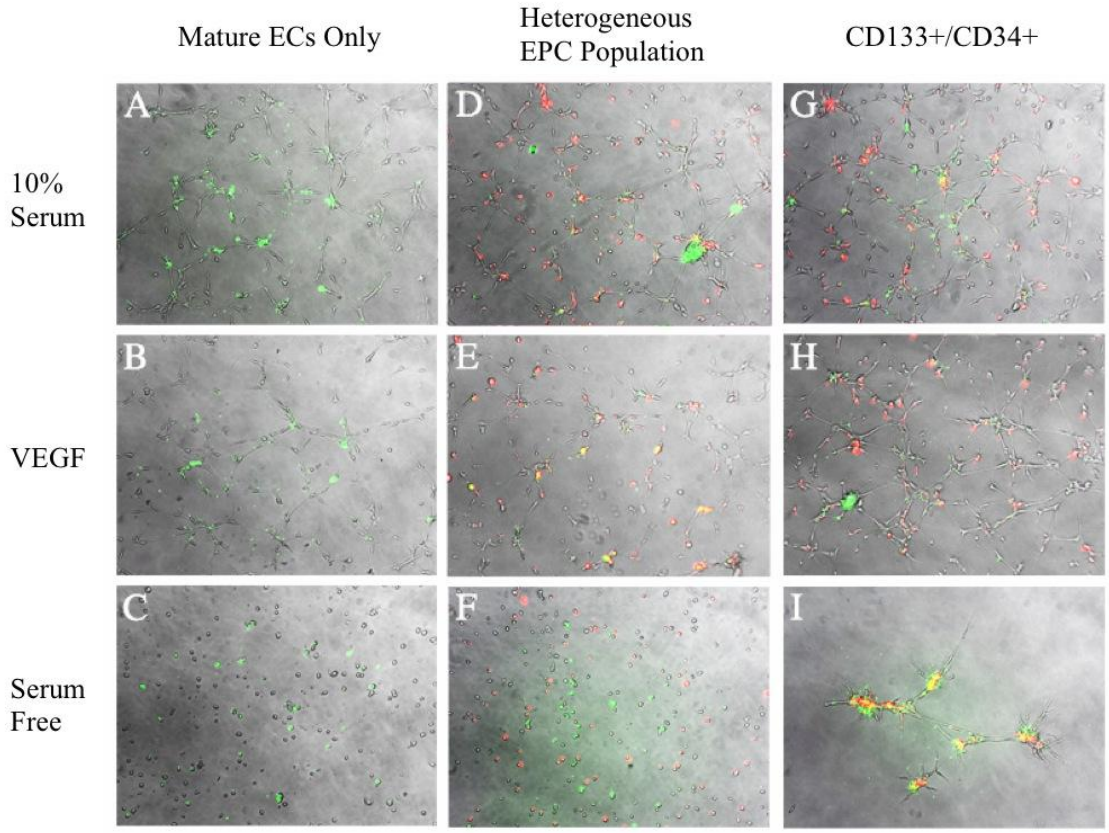

Figure 4.4. These panels show the varied qualitative responses of the mature endothelial cells and EPCs in a tube formation assay stimulated with either 10% serum or 50ng/ml rat VEGF. In these experiments the mature endothelial cells were prelabeled with a green fluorescent tracker and the EPC subpopulations were labeled with a red fluorescent tracker.

Figure 4.5 shows a graphically quantified representation of the panels in **Figure 4.4**. Again, relative to the endothelial cell controls, the heterogeneous population of the whole bone-marrow cells was more varied with a potentially decreased response to VEGF and an increased response to serum. The CD133+/CD34+ cells, however, demonstrated a strong and significant influence to increase tube formation of the endothelial cells in serum free, VEGF-stimulated and serum stimulated conditions. This population of EPCs had a 6.5-fold increase on the tube length in serum free conditions and a 1.7-fold increase on tube length in both VEGF- and serum-stimulated conditions. Tie2+/CD133+ cells were also used in this assay and did demonstrate a slightly increased and significant tube formation effect of 1.4-fold in both of the stimulated conditions. This subpopulation, however, did have any effect on the formation of tubes by the endothelial cells in the unstimulated (serum free) condition.

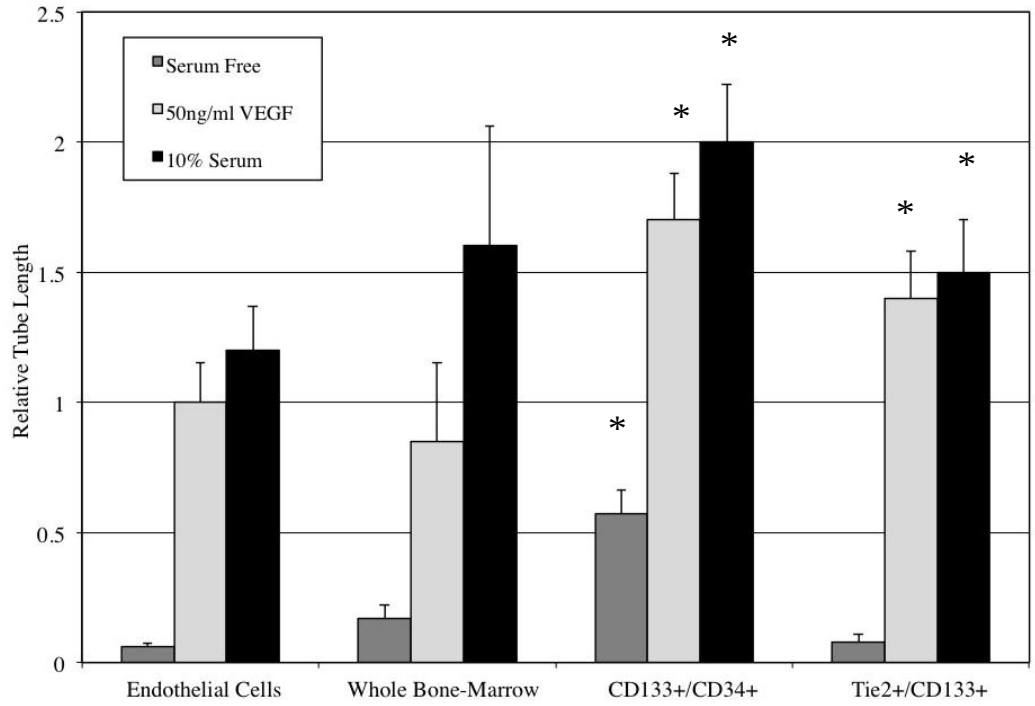

Figure 4.5. The graph shows the quantified tube lengths of the tube formation assay demonstrated in the **Figure 4.4** panels. In this assay the tube lengths were normalized to the mature endothelial cell response to VEGF stimulation. An "*" indicates a significance of $p<0.05$.

4.3.4 VEGF- and Serum-Mediated Proliferation of EPC Subpopulations

In **Figure 4.6**, the proliferation experiments showed a nearly 2-fold response of the control, mature endothelial cells and an even more robust 4-fold response of these cells to 10% serum. Of the EPC populations tested, the CD133+/CD34+ cells had the strongest proliferation in all of the treatments. These cells grew nearly 20% more in conditions without serum, but, additionally, had a 3-fold increase ($p<0.01$) in proliferation in response to VEGF and a 5-fold increase ($p<0.01$) in proliferation in response to the serum treatment. It is interesting to note that the Tie2+/CD133+ cells had an enhanced response to VEGF stimulated proliferation relative to mature endothelial cells, but did not have a statistically different response when stimulated with 10% serum. The heterogeneous population of EPCs had a decreased response to both proliferative stimuli and higher variability that is presumed to be the result of varied cell populations within this group and their respectively varied capacity to respond to the proliferative stimulants.

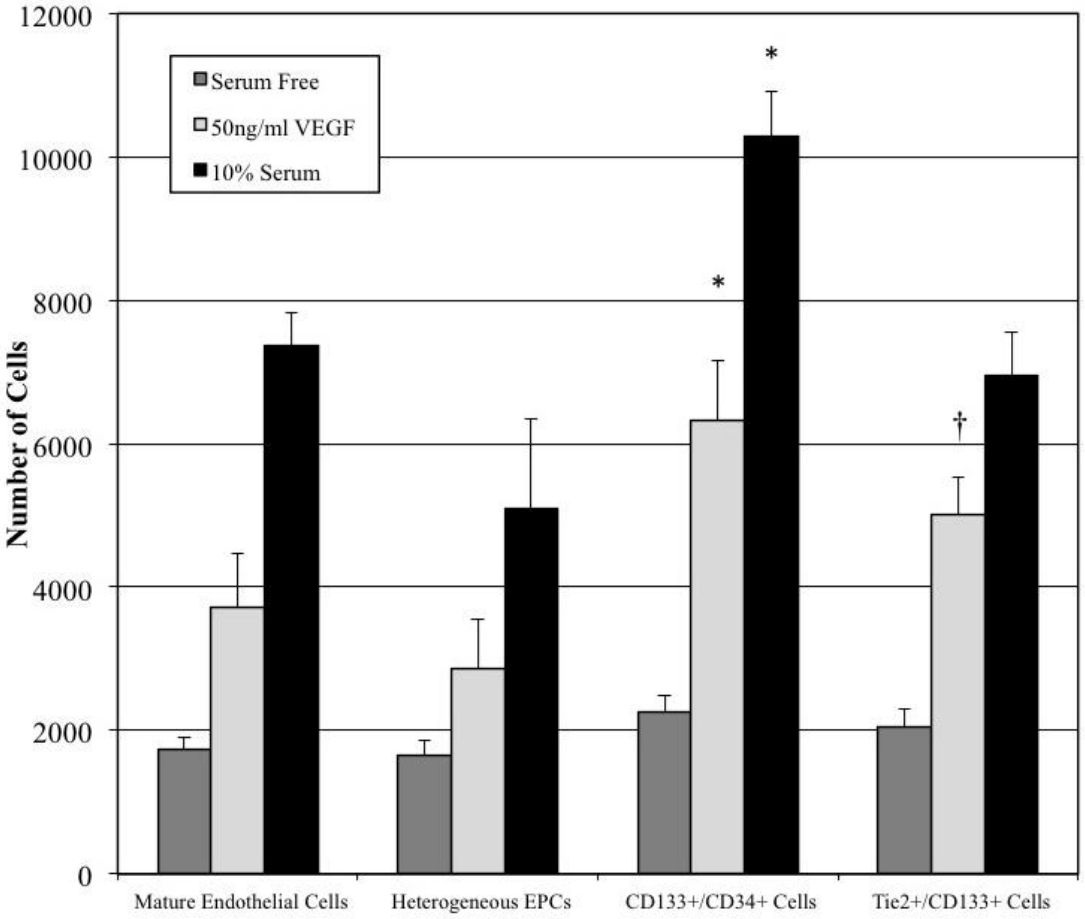

Figure 4.6. Analysis of EPCs subpopulation proliferation. An "*" indicates $p<0.01$ relative to mature ECs and $p<0.02$ from all other cell types; a "†" indicates a $p<0.05$ relative to mature ECs.

4.4 Discussion

Ultimately these studies show the importance of the CD133+/CD34+ subpopulation of EPCs in the homing, proliferation and tube formation models that have been tested. This subpopulation has consistently outperformed mature endothelial cells as well as a heterogeneous population of EPCs in all three assays. The CD133+/CD34+ subpopulation has also proven itself to be more influential than the CD133+/Tie2 subpopulation of cells in the proliferation assay as well as the tube formation assay. This demonstrates the potential of this cell population in the progression and exacerbation of the types of neovascular lesions that are seen in retinopathies. However, the CD133+/CD34+ subpopulation could be more thoroughly tested, and the EPC-associated antigens that were analyzed in **Figures 4.1** and **4.2** indicate some subpopulations to test against CD133+/CD34+ cells.

The Western blot protein analysis of EPC-associated antigens revealed the stem/progenitor cell antigen, CD133 and the antigen associated with cells originating from the bone marrow, CXCR4, both present in the retinal tissue at increased concentrations at times of peak neovascular proliferation. This suggests that progenitor cells from the bone marrow are in the retina during this time and may be involved in this neovascular proliferation. While CD34 and Tie2 were not found to change during these time points or between treatment groups, they are antigens found on proliferating endothelial cells. The overwhelming levels of these proteins on the endogenous endothelial cell populations may overwhelm any additional quantities that would be added by EPCs homing to these neovascular sites. However, the *in vitro* experiments in

this study have outlined a clear difference between the subpopulation of EPCs isolated with CD34 and those isolated with Tie2.

Additionally, it may be useful to continue using the western blot analysis screening method for several more promising antigens. If neither of these ligand/receptor pair antigens are present in the retinal tissue, they could be more easily dismissed as unlikely to be involved in this process. CD44, c-kit, and VEGFR3 should still be examined in OIR and room air-raised tissue.

With another subpopulation or two for comparison, the *in vitro* assays will carry much more meaningful results. These legitimate head to head comparisons of the subpopulations will help to identify the subpopulations that have the greatest involvement and influence in retinal neovascularization. Then these subpopulations can be validated and manipulated within animal models.

Further studies using these in vitro models will help to expand the understanding of the specific role of individual EPC subpopulations within retinal neovascular lesions. Pharmacological manipulation as well as the incorporation of isolated EPC subpopulations into the models will also facilitate further understanding of EPC involvement in ocular diseases as well as how these cells can be used to deliver preventative therapeutics to specific neovascular regions. The method outlined here for the influence of endothelial capillary tube formation will be invaluable in these studies along with the homing assay. These assays could allow for the simultaneous observation of several subpopulations and their interactions in an environment that is relevant to the aspects of the hypoxic and neovascular tissue of the diseased retina. The assays are easy to manipulate, and relatively easy to replicate quickly. There were several more aspects

of the tube formation assay that could have been measured such as the percentage of tubes that were formed by the mature endothelial cells relative to the EPCs or the length of the EPC tubes to those of the mature endothelial cells within the same treatment groups. These aspects of this assay will be addressed in future experiments.

CHAPTER V

BLOCKING ENDOGLIN REDUCES ENDOTHELIAL PROGENITOR CELL ANGIOGENIC CAPACITY AND RETINAL NEOVASCULARIZATION

5.1 Introduction

Angiogenesis and neovascularization are common pathological processes in age-related macular degeneration and retinopathies. Endoglin (CD105) has been reported as being upregulated in proliferative tumor vasculature and neovascular tissues. As an acillary receptor in the TGFβ super family it is suggested to be involved in cell proliferation, migration and differentiation. This study sought to examine the role of endoglin in endothelial progenitor cell (EPC) angiogenic capacity and retinal neovascularization. Endoglin was characterized and effectively blocked in models of endothelial progenitor cell homing, capillary tube formation and incorporation, and proliferation. Additionally endoglin was blocked in a rat model of oxygen induced retinopathy (OIR). Endoglin protein was found to be upregulated in OIR tissue relative to animals raised in room air conditions. This increase in endoglin could be reduced through the treatment of the animals with a CXCR4 antagonist (AMD3100) to inhibit the ability of EPCs home to neovascular areas. Endoglin targeted treatments were additionally able to inhibit both EPC proliferation and tube formation. However, EPC *in vitro* homing was unaffected by anti-CD105 treatment. The anti-CD105 was found to be effective in reducing the neovascular lesion size in the OIR model and worked additively with anti-VEGF treatments. Endoglin has an angiogenic role in retinal neovascularization and

blocking endoglin function is an effective method of reducing neovascularization partially through a reduced angiogenic capacity of EPCs.

Angiogenesis, the formation of new capillaries from existing blood vessels, occurs during physiologic processes such as reproduction, growth and development, and wound healing(72-77). Conversely, diseases such as arthritis, tumor growth and retinopathies are characterized by pathological, persistent angiogenesis(77-79). In the context of the retina, pathological, persistent angiogenesis is often referred to as retinal neovascularization (NV). Age-related macular degeneration (AMD), diabetic retinopathy (DR), and retinopathy of prematurity (ROP) are potentially blinding conditions characterized by choroidal or retinal NV.

The neovascularization that is seen in all of these ocular diseases is widely viewed to be driven primarily by vascular endothelial growth factor (VEGF)(80-82). As a result of this common vasoactive factor, the current pharmacologic therapies used clinically target VEGF(83, 84). Bevacizumab (Avastin, Genentech) and Ranibizumab (Lucentis, Genentech) are humanized monoclonal antibodies with high affinities for VEGF-A. As useful and efficacious as these therapies have been there are still concerns about their use and patients that do not improve with VEGF targeted therapy. There are concerns about anti-VEGF therapies leaking into the serum and circulatory system potentially damaging unintended vascular systems, particularly in younger patients(85). Additionally, there is evidence that VEGF plays an important survival role for neurons(86, 87). This could mean neuronal damage with prolonged VEGF targeted therapy. When visual outcome is the analyzed parameter in studies using VEGF targeted therapies, as many as 45% of the patients were found to be nonresponsive to the treatment(88, 89). With these concerns in

mind, it would be useful to have non-VEGF pathway therapies to target in ocular neovascularization.

Endoglin (CD105) is a potential non-VEGF pathway protein that could be targeted in the treatment of neovascularization. It is a transmembrane glycoprotein that is an accessory to the transforming growth factor β (TGFβ) receptor system(18). Endoglin is also expressed on proliferating endothelial cells (ECs) and tumor types characterized by hypoxia(19-24). On endothelial and tumor cells, it is thought to be involved in differentiation, migration and proliferation(20, 25). Monoclonal antibody therapies have been shown to have some antiproliferative effects in cancer studies(26, 27). Furthermore, subsets of endothelial progenitor cells (EPCs) have been found to highly express CD105(28-30). Additionally, as marker of mesenchymal stem cells, endoglin has been shown on progenitor cells that increase vascular remodeling in models of myocardial infarction and rheumatic diseases(31, 32).Many investigators suggest that EPCs play a significant role in ocular neovascularization and that these cells could be targeted to influence that neovascularization(33, 34). Perhaps targeting EPCs through CD105 could prevent their differentiation and proliferation in the neovascular lesions seen in the angiogenic pathology of the eye.

In these studies, the role of endoglin in EPC angiogenic capacity and retinal neovascularization was explored. By analyzing mature ECs and EPCs for CD105 in models of neovascular conditions, we sought to determine any connections between developing neovascularization and endoglin. Then through *in vitro* modeling of the homing, capillary incorporation and proliferation capabilities of EPCs, the effect of endoglin blockade on EPC function could be determined. Finally, we examined the effect

of blocking endoglin in a model of oxygen-induced retinal neovascularization. These experiments were performed concomitantly with anti-VEGF therapy in order to directly compare the two different strategies.

5.2 Experimental Procedures

5.2.1 Cell Isolation and Preparation

Cells were isolated from six, four- to six-week-old Brown Norway rats. The animals were sedated with methoxyflurane vapors, and then euthanized by decapitation. Their tibias and femurs were removed, and the bone marrow was isolated from these bones. The marrow tissue was then triturated and then the remaining cells were washed once with erythrocyte-lysing solution (154mM NH_4Cl, $KHCO_3$ 10mM, EDTA 82μM) by centrifugation. The cells were then washed three times by centrifugation with phosphate buffered saline to remove extracellular matrix debris. At this point, EPC subpopulations were further isolated and characterized first by immunopanning for cells expressing CD133 and then by FACS for CD34+ cells as described in section 4.2.3. These individual cell mixtures were then plated onto plastic dishes and grown in EGM-2 media (Clonetics) containing 10% fetal bovine serum, 1ug/ml hydrocortisone, 10ng/ml epidermal growth factor and 5ml/500ml of 100X antibiotic/antimycotic solution (Sigma) for one full passage before use *in vitro* or labeled directly and used in the FACS assay to confirm the lack of significant surface antigen drift.

In order to label these cells with QD-acLDL or Qtracker (Invitrogen), the cells were incubated with 2ug/ml of QD-acLDL or 1ug/ml of Qtracker (as directed) for four to six hours, then removed from the dish using Accutase™ (Sigma) followed by

centrifugation and resuspension to the desired concentration in PBS before use in the *in vitro* assays.

5.2.2 Fluorescence Activated Cell Sorting (FACS)

For all of the surface antigens investigated, isolated bone marrow was taken from the rats as described above and incubated in a 200 μg/ml of the appropriate blocking IgG for 10 minutes in an ice bath. A 1:500 dilution of the unconjugated primary antibody was then added to the solution. The antibodies used were anti-CD34 (Abcam). Appropriate non-labeled controls were set aside at this time as well. This suspension was incubated on ice for another 15 minutes. The cells were centrifuged at 1500×g for 3 minutes at 4°C and then resuspended in a 1:2000 dilution of the secondary antibody (Jackson Labs) conjugated to quantum dots (em. 655 and 525) using an the Invitrogen antibody conjugation kit. This solution was also incubated 15 minutes in an ice bath. The cells were then centrifuged for 3 minutes at 1500×g and 4°C. The cells were sorted on a 3-laser BD LSRII cell sorter (BD Biosciences) at the Vanderbilt Flow Cytometry Core.

5.2.3 In Vitro Hypoxia Treatment

EPCs that were isolated from bone marrow, according the procedure described sections 5.2.1 and 5.2.2. Cells from passages two to three were used in the following experiments. The cells were grown in EGM-2 media (Clonetics) containing 10% fetal bovine serum, 1ug/ml hydrocortisone, 10ng/ml epidermal growth factor and 5ml/500ml of 100X antibiotic/antimycotic solution (Sigma) to 70% confluence, and then maintained in normoxia for 24 hours. After 24 hours, cells were exposed to hypoxia for 18 hours

(using a BBL GasPak™ system; Becton, Dickinson and Company, Sparks, MD). Some cultures were lysed for Endoglin ELISAs, (Quantikine Colorimetric Sandwich ELISA; R&D Systems) while others were prepared for immunocytochemistry staining with anti-CD105 (Millipore). These experiments were conducted four times, with n = 4 for each treatment group.

5.2.4 Rat Oxygen Treatment

All animal experiments were approved by the Vanderbilt University School of Medicine Animal Care and Use Committee, and they were conducted according to the principles expressed in the ARVO statement for the Use of Animals in Ophthalmic and Vision Research. Within 4 hours after birth, litters of Sprague-Dawley rat pups and their mothers were exposed to alternating periods of 24 hrs at 50% and10% oxygen, for 14 days. This variable oxygen treatment protocol predisposes the rat pups to OIR. Hereafter, these rats are referred to as OIR rats. Age-matched control rats were maintained in ambient (20.9% oxygen) normoxia. These rats are referred to as room air (RA) rats. After the variable oxygen treatment, the OIR rats were returned to room air for up to six days, allowing time for retinal NV to develop. We refer to the timing of sacrifice and assessment with two numbers, one representing the time in variable oxygen and one representing the post-exposure period. Hence, rats sacrificed immediately upon removal from exposure are termed 14(0), while rats sacrificed at the end of the six-day post-exposure period are referred to as 14(6).

5.2.5 Western Blot Analysis

For Western blot analysis, the retinas of three eyes were pooled in 300 μL cold lysis buffer (150 mM NaCl, 1.0% TritonX-100, 0.1% SDS, 50 mM Tris-HCl, 100 μg/mL PMSF, 1 mM orthovanadate, 0.3 μg/mL EDTA, 0.5% deoxycholate acid, 50 μM NaF, 0.5 μg/mL leupeptin, 0.7 μg/mL pepstatin A, and 1.0 mg/mL aprotinin) and homogenized by sonication at 4°C. The samples were incubated at 4°C for 30 minutes and then centrifuged at 5000 rpm for 15 minutes at 4°C. Protein concentrations of the supernatants were determined with the BCA kit (Pierce). The volume of each sample was adjusted to a protein concentration of 2.5 μg/μL with cold lysis buffer containing protease inhibitors. Twenty microliters (50 μg) was mixed with 20 μL of 2× Laemmli buffer (Sigma, St Louis, MO) and heated at 95°C for 10 minutes. The samples were resolved by SDS-PAGE and were transferred to 0.2 μm nitrocellulose membranes (Bio-Rad). Nitrocellulose membranes were blocked with TBST-1% bovine serum albumin (Sigma) and were probed with primary antibodies. Either goat anti-mouse IgG HRP (Chemicon, Temecula, Ca), goat anti-rabbit IgG-HRP (Chemicon), or donkey anti-goat IgG-HRP (Santa Cruz Biotechnology, Santa Cruz, CA) secondary antibodies were applied to the membranes and were developed with enhanced chemiluminescence (ECL; Amersham, Piscataway, NJ). The following primary antibodies were used in this study: anti–CD105 (NeoMarkers). Each Western blot was repeated at least three times.

5.2.6 Vascular and Immunohistochemical Staining

At post natal days 17 and 20, the eyes of the mice were removed, and retinal flat-mounts were prepared by removing the cornea and lens in 10% phosphate-buffered

formalin. The retina was then dissected from the eyecup, and radial cuts were made from the edge of the eyecup in all four quadrants to the equator. In these flat-mounts the endothelial cells were identified using Isolectin B4, FITC conjugate (Sigma-Aldrich, Inc.), and anti-CD105 (Millipore). The tissue was then flat-mounted in Gel Mount (Biomedia, Victoria, Australia). Areas of vascular and avascular growth were measured via computer-assisted image analysis using high-resolution digital images of the stained retinal flat-mounts. All measurements were made using tools in Adobe Photoshop CS (Adobe Systems Inc.).

5.2.7 In Vitro Parallel Plate Flow Chamber (PPFC) Assay

PPFC and Hypoxic Endothelial Monolayer Adherence assay

Cells grown in culture and labeled with either QD-acLDL or Qtracker were using at 1-2 X 10^6 cells/ml. The cells were placed into a parallel plate flow chamber (PPFC) (Glycotech Corporation). The chamber used has a flow width of 1.00cm and a height of 0.010 in. Throughout these studies, a flow rate consistent with a shear stress of 15 dynes/cm^2 was used. Slides in these experiments had a confluent monolayer of endothelial cells on their surface. These cells were either mature endothelial cells cultured under normoxic conditions or hypoxic conditions for 24 hours prior to their use in the PPFC. Some cells were treated with anti-CD105 (Millipore) at concentrations ranging from 1-100 ug/ml for 10 minutes prior to and during their flow over the monolayers. An anti-rat IgG and AMD3100 (CXCR4 antagonist) were also used at 100 ug/ml and 5 ug/ml, respectively, as controls in these experiments. The slides were assembled as the lower wall of the PPFC and mounted on the stage of an inverted

microscope. Images of the flowing cells were captured every 300ms for 5 to 15 minutes and cell counts and rolling velocities were determined at frequent time points using Image Pro-Plus tracking software.

5.2.8 Proliferation and Tube Formation Assays

Rat endothelial progenitor cells as well as rat retinal microvascular endothelial cells (RRMECs) were seeded in 10% serum EBM at 3000 cells/well in a 96-well plate and were allowed to attach and settle. The cells were serum-starved for 12 hours and then treated with 1% serum medium in the absence or presence of 50 ng/mL VEGF or 10% serum. On these back grounds some cells were also treated with anti-CD105 (Millipore) at concentrations ranging from 1-100 ug/ml or anti-VEGF at 100ug/ml (Sigma). Cells were then labeled with BrdU for 12 hours, and BrdU incorporation was quantified with a colorimetric ELISA (Roche, Indianapolis, IN) according to the manufacturer's instructions. The experiment was independently repeated three times.

Twelve-well tissue culture plates were coated with 200 μL growth factor-reduced basement membrane matrix (Matrigel; Becton Dickinson, Franklin Lakes, NJ). RRMECs labeled with 525nm Qtracker (Invitrogen) were seeded at 20,000 cells/well and treated with serum-free EBM alone, EBM containing 50ng/ml VEGF, or 10% serum. The cells were cultured for 4 hours at 37°C in a 5% CO_2 atmosphere to allow tubes to begin to form. Then mature endothelial cells or specific subpopulations of EPCs were added at 20,000 cells/well and kept in culture for 12 hours more. On these back grounds some cells were also treated with anti-CD105 (Millipore) at concentrations ranging from 1-100 ug/ml or anti-VEGF at 100ug/ml (Sigma). Tubes were observed with an IMT-2 inverted

microscope (Olympus, Melville, NY), and images were captured with a DMC digitizing camera (Polaroid Corporation, Waltham, MA). Six fields per well were captured for quantitative analysis. The digitized images were imported into ImageJ software (developed by Wayne Rasband, National Institutes of Health, Bethesda, MD; available at http://rsb.info.nih.gov/ij/index.html). Capillary-like structures of more than two cell lengths were assessed, and the mean tube length per field of each well was calculated. The average tube length of each treatment group was reported. The experiment was independently repeated three times.

5.2.9 Intravitreal Injections

Rats were anesthetized by isoflurane (TerrellTM; Meridian, ID) inhalation, and a single drop of 0.5% proparacaine (Allergan; Hormigueros, PR) was topically applied to the cornea prior to intravitreal injection. For all intravitreal injections, the globe was penetrated posterior to the ora ciliaris retinal using a 30-gauge needle with a 19° bevel and a 10 l syringe (Hamilton Co.; Reno, NV). The needle was advanced to the posterior vitreous while maintaining a steep angle to avoid contact with the lens. The injection bolus (5 l) was delivered near the trunk of the hyaloids artery, proximal to the posterior pole of the retina. Following injection, a topical antibiotic suspension (neomycin and polymyxin B sulfates and gramicidin; Monarch Pharmaceuticals; Bristol, TN) was applied. Non-injected eyes were also treated with topical proparacaine and antibiotic to control for the potential of these agents to influence retinal vessel growth.

5.2.10 Drug Treatment

At 14(0), a time of high retinal VEGF expression in this model, eyes from OIR and RA rats remained uninjected, or were injected with 5 ul of vehicle (PBS), rat anti-VEGF (sigma) at 1.0 mg/ml or anti-CD105 at doses ranging from 0.01-1.0 mg/ml. These doses were initially chosen based on published data for the use of anti-VEGF treatments(90, 91).

5.2.11 Quantification of Retinopathy

OIR rats were euthanized by decapitation on 14(6). Rats were enucleated and the neural retinas were dissected and placed in cmf-PBS with 10% formaldehyde solution (37% formaldehyde solution; Fisher Scientific Fair Lawn, NJ) overnight at 4 C. The retinal vasculature was stained for ADPase activity, according to a previously described method(92) adapted for use herein(70, 93). Images of ADPase-stained retinas were digitized, captured, and displayed at 20X magnification. The total retinal area and the retinal area containing blood vessels were traced on the monitor face. The number of pixels within these areas was converted to mm^2. Measurements of this parameter were recorded. To determine the effect of the various treatments on pathological angiogenesis, the extent of retinal NV was assessed in flat-mounted retinas stained for ADPase activity. Representative retinal flatmounts quadrants are shown. Abnormal preretinal NV was assessed by digitally measuring NV area. Digitized images of the retinas were captured and displayed at 65X magnification. Preretinal vessels were then traced on a computer monitor. The pixels contained in the areas of NV were totaled for each retina and converted to mm^2 (Photoshop CS; Adobe Systems Inc.). The operator was masked with

respect to the treatment. Where there was a question of the preretinal nature of a vessel tuft, the tissue was evaluated with a light microscope at 200X magnification using the plane of focus. This method of estimation correlates well ($r^2 = 0.947$) with the clockhour method of estimation(94), and yields normally distributed data that allow statistically significant differences between treatment groups to be determined by analysis of variance. The retinas of age-matched RA rats showed no pathology and were not included in statistical analyses.

5.2.12 Statistical Analysis

Statistically significant differences between treatment and control groups throughout this study were determined by analysis of variance with a Dunnett's post hoc procedure $p \leq 0.05$ was considered significant. Unless otherwise stated, error bars on the graphs indicate standard deviation. Unless otherwise stated, each experiment was repeated three times. For each experiment, n = 8 – 12 eyes for each treatment group.

5.3 Results

5.3.1 In Vitro Protein Expression of Endoglin During Normoxia or Hypoxia

In this set of experiments, mature endothelial cells and EPCs were exposed to 24 hours of either hypoxia or normoxia. There was very little positive immunocytochemical staining for CD105 in normoxic EPCs, however, there were a small number of cells that were clearly positive for the protein. Similarly, there was almost no positive CD105 staining of the normoxic ECs and less in comparison to the normoxic EPCs. Having been affected by the hypoxic treatment, the hypoxic EPCs demonstrated a large upregulation

of CD105 protein expression; however, it stained more strongly on some cells than others. The hypoxic mature ECs also exhibited an increase in CD105 staining relative to normoxic ECs, but it is less than the hypoxic EPCs. The hypoxic mature EC CD105 staining intensity was closest to that of the normoxic EPC staining. This is depicted in **Figure 5.1.**

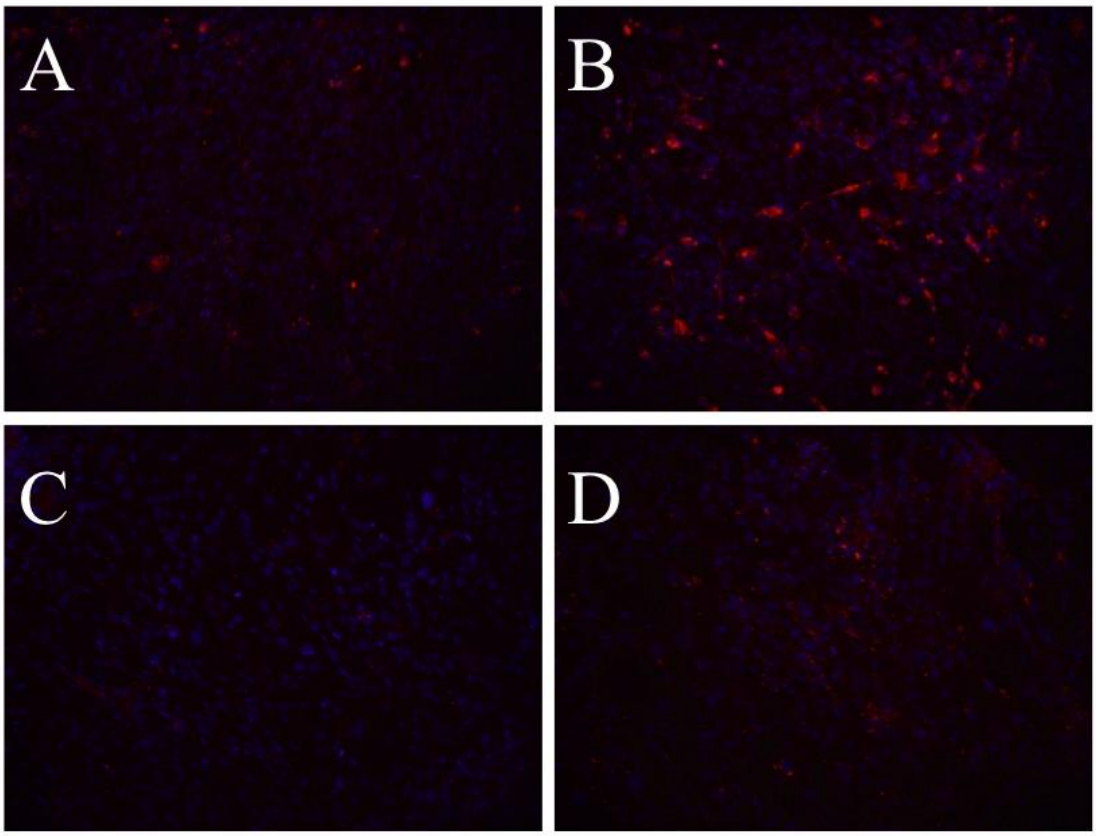

Figure 5.1. Endoglin staining in CD133+/CD34+ EPCs and mature ECs treated for hypoxia and normoxia for 24 hours. Endoglin is shown in red while DAPI stained cell nuclei are shown in blue. A and B are CD133+/CD34+ EPCs. C and D are mature ECs. A and C are normoxia treated, and B and D are hypoxia treated.

The results of endoglin protein levels measured by ELISA are shown in **Figure 5.2**. This figure demonstrates a similar finding to what can be observed in the immunocytochemical staining. There was no significant difference in protein levels between the hypoxic and normoxic mature endothelial cell samples; nor was there a significant difference between either of the mature EC sample endoglin levels and those of the normoxic EPC protein levels. However, the hypoxic EPC samples demonstrated a 3.2-fold upregulation of CD105 protein ($p<0.01$) relative to the normoxic samples of this cell type.

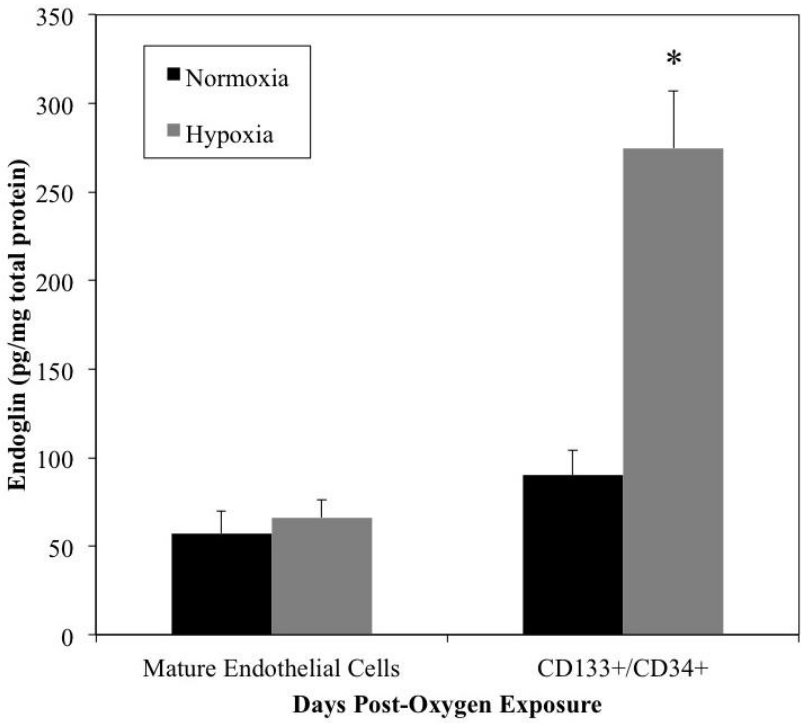

Figure 5.2. Endoglin protein levels from mature ECs and CD133+/CD43+ EPCs after 24 hours of treatment with either normoxia or hypoxia. * - $p<0.01$.

5.3.2 Assessment of Rat Oxygen-Induced Retinopathy (OIR) Tissue for Endoglin Levels and Association with Neovascularization

In westerns blots from retinal tissue lysates, the CD105 levels appear higher in all of the OIR sample time points, and are significantly higher at two, three and six days post-oxygen treatment ($p<0.02$). While the room air-treated samples remain low and constant over the times observed, the OIR samples appear to increase, throughout the sample times with the largest amplification between day zero and day two post treatment. A representative western blot and graph depicting the relative quantified CD105 values from four separate experiments is shown in **Figure 5.3**.

Retinal tissue samples taken from animals three days post-oxygen treatment were flatmounted and examined for CD105 and a marker of endothelial cells (Isolectin B4). This immunohistochemical staining is shown in **Figure 5.4**. Panel A shows strong endoglin staining in many of the neovascular lesions and some additional strong staining in a bit of the vessels. However, not all of the neovascular lesions are positive for CD105 and the lesions that are positive are not uniformly staining for endoglin. Panel B depicts three large vessels in the retinal mid periphery between the vascular and avascular interface: two veins on either side of an artery. This panel demonstrates the increased endoglin levels in the veins at the vascular and avascular interface at the ends of the veins, relative to the endoglin levels in and at the end of the artery. Panel C illustrates more closely associated CD105 protein with the vessels at the end of a vein. Additionally, this panel shows strong endoglin protein overlap in most of the neovascular lesions.

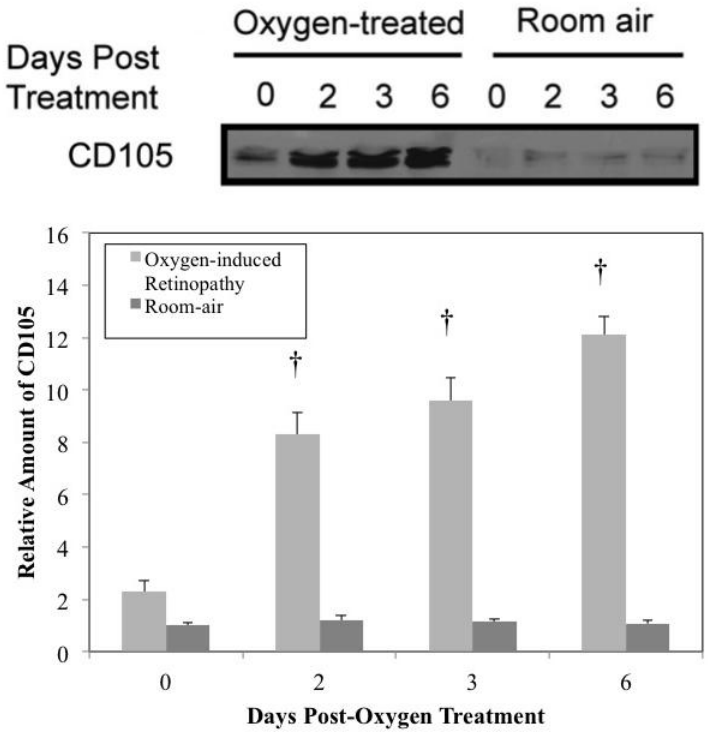

Figure 5.3. Western blots showing endoglin at several time points in post-oxygen treated retinal tissue from OIR and room air-raised control animals. Samples in every lane were matched for protein concentration and ultimately compared to one another after being normalized to relative beta-actin levels. The bottom graph shows the normalized and averaged results of the western protein quantities. Each band was normalized to beta-actin and every western was independently repeated at least three times. † - $p<0.02$.

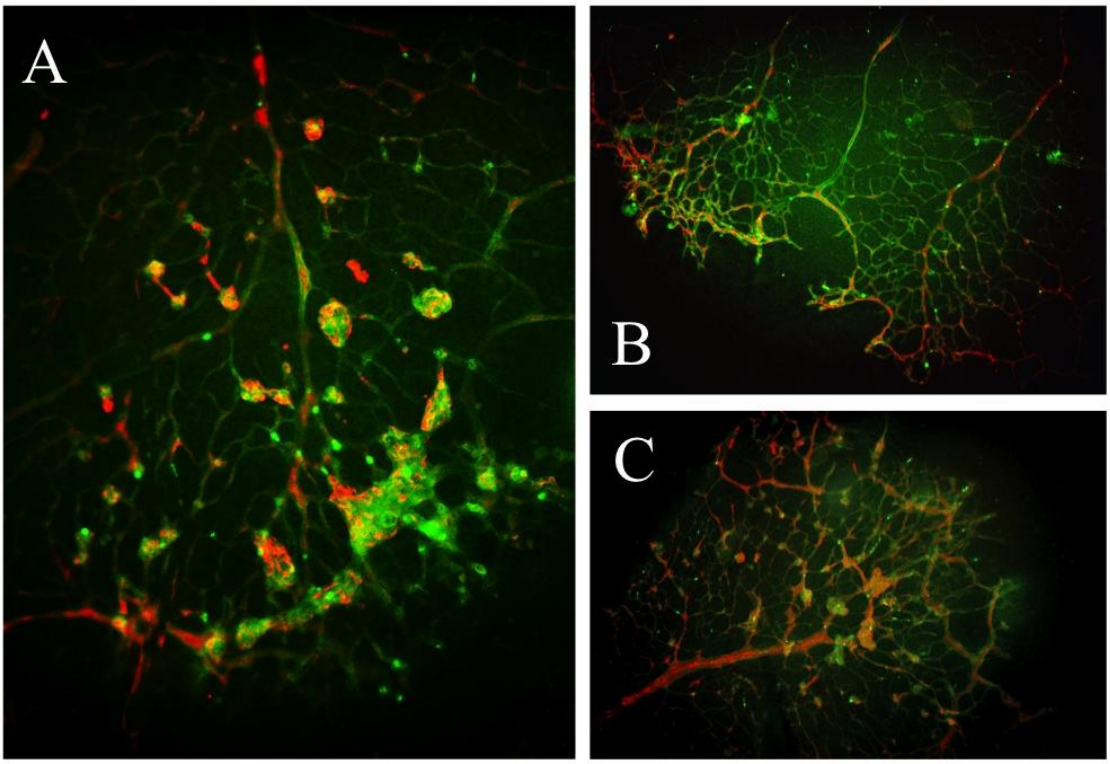

Figure 5.4. Endoglin and vascular staining on retinal flatmounted tissue from animals three days post-oxygen treatment, 14(3). Endoglin is shown in the red, and Isolectin B4 staining of the vasculature is green. (A) Endoglin is mostly associated with neovascular lesions, but not all lesions are CD105 positive. (B) Endoglin is more associated with veins. (C) Endoglin associated with neovascular lesions and vasculature tissue.

Retinal tissue samples taken from animals six days post-oxygen treatment were flatmounted and examined for CD105 and a marker of endothelial cells (isolectin B4). This immunohistochemical staining is shown in **Figure 5.5**. The left image panels are a low magnification of the entire retinal flatmount and the right panels are a higher magnification of the neovascular lesions at the end of a vein. The top panels show the relatively endothelial specific isolectin B4. These panels demonstrate the typical vascular and neovascular staining pattern seen at this time in the OIR model. The neovascular lesions are predominately at the ends of veins, just on the vascular side of the vascular to avascular interface of the retinal mid-periphery. The middle panel shows endoglin staining in red. The areas of most intense staining seem to correspond with neovascular lesions seen in the green, isolectin B4 panels. The bottom panels demonstrate the combined isolectin B4 and endoglin staining. This reveals a strong association of endoglin with the neovascular lesions and the incompletely formed vessels right at the vascular border with the avascular zone. There is also a much less intense overlap of endoglin staining with more mature vessels found more centrally in the retinal flatmount.

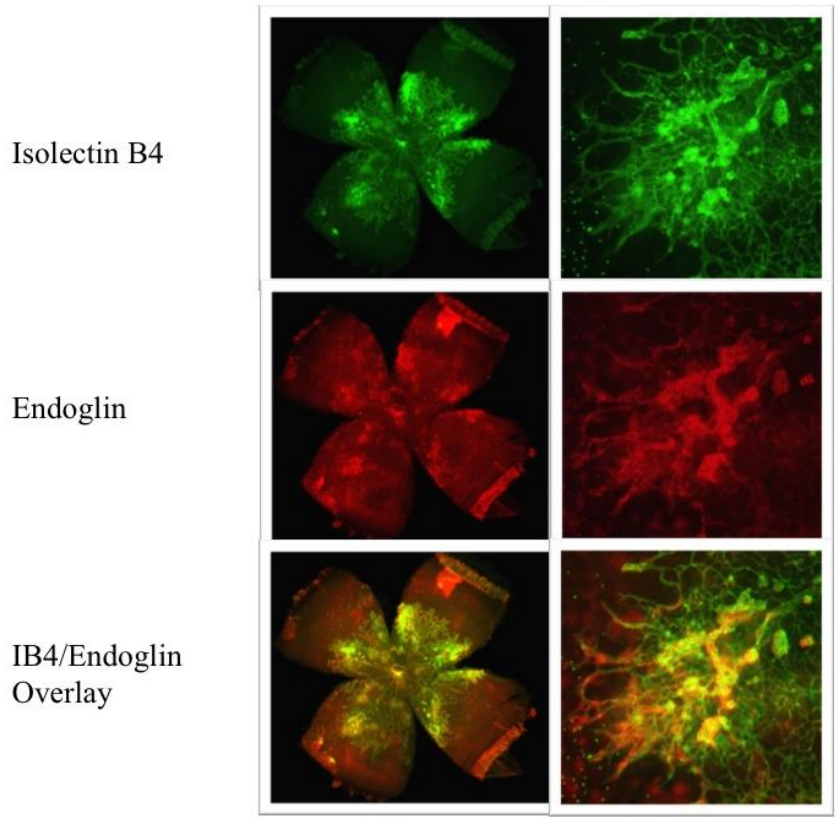

Figure 5.5. Endoglin and vascular staining on retinal flatmounted tissue from animals six days post-oxygen treatment, 14(6).

The results of endoglin protein levels in OIR tissue measured by ELISA are shown in **Figure 5.6**. In this experiment, some of the animals were treated with an intraperitoneal injection of a CXCR4 antagonist (AMD3100) at 40mg/kg on zero and three days post-oxygen treatment. This antagonist has been shown to potently and specifically antagonize CXCR4(95-97), prevent CXCR4/SDF-1 mediated binding and homing of progenitor cells(98, 99), and reduce progenitor cell mediated neovascularization(100). This figure demonstrates a similar finding to what can be observed in the western blot analysis of this tissue in **Figure 5.3**. There was no significant difference in protein levels between the room air-raised samples at either time; nor was there a significant difference between either of OIR sample endoglin levels at either time. However, the OIR samples demonstrated a 3.7-fold upregulation of CD105 protein ($p<0.01$) relative to the room air-raised samples at three days post-oxygen treatment, and a 4.8-fold upregulation ($p<0.01$) at six days post-oxygen treatment. Additionally, there was a 46% ($p<0.05$) and 50% ($p<0.05$) reduction in CD105 protein levels in the samples treated with AMD3100 relative to the OIR samples at days three and six post-oxygen removal.

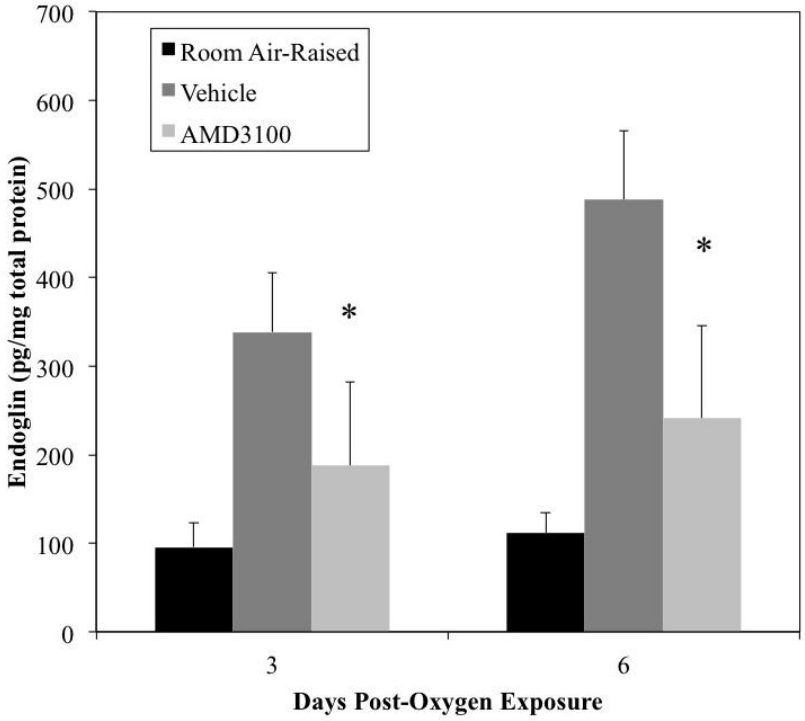

Figure 5.6. Endoglin protein levels in retinal tissue from OIR and room air-raised animals. This tissue was collected at three and six days post-oxygen exposure. * - $p<0.02$.

5.3.3 Assessment of EPC Homing and Recruitment in a Hypoxic Endothelial Monolayer Adherence Model

The findings in **Figure 5.7** demonstrate the increased adherence CD133+/CD34+ EPCs on hypoxic endothelial monolayers, was unaffected by treatment with anti-rat IgG at 100µg/ml. In these samples there was a 36% reduction ($p<0.05$) in rolling velocity on the hypoxic monolayer relative to the normoxic control. Treatment with 5µg/ml of the CXCR4 antagonist prevented this reduction in rolling velocity to non-significant levels. However, treatment of the EPCs with anti-CD105 at 100µg/ml had no effect on the adherence of the cells. In these samples, there was a 44% reduction ($p<0.05$) in the rolling velocity on the hypoxic monolayer relative to the normoxic control. This difference was not significantly different from that of the anti-rat IgG control.

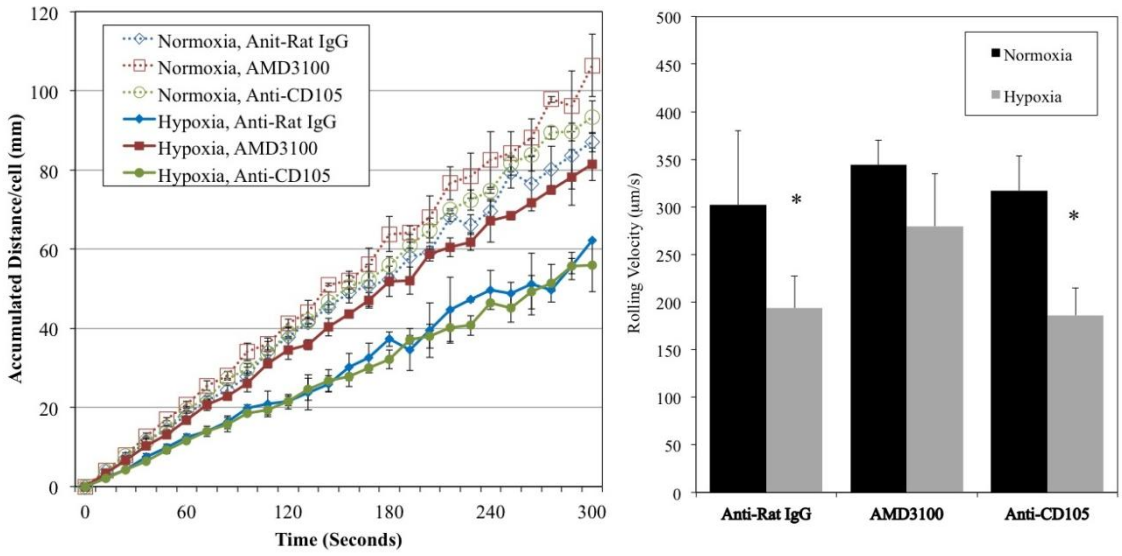

Figure 5.7. The effect of anti-CD105 treatment on mature EC and EPC homing ability. Rolling velocities of the cells are measured and a slower rolling velocity is indicative of increased adherence to the endothelial monolayer. The graph to the left is the average accumulated distance of the cells at each time point during the assay and the graph to the right shows the average rolling velocity of each cell type for the entire assay. * - $p<0.05$.

5.3.4 VEGF- and Serum-Mediated Endothelial Cell Capillary Tube Formation and Incorporation by EPCs

This assay should model the effect that homing EPCs would have on endogenous endothelial cells that are proliferating and forming new capillary networks in angiogenic or neovascular tissue. The top row (A-C) of **Figure 5.8** shows control anti-rat IgG at 100µg/ml treatment conditions, and the bottom row (D-F) is a treatment of anti-CD105 at 100µg/ml. The first column (A, D) of the figure shows how the endothelial cells and EPCs react in an environment that is free of serum, Here the cells clump, with addition of the EPCs and grow out from these clumped cell colonies. The anti-CD105 treatment reduces the tubes that are formed from these cell colonies. The middle column of the figure (B, E) is stimulated with 50ng/ml VEGF. There appears to be a slight effect of the anti-endoglin treatment with some reduction in tube formation in panel E. The right most column of the figure (C, F) is treated with the strongest tube forming stimulant, 10% serum. These panels show no apparent difference with anti-CD105 treatment.

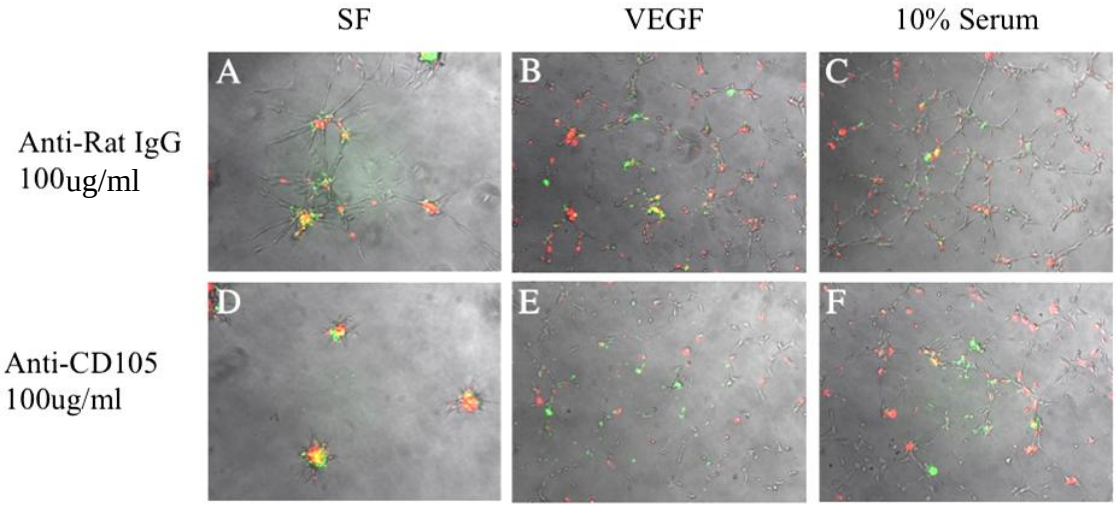

Figure 5.8. The effect of anti-CD105 treatment on mature EC tube formation and the ability of EPCs to incorporate into capillaries. In these experiments the mature endothelial cells were prelabeled with a green fluorescent tracker and the EPC subpopulations were labeled with a red fluorescent tracker.

Figure 5.9 shows a graphically quantified representation of the panels in **Figure 5.8,** however, the tube formation was quantified by the cell type: EPCs (red cells) or mature ECs (green cells). The data in this figure generally agrees with that from the figures, showing significant increases in tube formation from serum free with the addition of either VEGF or 10% serum, $p<0.01$ for both. Anti-VEGF therapy was able to produce a 42% reduction ($p<0.05$) in tube length in ECs and a 31% reduction ($p<0.05$) in EPCs. Anti-CD105 had no significant effect on EC tube formation, but did result in a 15% reduction in EPCs ($p<0.05$). Finally, the combination of anti-CD105 and anti-VEGF produced a 48% reduction ($p<0.05$) in ECs tube length, however, this reduction was not significantly different from anti-VEGF alone. In EPCs, the combination treatment resulted in a 44% reduction ($p<0.02$) in tube length relative to10% serum, however, it was not significantly different than the reduction as a result of anti-VEGF alone.

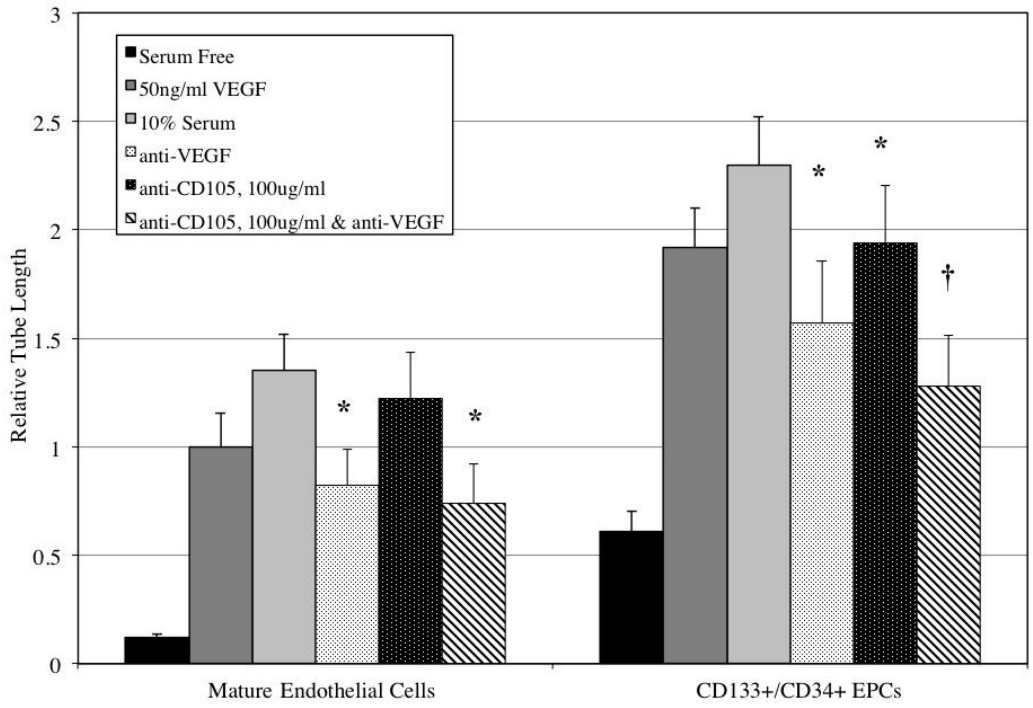

Figure 5.9. Graph of anti-CD105 effect on relative tube length in ECs and EPCs. The graph shows the quantified tube lengths of the tube formation assay demonstrated in the **Figure 5.8** panels. All antibody treatments were performed on a 10% serum background. In this assay the tube lengths were normalized to the mature endothelial cell response to VEGF stimulation. * - $p<0.05$, † - $p<0.02$, relative to 10% serum. Statistics were determined by analysis of variance with a Dunnett's post hoc procedure.

5.3.5 VEGF- and Serum-Mediated Proliferation

In **Figure 5.10**, the proliferation experiments for mature ECs showed a 2-fold response of the cells to VEGF, and a more robust 4.3-fold response of these cells to 10% serum. Anti-VEGF reduced proliferation by 31% ($p<0.05$). Anti-CD105 treatment reduced the proliferation in a dose dependant manner at 17% ($p<0.05$), 34% ($p<0.05$), and 57% ($p<0.02$), respectively, for each of the doses: 1-100ug/ml. The combination of anti-VEGF and the middle concentration of anti-CD105 (10ug/ml) significantly reduced proliferation by 44% ($p<0.05$). This combination treatment was not significant from either of the anti-VEGF or anti-CD105 treatments alone.

The proliferation experiments for mature EPCs showed a 2.5-fold response of the cells to VEGF, and a more robust 4.2-fold response of these cells to 10% serum. Anti-VEGF reduced proliferation by 22% ($p<0.05$). Anti-CD105 treatment reduced the proliferation in a dose dependant manner at 13% ($p<0.05$), 37% ($p<0.05$), and 59% ($p<0.02$), respectively, for each of the doses: 1-100ug/ml. The combination of anti-VEGF and the middle concentration of anti-CD105 (10ug/ml) significantly reduced proliferation by 57% ($p<0.05$). This combination therapy was significantly different from both anti-VEGF and anti-CD105 at 10ug/ml ($p<0.05$)

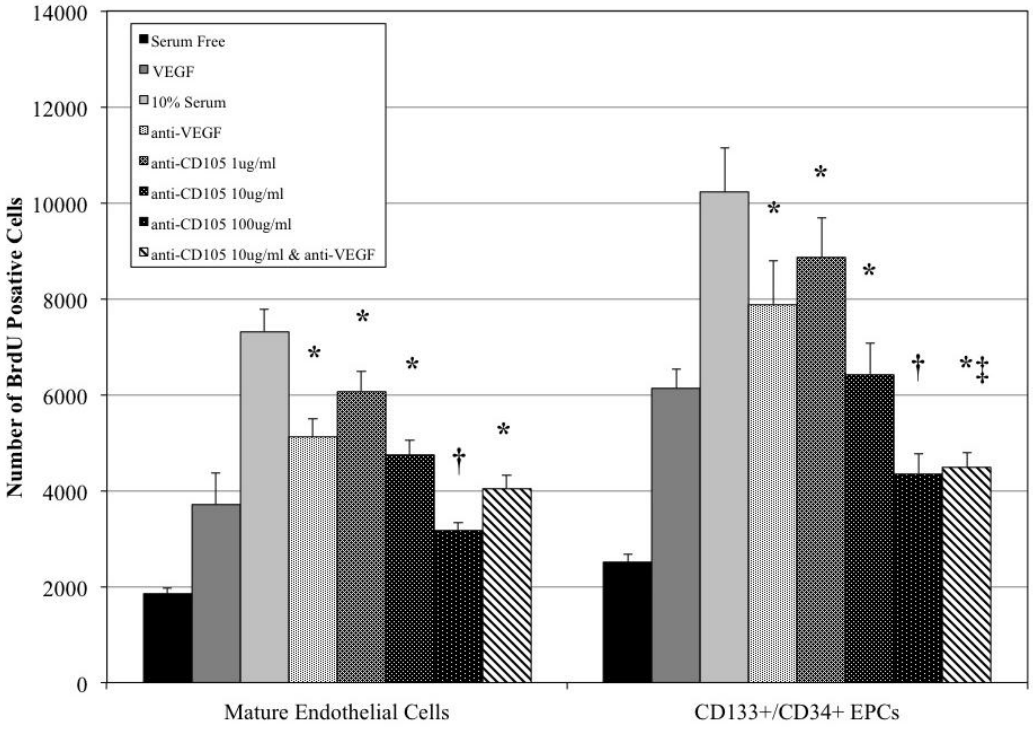

Figure 5.10. Analysis of anti-CD105 treatment on mature EC and EPCs proliferation. All antibody treatments were performed on a 10% serum background. * - $p<0.05$, relative to 10% serum. † - $p<0.02$, relative to 10% serum. ‡ - $p<0.05$, relative to anti-CD105 10ug/ml. Statistics were determined by analysis of variance with a Dunnett's post hoc procedure.

5.3.6 In Vivo Endoglin Targeted Neovascular Inhibition in the Rat Oxygen-Induced Retinopathy (OIR) Model

Figure 5.11 shows representative retinal quadrants of OIR animals in an experiment looking at the effect of anti-CD105 treatment on neovascularization. The vasculature is stained dark brown with a lead precipitate according to the ADPase staining method(92). Panels A and B are non-injected and vehicles controls showing large neovascular lesions. Panel C illustrates an anti-VEGF treated animal with slightly reduced neovascularization. Panels D and E are anti-CD105 treatments at 0.1mg/ml and 1.0mg/ml treatments, respectively. These panels show a bit of reduced neovascularization relative to the controls. Panel F is of a retinal quadrant from an animal treated with a combination of 1.0mg/ml of both anti-CD105 and anti-VEGF. This panel shows the most apparent reduction in neovascularization.

Figure 5.12 is a graphical representation of the quantified neovascular lesion areas from the retinas depicted in **Figure 5.11**. Relative to vehicle, anti-VEGF treatment reduced neovascular area by 32% ($p<0.05$). Anti-CD105 treatment reduced the neovascular area in a dose dependant manner by 18%, 31% ($p<0.05$), and 47% ($p<0.05$), respectively, for each of the doses: 0.01-1.0mg/ml. The combined treatment with anti-CD105 and anti-VEGF resulted in the greatest neovascular reduction of 62% ($p<0.02$), and this reduction in neovascular area was significantly different from the highest dose of anti-CD105 and the dose of anti-VEGF alone ($p<0.05$).

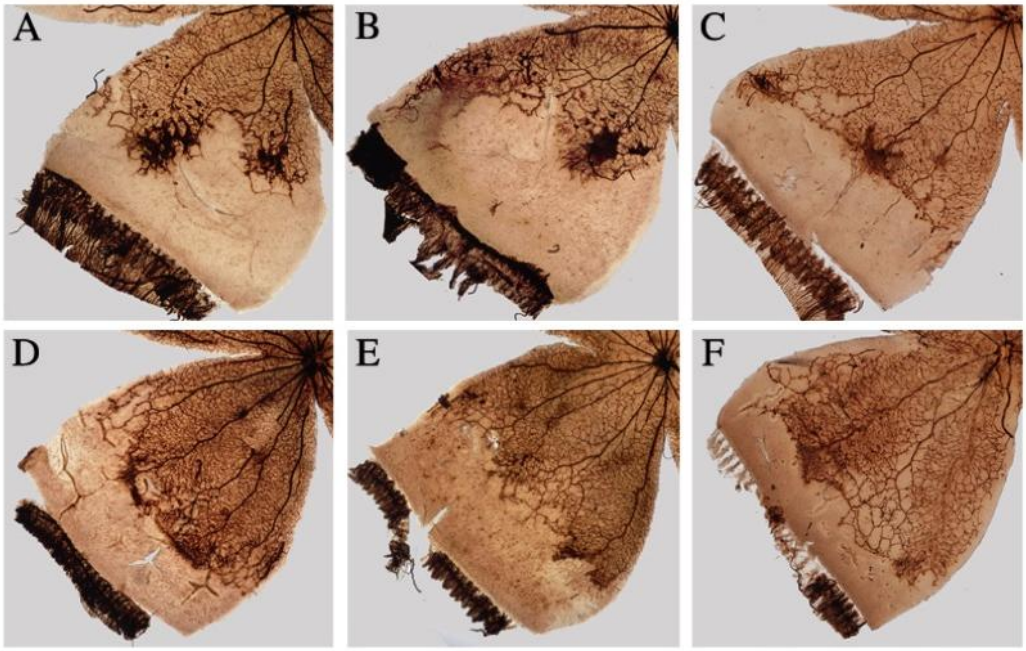

Figure 5.11. Comparison of representative retinal quadrants from eyes treated with anti-CD105. (A) No injection (B) Vehicle (C) anti-VEGF, 1.0mg/ml (D) anti-CD105, 0.1mg/ml (E) anti-CD105, 0.1mg/ml (F) anti-CD105, 1.0mg/ml and anti-VEGF, 1.0mg/ml.

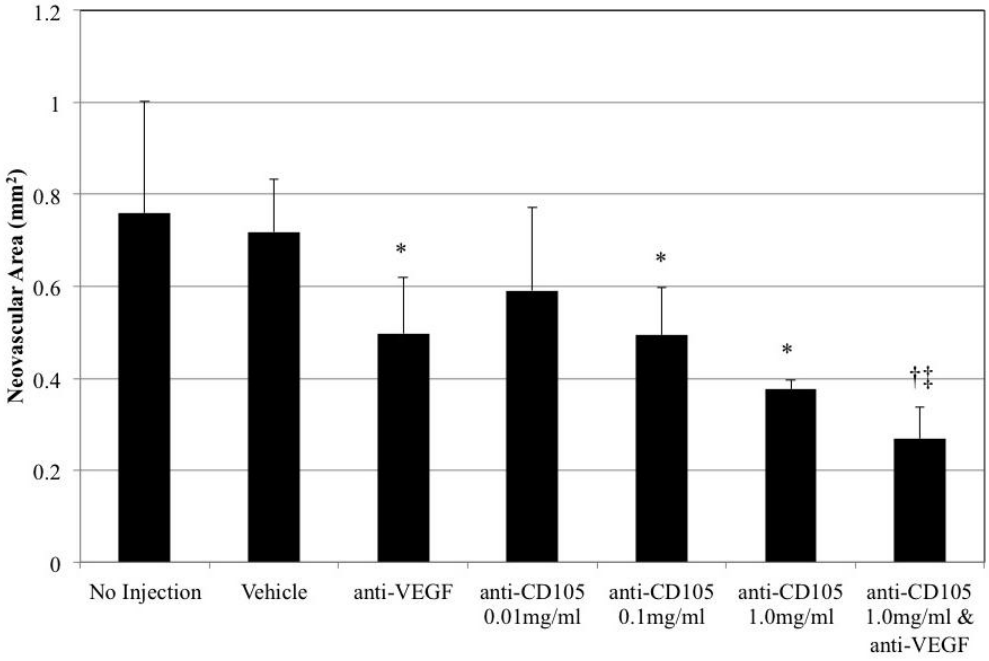

Figure 5.12. The effect of anti-CD105 treatment on neovascular area in rat OIR. * - $p<0.05$, relative to vehicle. † - $p<0.02$, relative to vehicle. ‡ - $p<0.05$, relative to anti-CD105 1.0mg/ml.

5.4 Discussion

The experiments from this study considered as a whole suggest a role for endoglin in the promotion of retinal neovascularization that is associated with disease pathology in diabetic retinopathy and retinopathy of prematurity. Additionally, endoglin appears to be functioning in this angiogenic role largely through its association with endothelial progenitor cells involved in neovascular lesion formation.

In the initial *in vitro* experiments, endoglin was expressed at slightly higher levels in the EPCs than the mature ECs under normoxic conditions and then only significantly upregulated in the hypoxic EPCs. This was reflected and reinforced in the *in vivo* OIR model, with the significantly increased amounts of endoglin at days two, three and six post-oxygen exposure. Additionally, this increase in endoglin could be reduced by the inhibition of EPC homing to sights of neovascularization with the CXCR4 antagonist AMD3100. Finally, the protein expression patterns of endoglin associated closely with neovascular lesions and proliferative vascular areas at both 14(3) and 14(6). Three days post-oxygen exposure is a significant time point because this is when neovascular tufts are beginning to form and grow rapidly. The 14(6) time point is also significant because it is the peak of neovascular growth. At 14(3), there is a heterogeneous overlap of endoglin with the developing neovascular lesions as they begin to grow. This is possibly the result of a heterogeneous population of cell contributing to those lesions, such as EPCs and native mature ECs. Also, it is important to note the association of endoglin at the ends of veins at 14(3). This is particularly important because neovascular lesions predominantly form at these locations, at the end of veins. At the later 14(6) time, the

lesions are more fully developed. The association between intense endoglin staining and the vessels seems to be decreased and there is an increased homogeneous association of intense endoglin staining with large neovascular lesions.

In the assays examining the angiogenic capacities of EPCs, endoglin demonstrated significant effects on EPC proliferation. Specifically, the tube formation and proliferation assays were preformed with the antibody treatments on a 10% serum background in an effort to account for more of the growth factors responsible for neovascularization than VEGF alone, but also being inclusive of VEGF. In a dose dependent fashion, anti-CD105 treatment reduced proliferation in both ECs and EPCs, but having a greater effect on reducing EPC proliferation. Additionally, the combined therapy of anti-VEGF with anti-CD105 significantly reduced the EPC proliferation more than either treatment alone. In the parallel plate flow chamber cell homing assay, anti-CD105 treatment had no significant effect on the ability of EPCs to home, however, there was evidence that it affected capillary tube formation and incorporation. Furthermore, in the tube formation assay, there wasn't a significant difference in a combined anti-CD105 and anti-VEGF treatment for mature ECs, however, for EPCs there was a significant response reducing tube length with anti-endoglin alone and the combined treatment.

Finally, through the analysis of neovascular area in the OIR model, endoglin blockade is shown to significantly reduce the pathological lesion sizes. This reduction was done in a dose dependent manner, like that of the *in vitro* assays. Additionally, at equivalent concentrations anti-CD105 was more effective than anti-VEGF treatment, but also worked additively with anti-VEGF treatment when the two were combined to cause the largest reduction in neovascular lesion size.

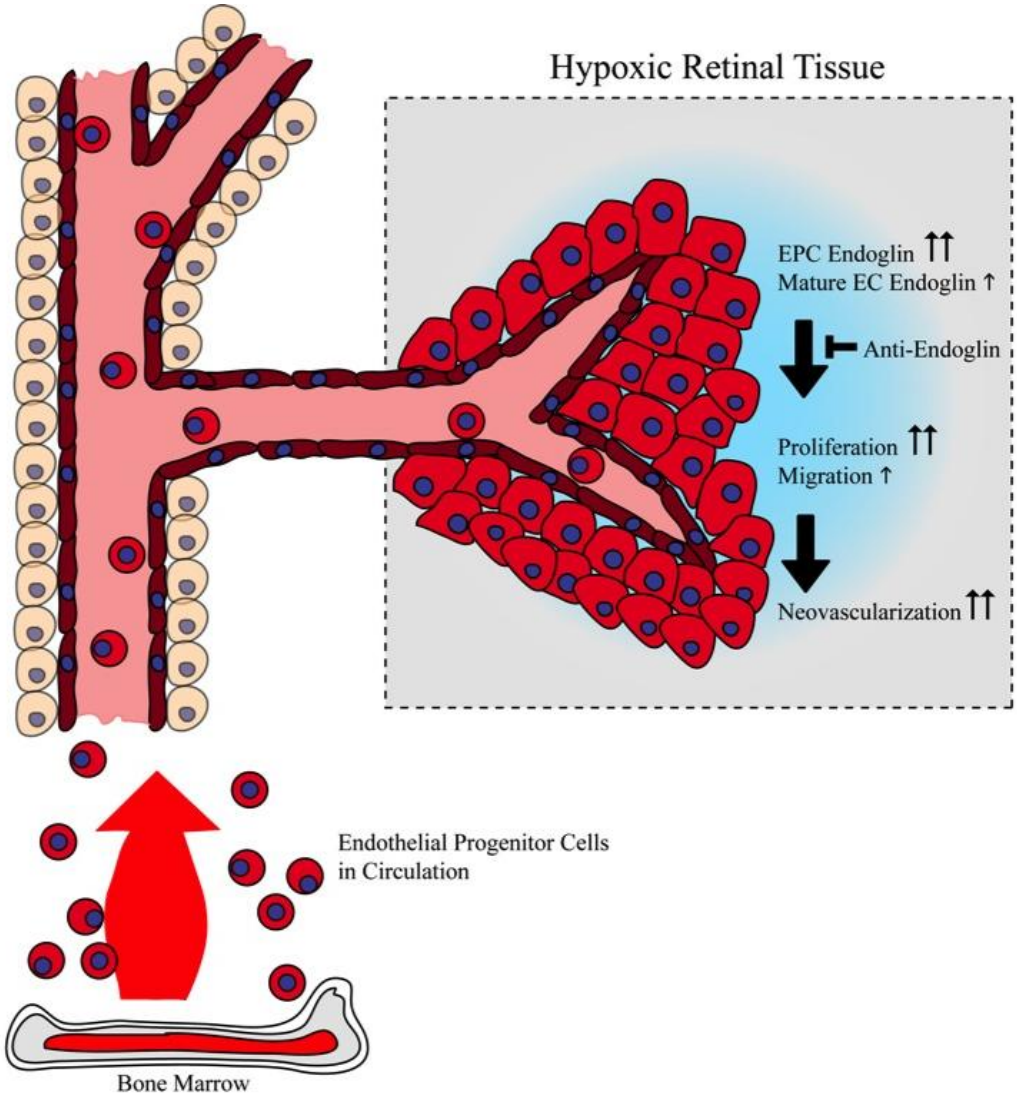

Figure 5.13. Diagram demonstrating the role of endoglin in tissue-specific, EPC-mediated retinal neovascularization. Here the endothelial progenitor cells are originating in the bone marrow and entering systemic circulation. These EPCs home to and incorporate into retinal tissue that is hypoxic and in a proangiogenic state. In this hypoxic condition, the level of endoglin on the surface of EPCs is greatly increased relative to the normoxic levels and there is also a slight increase of endoglin on the resident mature endothelial cells in this tissue. This increased endoglin on the EPCs causes them to proliferate rapidly and migrate more quickly leading to a larger neovascular lesion. This system can be inhibited by blocking endoglin.

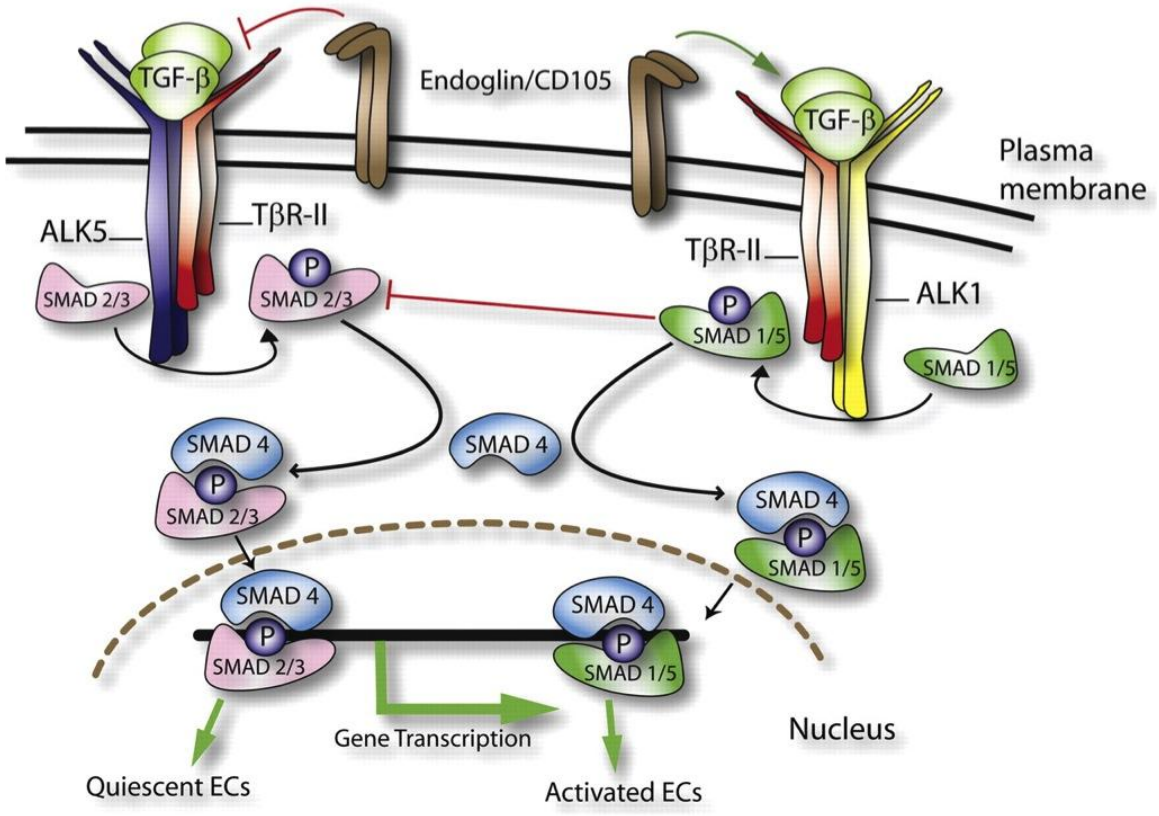

Figure 5.14. Diagram demonstrating a speculative, theoretical mechanism by which endoglin may be affecting EPC activity in retinal neovascularization. EPCs homing to hypoxic retinal tissue as well as resident mature endothelial cells in the hypoxic retinal tissue are activated to a more proliferative state through either the ALK1 or ALK5 pathways. (This diagram is a reproduction and originally published in Fonsatti et al. Cardiovasc Res. 2010 Apr 1;86(1):12-9. – (101).

All of these experiments suggest a critical role for endoglin in the EPC-mediated retinal neovascularization that is seen in these OIR animals. **Figure 5.13** demonstrates the tissue specific mechanism for endoglin, while **Figure 5.14** shows a more detailed biochemical, signaling mechanism that utilizes endoglin's interaction with TGFβ/ALK1 and TGFβ/ALK5 signaling. While there aren't experiments in this chapter directly targeting the signaling mechanism of endoglin's effects on EPCs, there are a number of published studies that indicate what this mechanism might be. Tian et al. have demonstrated that endoglin can be upregulated by hypoxia in mature cardiovascular endothelial cells(102). Additionally, endoglin, through activation of TGFβ/ALK1, can phosphorylate SMAD1/5/8 to promote endothelial proliferation and migration or, through inhibition of TGFβ/ALK5 and SMAD2/3 phosphorylation can prevent endothelial cell quiescence(25, 101, 102). Yet another study pointing to the importance of this pathway demonstrated that over expression of ALK1 was able to promote the remodeling of retinal blood vessels(103). The experiments conducted in this chapter have shown EPCs to be more reactive to endoglin upregulation in hypoxia and highly active in the formation of neovascular lesions in OIR. It is likely that the same CD105/ALK/SMAD pathways that have been shown to control mature endoglin proliferation also play a role in EPC proliferation and migration signaling pathways.

The results from this study are encouraging as a potentially new treatment pathway for ocular neovascularization that is, at least, partially independent of VEGF and targets endothelial progenitor cell. It is additionally promising that the endoglin and VEGF targeted therapies seem to work additively, which potentially would make them more effective when used to treat individuals with little or no effect from either therapy

strategy alone. Also, since they work additively, smaller doses of each could be given in combination. This reduced dosing may decrease any side effects that are associated with the treatments. Ultimately, more studies will be necessary, and endoglin seems like an ideal candidate for future clinical trials for ocular neovascularization.

CHAPTER VI

CONCLUSIONS AND FUTURE WORK

This dissertation is composed of four chapters that define a framework for studying EPCs in the context of ocular neovascularization. Using the methods developed in this work can help to determine the biological role of an EPC subpopulation, EPC associated protein, or EPC directed therapies either through their inhibition or utility as a drug delivery device. With this outline as an example, multiple EPC subpopulations can be compared, and their surface antigens and angiogenic signaling can be effectively examined in the context of ocular angiogenesis. Chapter II was concerned with the goal of developing sufficient EPC labeling and tracking methods so that a population of cells could be marked in an EPC specific manner (ie. the scavenger receptors that pick up the acLDL, one of the tools used regularly to identify EPCs). One secondary condition of this labeling was that it be sufficiently bright to see relatively small quantities of the fluorescent reagent in cells through many cellular divisions and this fluorescence needed to be photostable over long observation periods. Another condition was the necessity to label several subpopulations with an individual color. All of these conditions were met using acLDL conjugated quantum dots. This labeling system allowed us to sufficiently track EPCs in a model of laser-induced choroidal neovascularization (LCNV). This met the goals of specific aim 1 of this work. Future studies should concentrate on tracking multiple different cell types *in vivo* simultaneously and in both LCNV and oxygen-induced retinopathy.

Chapters III and IV were concerned with the goal of developing high throughput, *in vitro* methods to analyze the angiogenic capacity of EPCs using quantum dot coded subpopulations. This was first approached with the development of the parallel plate flow chamber (PPFC) system for analyzing EPC homing capabilities in chapter III. The work from chapter II was built on here through the use of the quantum dot labeling of the EPCs. This analysis was made possible through the adherence of the cells to coated surfaces and treated endothelial monolayers. The coated surfaces allow specific proteins like SDF-1 and extracellular matrix components like hyaluronic acid to be studied in terms of their influence on EPC homing. The endothelial monolayers treated with hypoxia, normoxia, or a mechanical injury allow the PPFC to act as a model of the inner luminal wall of a blood vessel. In this way the EPCs can be studied in terms of how they react to vessels in a variety of injury scenarios. Future studies should try to add insults to the endothelial monolayers, like inflamitory stimuli (ie. LPS, or interleukins) or diabetic modeling by pretreating the monolayers in high glucose (~25mM glucose) conditions before examining the EPC adherence.

Chapter IV built again on the work of chapters II and III by utilizing those methods in a more complete analysis of EPC angiogenic capacity. Here the homing ability of the cells was analyzed with the PPFC system. The tube formation and proliferation capabilities of the cells were analyzed using a unique assay that incorporated the quantum dot labeling method developed in chapter II to follow and distinguish EPC subpopulations and mature ECs. Additionally, proliferation was studied using a BrdU assay. Together this analytical system explored the homing, tube formation and incorporation, and proliferative abilities of the EPCs. Ultimately we discovered that

CD133+/CD34+ cells had a higher angiogenic capacity in retinal angiogenesis compared to Tie2+/CD133+ cells or a heterogeneous population of EPCs. This work concluded the goals set in specific aim 2 of this work, which was to develop this analytical system. Future studies into this work should concentrate on analyzing more subpopulations of cells for their specific differences and characteristic activities in retinal neovascularization.

Chapter V built on the progress of the previous three chapters to determine the biological role of an EPC associated protein demonstrating the utility of this system of analysis. Endoglin was studied in the context of retinal neovascularization and determined to have an angiogenic role in neovascularization, largely through its proliferative effects on EPCs. This study fulfilled the goals of specific aim three, identifying, validating and examining the EPC associated protein and finding it to be a valid therapeutic target for the inhibition of neovascularization using an antibody to block its cellular function. Future studies should use this system to analyze more EPC associated proteins, more EPC subpopulations in the context of these assays, and track multiple EPC subpopulations *in vivo* in order to validate an EPC associated protein target. Additionally, the signaling pathways of endoglin on both EPCs and retinal endothelial cells should be further explored. There is promising evidence in the literature that endoglin is functioning through TGFβ/ALK1/SMAD1/5/8 to promote endothelial proliferation and through inhibition of TGFβ/ALK5/SMAD2/3 to prevent endothelial quiescence. There are a number of ALK1 and ALK5 inhibitors available that would make studying these pathways more feasible(104, 105), and many of the natural agonists like TGFβ and the BMPs should be explored as well.

There are a number of other studies that could be done involving endoglin and haplotype patient studies or animal endoglin deletion studies. Endoglin has a human correlative disease related to missense mutations in CD105, ALK1 or SMAD4(106-108). These mutations lead to hereditary hemorrhagic telangiectasia (HHT), also known as Osler-Weber-Rendu disease. This is an autosomal dominant genetic disorder characterized by arteriovenous malformations, hemorrhages, fistulas, and ulcers. These malformations can range from irritable ulcers in the mouth, skin and sclera to life-threatening hemorrhages in the lungs, liver or brain. While there are not many studies looking directly at the effects of HHT on retinal vascular development or formation, there are a small number of case studies that suggest an interesting role. Studies have shown that patients with HHT can present with retinopathy similar to that of diabetic retinopathy(109) and retinal abnormalities consisting mainly of choriocapillaris atrophy(110). These would suggest that endoglin pathway loss leads to a lack of vascular growth in the retina. Additionally, HHT patients demonstrate high plasma VEGF levels and correspondingly high focal areas of high tissue VEGF levels(111). This may be a constitutive tissue response to the absence of endoglin in an attempt to achieve vascular homeostasis. Without the proliferative and developmental cues from endoglin, an underdevelopment of the vasculature occurs resulting in an over production of VEGF from the surrounding, undernourished tissue. This would also suggest that the VEGF and endoglin pathways are separate. Interestingly, the anti-VEGF therapy, Avastin, has been successfully used in HHT patients to treat liver hemorrhaging preventing the need for transplants(112) and epistaxis(113). These findings also suggest separate signaling pathways for VEGF and endoglin. With these findings in mind, it may be beneficial to

perform a retrospective patient study comparing HHT patients and controls while focusing on the incidences of vascular diseases in the eye such as retinopathy of prematurity, diabetic retinopathy and age-related macular degeneration. Animal models could be useful to this end as well. While, an endoglin knockout mouse has embryonic lethality, an endoglin conditional knockout is available and demonstrates vascular abnormalities including delayed vascular remodeling and reduced numbers of new blood vessels(114, 115). Additionally, the heterogenous knockout mouse, which has no embryonic lethality would be an ideal model animal for HHT and studying both the vascular disorders of the eye in these patients and the influence of endoglin pathway signaling in these disorders. These animals could be invaluable through their use in the oxygen-induced retinopathy model and the laser-induced choroidal neovascularization model. The combination of these biological tools, the easy access of the retinal vasculature, and the continued research developments pointing to the importance of endoglin in vascular biology indicate that it is a prime moment to explore this molecule. With its many developing roles in vascular growth and development, endoglin should be carefully studied particularly in terms of its potential therapeutic targeting in vascular diseases of the eye.

REFERENCES

1. Liekens S, De Clercq E, Neyts J. Angiogenesis: regulators and clinical applications. *Biochem Pharmacol* 2001;61(3):253-270.

2. Asahara T, Murohara T, Sullivan A, et al. Isolation of putative progenitor endothelial cells for angiogenesis. *Science* 1997;275(5302):964-967.

3. Sengupta N, Caballero S, Mames RN, et al. The role of adult bone marrow-derived stem cells in choroidal neovascularization. *Invest Ophthalmol Vis Sci* 2003;44(11):4908-4913.

4. Sengupta N, Caballero S, Mames RN, et al. Preventing stem cell incorporation into choroidal neovascularization by targeting homing and attachment factors. *Invest Ophthalmol Vis Sci* 2005;46(1):343-348.

5. Kawamoto A, Gwon HC, Iwaguro H, et al. Therapeutic potential of ex vivo expanded endothelial progenitor cells for myocardial ischemia. *Circulation* 2001;103(5):634-637.

6. Shintani S, Murohara T, Ikeda H, et al. Mobilization of endothelial progenitor cells in patients with acute myocardial infarction. *Circulation* 2001;103(23):2776-2779.

7. Shirakawa K, Shibuya M, Heike Y, et al. Tumor-infiltrating endothelial cells and endothelial precursor cells in inflammatory breast cancer. *Int J Cancer* 2002;99(3):344-351.

8. Sata M, Saiura A, Kunisato A, et al. Hematopoietic stem cells differentiate into vascular cells that participate in the pathogenesis of atherosclerosis. *Nat Med* 2002;8(4):403-409.

9. Caplice NM, Bunch TJ, Stalboerger PG, et al. Smooth muscle cells in human coronary atherosclerosis can originate from cells administered at marrow transplantation. *Proc Natl Acad Sci U S A* 2003;100(8):4754-4759.

10. Hess DC, Hill WD, Martin-Studdard A, et al. Bone marrow as a source of endothelial cells and NeuN-expressing cells After stroke. *Stroke* 2002;33(5):1362-1368.

11. Zhang ZG, Zhang L, Jiang Q, Chopp M. Bone marrow-derived endothelial progenitor cells participate in cerebral neovascularization after focal cerebral ischemia in the adult mouse. *Circ Res* 2002;90(3):284-288.

12. Otani A, Dorrell MI, Kinder K, et al. Rescue of retinal degeneration by intravitreally injected adult bone marrow-derived lineage-negative hematopoietic stem cells. *J Clin Invest* 2004;114(6):765-774.

13. Otani A, Kinder K, Ewalt K, et al. Bone marrow-derived stem cells target retinal astrocytes and can promote or inhibit retinal angiogenesis. *Nat Med* 2002;8(9):1004-1010.

14. Fadini GP, Sartore S, Baesso I, et al. Endothelial progenitor cells and the diabetic paradox. *Diabetes Care* 2006;29(3):714-716.

15. Galiano RD, Tepper OM, Pelo CR, et al. Topical vascular endothelial growth factor accelerates diabetic wound healing through increased angiogenesis and by mobilizing and recruiting bone marrow-derived cells. *Am J Pathol* 2004;164(6):1935-1947.

16. Fadini GP, Miorin M, Facco M, et al. Circulating endothelial progenitor cells are reduced in peripheral vascular complications of type 2 diabetes mellitus. *J Am Coll Cardiol* 2005;45(9):1449-1457.

17. Krankel N, Adams V, Linke A, et al. Hyperglycemia reduces survival and impairs function of circulating blood-derived progenitor cells. *Arterioscler Thromb Vasc Biol* 2005;25(4):698-703.

18. Barbara NP, Wrana JL, Letarte M. Endoglin is an accessory protein that interacts with the signaling receptor complex of multiple members of the transforming growth factor-beta superfamily. *J Biol Chem* 1999;274(2):584-594.

19. Dallas NA, Samuel S, Xia L, et al. Endoglin (CD105): a marker of tumor vasculature and potential target for therapy. *Clin Cancer Res* 2008;14(7):1931-1937.

20. Li C, Hampson IN, Hampson L, et al. CD105 antagonizes the inhibitory signaling of transforming growth factor beta1 on human vascular endothelial cells. *Faseb J* 2000;14(1):55-64.

21. Beresford MJ, Harris AL, Ah-See M, et al. The relationship of the neo-angiogenic marker, endoglin, with response to neoadjuvant chemotherapy in breast cancer. *Br J Cancer* 2006;95(12):1683-1688.

22. Brewer CA, Setterdahl JJ, Li MJ, et al. Endoglin expression as a measure of microvessel density in cervical cancer. *Obstet Gynecol* 2000;96(2):224-228.

23. El-Gohary YM, Silverman JF, Olson PR, et al. Endoglin (CD105) and vascular endothelial growth factor as prognostic markers in prostatic adenocarcinoma. *Am J Clin Pathol* 2007;127(4):572-579.

24. Wikstrom P, Lissbrant IF, Stattin P, Egevad L, Bergh A. Endoglin (CD105) is expressed on immature blood vessels and is a marker for survival in prostate cancer. *Prostate* 2002;51(4):268-275.

25. Lebrin F, Goumans MJ, Jonker L, et al. Endoglin promotes endothelial cell proliferation and TGF-beta/ALK1 signal transduction. *Embo J* 2004;23(20):4018-4028.

26. Maier JA, Delia D, Thorpe PE, Gasparini G. In vitro inhibition of endothelial cell growth by the antiangiogenic drug AGM-1470 (TNP-470) and the anti-endoglin antibody TEC-11. *Anticancer Drugs* 1997;8(3):238-244.

27. Takahashi N, Haba A, Matsuno F, Seon BK. Antiangiogenic therapy of established tumors in human skin/severe combined immunodeficiency mouse chimeras by anti-endoglin (CD105) monoclonal antibodies, and synergy between anti-endoglin antibody and cyclophosphamide. *Cancer Res* 2001;61(21):7846-7854.

28. Waller EK, Olweus J, Lund-Johansen F, et al. The "common stem cell" hypothesis reevaluated: human fetal bone marrow contains separate populations of hematopoietic and stromal progenitors. *Blood* 1995;85(9):2422-2435.

29. Pierelli L, Bonanno G, Rutella S, et al. CD105 (endoglin) expression on hematopoietic stem/progenitor cells. *Leuk Lymphoma* 2001;42(6):1195-1206.

30. Rokhlin OW, Cohen MB, Kubagawa H, Letarte M, Cooper MD. Differential expression of endoglin on fetal and adult hematopoietic cells in human bone marrow. *J Immunol* 1995;154(9):4456-4465.

31. Britten MB, Abolmaali ND, Assmus B, et al. Infarct remodeling after intracoronary progenitor cell treatment in patients with acute myocardial infarction (TOPCARE-AMI): mechanistic insights from serial contrast-enhanced magnetic resonance imaging. *Circulation* 2003;108(18):2212-2218.

32. Jones EA, Kinsey SE, English A, et al. Isolation and characterization of bone marrow multipotential mesenchymal progenitor cells. *Arthritis Rheum* 2002;46(12):3349-3360.

33. Li Calzi S, Neu MB, Shaw LC, et al. EPCs and pathological angiogenesis: when good cells go bad. *Microvasc Res* 2010;79(3):207-216.

34. Friedlander M, Dorrell MI, Ritter MR, et al. Progenitor cells and retinal angiogenesis. *Angiogenesis* 2007;10(2):89-101.

35. Chavakis E, Aicher A, Heeschen C, et al. Role of beta2-integrins for homing and neovascularization capacity of endothelial progenitor cells. *J Exp Med* 2005;201(1):63-72.

36. Biancone L, Cantaluppi V, Duo D, et al. Role of L-selectin in the vascular homing of peripheral blood-derived endothelial progenitor cells. *J Immunol* 2004;173(8):5268-5274.

37. Gulati R, Simari RD. Cell therapy for angiogenesis: embracing diversity. *Circulation* 2005;112(11):1522-1524.

38. Dzau VJ, Gnecchi M, Pachori AS. Enhancing stem cell therapy through genetic modification. *J Am Coll Cardiol* 2005;46(7):1351-1353.

39. Gulati R, Jevremovic D, Peterson TE, et al. Diverse origin and function of cells with endothelial phenotype obtained from adult human blood. *Circ Res* 2003;93(11):1023-1025.

40. Rohde E, Malischnik C, Thaler D, et al. Blood monocytes mimic endothelial progenitor cells. *Stem Cells* 2006;24(2):357-367.

41. Suzuki H, Watabe T, Kato M, Miyazawa K, Miyazono K. Roles of vascular endothelial growth factor receptor 3 signaling in differentiation of mouse embryonic stem cell-derived vascular progenitor cells into endothelial cells. *Blood* 2005;105(6):2372-2379.

42. Friedrich EB, Walenta K, Scharlau J, Nickenig G, Werner N. CD34-/CD133+/VEGFR-2+ endothelial progenitor cell subpopulation with potent vasoregenerative capacities. *Circ Res* 2006;98(3):e20-25.

43. Aiello LP. Vascular endothelial growth factor. 20th-century mechanisms, 21st-century therapies. *Invest Ophthalmol Vis Sci* 1997;38(9):1647-1652.

44. Rafii S, Lyden D. Therapeutic stem and progenitor cell transplantation for organ vascularization and regeneration. *Nat Med* 2003;9(6):702-712.

45. McHale JF, Harari OA, Marshall D, Haskard DO. TNF-alpha and IL-1 sequentially induce endothelial ICAM-1 and VCAM-1 expression in MRL/lpr lupus-prone mice. *J Immunol* 1999;163(7):3993-4000.

46. Sans M, Panes J, Ardite E, et al. VCAM-1 and ICAM-1 mediate leukocyte-endothelial cell adhesion in rat experimental colitis. *Gastroenterology* 1999;116(4):874-883.

47. Nishiwaki H, Ogura Y, Kimura H, Kiryu J, Honda Y. Quantitative evaluation of leukocyte dynamics in retinal microcirculation. *Invest Ophthalmol Vis Sci* 1995;36(1):123-130.

48. Kimura H, Sakamoto T, Hinton DR, et al. A new model of subretinal neovascularization in the rabbit. *Invest Ophthalmol Vis Sci* 1995;36(10):2110-2119.

49. Kelly KA, Allport JR, Tsourkas A, et al. Detection of vascular adhesion molecule-1 expression using a novel multimodal nanoparticle. *Circ Res* 2005;96(3):327-336.

50. Tsourkas A, Shinde-Patil VR, Kelly KA, et al. In vivo imaging of activated endothelium using an anti-VCAM-1 magnetooptical probe. *Bioconjug Chem* 2005;16(3):576-581.

51. Jin H, Su J, Garmy-Susini B, Kleeman J, Varner J. Integrin alpha4beta1 promotes monocyte trafficking and angiogenesis in tumors. *Cancer Res* 2006;66(4):2146-2152.

52. Barnett JM, McCollum GW, Penn JS. Role of cytosolic phospholipase A(2) in retinal neovascularization. *Invest Ophthalmol Vis Sci* 2010;51(2):1136-1142.

53. Jayagopal A, Russ PK, Haselton FR. Surface engineering of quantum dots for in vivo vascular imaging. *Bioconjug Chem* 2007;18(5):1424-1433.

54. Chan-Ling T, Baxter L, Afzal A, et al. Hematopoietic stem cells provide repair functions after laser-induced Bruch's membrane rupture model of choroidal neovascularization. *Am J Pathol* 2006;168(3):1031-1044.

55. Peled A, Grabovsky V, Habler L, et al. The chemokine SDF-1 stimulates integrin-mediated arrest of CD34(+) cells on vascular endothelium under shear flow. *J Clin Invest* 1999;104(9):1199-1211.

56. Avigdor A, Goichberg P, Shivtiel S, et al. CD44 and hyaluronic acid cooperate with SDF-1 in the trafficking of human CD34+ stem/progenitor cells to bone marrow. *Blood* 2004;103(8):2981-2989.

57. Lima e Silva R, Shen J, Hackett SF, et al. The SDF-1/CXCR4 ligand/receptor pair is an important contributor to several types of ocular neovascularization. *Faseb J* 2007;21(12):3219-3230.

58. Yin AH, Miraglia S, Zanjani ED, et al. AC133, a novel marker for human hematopoietic stem and progenitor cells. *Blood* 1997;90(12):5002-5012.

59. de Wynter EA, Buck D, Hart C, et al. CD34+AC133+ cells isolated from cord blood are highly enriched in long-term culture-initiating cells, NOD/SCID-repopulating cells and dendritic cell progenitors. *Stem Cells* 1998;16(6):387-396.

60. Takahashi T, Kalka C, Masuda H, et al. Ischemia- and cytokine-induced mobilization of bone marrow-derived endothelial progenitor cells for neovascularization. *Nat Med* 1999;5(4):434-438.

61. Rafii S. Circulating endothelial precursors: mystery, reality, and promise. *J Clin Invest* 2000;105(1):17-19.

62. Su X, Sorenson CM, Sheibani N. Isolation and characterization of murine retinal endothelial cells. *Mol Vis* 2003;9:171-178.

63. Toma HS, Barnett JM, Penn JS, Kim SJ. Improved assessment of laser-induced choroidal neovascularization. *Microvasc Res* 2010;80(3):295-302.

64. Yanni SE, Barnett JM, Clark ML, Penn JS. The role of PGE2 receptor EP4 in pathologic ocular angiogenesis. *Invest Ophthalmol Vis Sci* 2009;50(11):5479-5486.

65. Kaplan HJ, Leibole MA, Tezel T, Ferguson TA. Fas ligand (CD95 ligand) controls angiogenesis beneath the retina. *Nat Med* 1999;5(3):292-297.

66. Bora PS, Hu Z, Tezel TH, et al. Immunotherapy for choroidal neovascularization in a laser-induced mouse model simulating exudative (wet) macular degeneration. *Proc Natl Acad Sci U S A* 2003;100(5):2679-2684.

67. Rahmani B, Tielsch JM, Katz J, et al. The cause-specific prevalence of visual impairment in an urban population. The Baltimore Eye Survey. *Ophthalmology* 1996;103(11):1721-1726.

68. Bressler NM, Bressler SB. Preventative ophthalmology. Age-related macular degeneration. *Ophthalmology* 1995;102(8):1206-1211.

69. Asahara T, Masuda H, Takahashi T, et al. Bone marrow origin of endothelial progenitor cells responsible for postnatal vasculogenesis in physiological and pathological neovascularization. *Circ Res* 1999;85(3):221-228.

70. Penn JS, Tolman BL, Lowery LA. Variable oxygen exposure causes preretinal neovascularization in the newborn rat. *Invest Ophthalmol Vis Sci* 1993;34(3):576-585.

71. Penn JS, Henry MM, Tolman BL. Exposure to alternating hypoxia and hyperoxia causes severe proliferative retinopathy in the newborn rat. *Pediatr Res* 1994;36(6):724-731.

72. Klagsbrun M. Regulators of angiogenesis: stimulators, inhibitors, and extracellular matrix. *J Cell Biochem* 1991;47(3):199-200.

73. Folkman J, Shing Y. Angiogenesis. *J Biol Chem* 1992;267(16):10931-10934.

74. Folkman J, D'Amore PA. Blood vessel formation: what is its molecular basis? *Cell* 1996;87(7):1153-1155.

75. Risau W. Mechanisms of angiogenesis. *Nature* 1997;386(6626):671-674.

76. Li J, Zhang YP, Kirsner RS. Angiogenesis in wound repair: angiogenic growth factors and the extracellular matrix. *Microsc Res Tech* 2003;60(1):107-114.

77. Folkman J, Browder T, Palmblad J. Angiogenesis research: guidelines for translation to clinical application. *Thromb Haemost* 2001;86(1):23-33.

78. Carmeliet P. Angiogenesis in health and disease. *Nat Med* 2003;9(6):653-660.

79. Folkman J. Angiogenesis in cancer, vascular, rheumatoid and other disease. *Nat Med* 1995;1(1):27-31.

80. Wells JA, Murthy R, Chibber R, et al. Levels of vascular endothelial growth factor are elevated in the vitreous of patients with subretinal neovascularisation. *Br J Ophthalmol* 1996;80(4):363-366.

81. Zhang X, Bao S, Hambly BD, Gillies MC. Vascular endothelial growth factor-A: a multifunctional molecular player in diabetic retinopathy. *Int J Biochem Cell Biol* 2009;41(12):2368-2371.

82. Chen J, Smith LE. Retinopathy of prematurity. *Angiogenesis* 2007;10(2):133-140.

83. Andreoli CM, Miller JW. Anti-vascular endothelial growth factor therapy for ocular neovascular disease. *Curr Opin Ophthalmol* 2007;18(6):502-508.

84. Abouammoh M, Sharma S. Ranibizumab versus bevacizumab for the treatment of neovascular age-related macular degeneration. *Curr Opin Ophthalmol* 2011;22(3):152-158.

85. van Wijngaarden P, Coster DJ, Williams KA. Inhibitors of ocular neovascularization: promises and potential problems. *Jama* 2005;293(12):1509-1513.

86. Storkebaum E, Lambrechts D, Carmeliet P. VEGF: once regarded as a specific angiogenic factor, now implicated in neuroprotection. *Bioessays* 2004;26(9):943-954.

87. Yourey PA, Gohari S, Su JL, Alderson RF. Vascular endothelial cell growth factors promote the in vitro development of rat photoreceptor cells. *J Neurosci* 2000;20(18):6781-6788.

88. Lux A, Llacer H, Heussen FM, Joussen AM. Non-responders to bevacizumab (Avastin) therapy of choroidal neovascular lesions. *Br J Ophthalmol* 2007;91(10):1318-1322.

89. Arias L, Caminal JM, Badia MB, et al. Intravitreal infliximab in patients with macular degeneration who are nonresponders to antivascular endothelial growth factor therapy. *Retina* 2010;30(10):1601-1608.

90. Ferrara N, Damico L, Shams N, Lowman H, Kim R. Development of ranibizumab, an anti-vascular endothelial growth factor antigen binding fragment, as therapy for neovascular age-related macular degeneration. *Retina* 2006;26(8):859-870.

91. Bakri SJ, Snyder MR, Reid JM, et al. Pharmacokinetics of intravitreal ranibizumab (Lucentis). *Ophthalmology* 2007;114(12):2179-2182.

92. Lutty GA, McLeod DS. A new technique for visualization of the human retinal vasculature. *Arch Ophthalmol* 1992;110(2):267-276.

93. Penn JS, Henry MM, Wall PT, Tolman BL. The range of PaO2 variation determines the severity of oxygen-induced retinopathy in newborn rats. *Invest Ophthalmol Vis Sci* 1995;36(10):2063-2070.

94. Bullard LE, Qi X, Penn JS. Role for extracellular signal-responsive kinase-1 and -2 in retinal angiogenesis. *Invest Ophthalmol Vis Sci* 2003;44(4):1722-1731.

95. Hatse S, Princen K, Bridger G, De Clercq E, Schols D. Chemokine receptor inhibition by AMD3100 is strictly confined to CXCR4. *FEBS Lett* 2002;527(1-3):255-262.

96. Rubin JB, Kung AL, Klein RS, et al. A small-molecule antagonist of CXCR4 inhibits intracranial growth of primary brain tumors. *Proc Natl Acad Sci U S A* 2003;100(23):13513-13518.

97. De Clercq E. The bicyclam AMD3100 story. *Nat Rev Drug Discov* 2003;2(7):581-587.

98. Broxmeyer HE, Orschell CM, Clapp DW, et al. Rapid mobilization of murine and human hematopoietic stem and progenitor cells with AMD3100, a CXCR4 antagonist. *J Exp Med* 2005;201(8):1307-1318.

99. Devine SM, Flomenberg N, Vesole DH, et al. Rapid mobilization of CD34+ cells following administration of the CXCR4 antagonist AMD3100 to patients with multiple myeloma and non-Hodgkin's lymphoma. *J Clin Oncol* 2004;22(6):1095-1102.

100. Grunewald M, Avraham I, Dor Y, et al. VEGF-induced adult neovascularization: recruitment, retention, and role of accessory cells. *Cell* 2006;124(1):175-189.

101. Fonsatti E, Nicolay HJ, Altomonte M, Covre A, Maio M. Targeting cancer vasculature via endoglin/CD105: a novel antibody-based diagnostic and therapeutic strategy in solid tumours. *Cardiovasc Res* 2010;86(1):12-19.

102. Tian F, Zhou AX, Smits AM, et al. Endothelial cells are activated during hypoxia via endoglin/ALK-1/SMAD1/5 signaling in vivo and in vitro. *Biochem Biophys Res Commun* 2010;392(3):283-288.

103. Li B, Yin W, Hong X, et al. Remodeling retinal neovascularization by ALK1 gene transfection in vitro. *Invest Ophthalmol Vis Sci* 2008;49(10):4553-4560.

104. Cunha SI, Pardali E, Thorikay M, et al. Genetic and pharmacological targeting of activin receptor-like kinase 1 impairs tumor growth and angiogenesis. *J Exp Med* 2010;207(1):85-100.

105. Geldenhuys WJ, Nakamura H. 3D-QSAR and docking studies on transforming growth factor (TGF)-beta receptor 1 antagonists. *Bioorg Med Chem Lett* 2010;20(6):1918-1923.

106. McAllister KA, Grogg KM, Johnson DW, et al. Endoglin, a TGF-beta binding protein of endothelial cells, is the gene for hereditary haemorrhagic telangiectasia type 1. *Nat Genet* 1994;8(4):345-351.

107. Johnson DW, Berg JN, Baldwin MA, et al. Mutations in the activin receptor-like kinase 1 gene in hereditary haemorrhagic telangiectasia type 2. *Nat Genet* 1996;13(2):189-195.

108. Gallione CJ, Repetto GM, Legius E, et al. A combined syndrome of juvenile polyposis and hereditary haemorrhagic telangiectasia associated with mutations in MADH4 (SMAD4). *Lancet* 2004;363(9412):852-859.

109. Davis DG, Smith JL. Retinal involvement in hereditary hemorrhagic telangiectasia. *Arch Ophthalmol* 1971;85(5):618-621 passim.

110. Rinaldi M, Buscarini E, Danesino C, et al. Ocular manifestations in hereditary hemorrhagic telangiectasia (Rendu-Osler-Weber disease): a case-series. *Ophthalmic Genet* 2011;32(1):12-17.

111. Sadick H, Naim R, Gossler U, Hormann K, Riedel F. Angiogenesis in hereditary hemorrhagic telangiectasia: VEGF165 plasma concentration in correlation to the VEGF expression and microvessel density. *Int J Mol Med* 2005;15(1):15-19.

112. Mitchell A, Adams LA, MacQuillan G, et al. Bevacizumab reverses need for liver transplantation in hereditary hemorrhagic telangiectasia. *Liver Transpl* 2008;14(2):210-213.

113. Simonds J, Miller F, Mandel J, Davidson TM. The effect of bevacizumab (Avastin) treatment on epistaxis in hereditary hemorrhagic telangiectasia. *Laryngoscope* 2009;119(5):988-992.

114. Jain RK. Molecular regulation of vessel maturation. *Nat Med* 2003;9(6):685-693.

115. Mahmoud M, Allinson KR, Zhai Z, et al. Pathogenesis of arteriovenous malformations in the absence of endoglin. *Circ Res* 2010;106(8):1425-1433.